THE RESPONSE OF IMPULSIVELY LOADED SANDWICH PLATES.

by

G.H. FARROW

1995

Submitted to the University of Cape Town
in partial fulfilment of the requirements for
the Degree of Master of Science.

DECLARATION

I, Gary Herbert Farrow, declare that this thesis is essentially my own work and has not been submitted in this or in a similar form for a Degree at any other University.

ABSTRACT

This thesis describes a numerical study of the response of impulsively loaded circular sandwich plates using the general purpose finite element programme called ABAQUS.

The sandwich plate studied consists of three layers. The two outer layers are of mild steel and the centre layer, or core, is of air. Because of this configuration, the analysis is split into two sections. The first is the study of impulsively loaded circular single plates and the second is the study of the interaction of the outer layers of the sandwich plate on each other. The plates are analysed in the impulse range that results in large plastic deformations known as Mode I Failure. Mode II and III failure of the plates, where failure by tearing occurs, is omitted.

The results of the single plate analysis are compared to experimental and analytical work. Criteria for comparison include mid-plate deflections, strain rate dependence, strain predictions, plate thinning, deformation shape and response time. The results of the sandwich plate analysis are compared to experimental data and the criteria for comparison include mid-plate deflections and the diameter of the contact area of the two outer layers. Other aspects of the plate behaviour such as response times and the amount of strain energy absorbed are also discussed.

The explicit integration scheme is considered the best finite element solution method to use for this dynamic response problem. The pressure loading model is found to give the best correlation with experimental data while velocity loading models tend to result in instabilities in the explicit solution scheme.

The presented results for both the single plates and the sandwich plates show good correlation with the experimental data. In the case of the sandwich plates, the predicted contact diameters show good correlation with the experimental work. The phases of deformation evident in the sandwich plate experimental work are not evident in the presented results, while the mid plate deflection predictions show correct trends, but over estimate the experimental data.

ACKNOWLEDGEMENTS

My sincere gratitude to the following:

Professor G.N. NURICK: for his valued advice, guidance and support throughout.

Dr G.P. MITCHELL: for his valued assistance with ABAQUS.

Mr M. W. EASTMAN: for his untiring help and guidance with the computer network.

Messrs. H. BOWLES and G. STARKE: for their help and encouragement.

The CENTRE FOR RESEARCH IN COMPUTATIONAL AND APPLIED MECHANICS and the FOUNDATION FOR RESEARCH DEVELOPMENT for their financial assistance.

TABLE OF CONTENTS

TABLE OF FIGURES

NOMENCLATURE

Upper case:

A	Plate area
D	Strain rate material constant
E	Energy
H	Plate thickness
I	Applied impulse
M	Plate mass
P	Applied pressure
R	Plate radius
C_e	Contact energy
E_e	Elastic strain
K_e	Kinetic energy
L_{min}	Minimum characteristic element length
P_e	Plastic strain energy
V_{amp}	Initial velocity amplitude
V_o	Initial uniform velocity
V(r)	Velocity shape function
W_e	Work energy
W_f	Deflection

Lower case:

c_d	Dilation wave speed
h	Overclosure
m	Radial mass of plate
n	Strain rate sensitivity factor
q	Strain rate material constant
t	Time
t_b	Explosive burn time

Greek:

Δt	Time step
$\dot{\varepsilon}$	Strain rate
Φ_c	Damage number
μ	Friction coefficient

ν	Poisson's ratio
ρ	Material density
σ_f	Flow stress
σ_o	Static yield stress
τ	Shear stress

CHAPTER 1. INTRODUCTION

An analysis of the response of blast loaded circular sandwich plates is presented. The analysis is an investigation using a general purpose finite element package and the results are compared with previously reported analytical, numerical and experimental results.

The sandwich plates analysed consist of three layers. The two outer layers are of mild steel 1.6mm thick while the centre layer, or core, of the sandwich plate is of air. The sandwich plates tested have a radius of 50mm. As the two outer plates of the sandwich plate are separated by a core of air, the problem can be separated into two parts. The first is the analysis of the behaviour of single impulsively loaded circular plates and the second is the interaction of the one plate with the other due to contact.

Experimental results on explosively loaded circular and square plates and analytical and numerical methods used to predict the behaviour of these plates have been widely reported.

The first part of the presented analysis is an attempt to model the behaviour of single circular plates subjected to impulsive loading. The results obtained are compared with previous experimental, analytical and numerical work. The criteria for comparison include plate mid-point deflection, strain rate dependence, strain predictions, plate thinning, deformed plate shape and response times.

There has been little reported in the literature on the sandwich plate of the configuration analysed in this work, i.e. with an air gap core. Some preliminary experimental work has been carried out by Milburn-Pyle [1] on blast loaded sandwich plates with air gaps as a core.

The second part of the analysis is an attempt to model the interaction of the outer layers under impulsive loading. The numerical predictions of this investigation are compared with experimental results. The criteria for comparison are plate mid-point deflections and the diameter of the area of contact between the two plates. An attempt is made to

understand the behaviour of the plates with regard to the response time and absorption of strain energy.

In Chapter 2 , a review of the single plate experimental and analytical work is presented. The plate behaviour and experimental set-up is described. The experimental work conducted by Milburn-Pyle [1], including a description of the plate set-up and results, are also presented.

Chapter 3 describes the finite element models used in this analysis to model the physical experiments. The integration schemes and finite element formulation are described as well as the material model, the loading models, the imposed boundary conditions and the contact model.

Chapter 4 sets out the results of the analysis. As the analysis has been separated into two parts, the single plate results are described separately from the results of the sandwich plates.

A discussion with conclusions are presented in Chapter 5 and the dissertation is concluded in Chapter 6 with recommendations for further work.

CHAPTER 2. PREDICTIONS AND EXPERIMENTAL DETAILS

Results of experimental work on impulsively loaded circular and square plates have been widely reported (see for example Nurick and Martin [2], Teeling-Smith [3], Thomas [4], Jones [5]). Analytical methods have also been used extensively to predict the behaviour of these plates (for example Wierzbicki and Florence [6], Jones [5]). In addition, there have been predictions using special dedicated numerical analyses (for example Nurick, Pearce and Martin [7,8], Shen and Jones [9], Olson, Nurick and Fagnan [10,11]). A brief description of the behaviour of the single plate follows.

It has been shown that as the impulse on a clamped beam is increased, three distinctly different failure modes occur (Menkes et al [12]). Mode I failure is the occurrence of large inelastic deformations, in Mode II failure tensile tearing at the outer boundary occurs, and in Mode III failure transverse shear failure at the outer boundary occurs. These same failure modes have also been recognised in the deformation of circular plates [3]. During all these modes of failure, non-linear material and geometry effects are introduced. The high impulses transmitted result in the structure undergoing rapid dynamic deflections and the overall response time of the deformation is in the order of 100 to 150 μ seconds. The plate response is initially dominated by bending moments and transverse shear forces. As transverse displacement increases, membrane forces develop and bending moments and shear forces play a less important role [5].

Nurick and Teeling Smith [13] have observed from experimental work on clamped circular plates that draw-through of material from between the clamping rings occurs at higher impulses. It was found that this caused thinning at the clamped outer edge of the plate. The boundary condition effects have further been studied by Thomas [4] who conducted tests on plates that are integral, or built in, at the boundary as opposed to being clamped. A numerical investigation by Olson et al [11] on the deformation and tearing of blast loaded circular plates studied the tearing failure models associated with Mode II and III failure. Impulsive loading in the range that causes Mode I failure is modelled in the present work. The presented results for single plates are compared to results published in a review by Nurick and Martin [2].

A brief overview of the experimental details are given in the following: The technique employed for single plate analysis uses explosives to impart an impulse on the clamped plate and a ballistic pendulum test rig is used to measure the impulse applied to the specimen. The plates used were 1.6mm thick with a radius of 50mm. In order to approximate a uniform pressure pulse over the entire plate, the explosives are placed in a two ring configuration [3]. The outer ring, placed on the plate at a radius of 41mm, is joined to the inner ring, placed at a radius of 21mm, and to the detonator in the centre by a cross leader of explosive. The explosive is separated from the outer plate by a disk of polystyrene 15mm thick in order to prevent spalation of the plate and to ensure an approximately uniform impulse over the whole plate.

Previous work on sandwich plates has been restricted mainly to impulses that result in only elastic deformation. Experimental work has, however, been conducted by Milburn-Pyle [1] on the plastic deformation of sandwich plates with air gap cores. It is this experimental data that this thesis attempts to model. These plates consist of two outer layers of cold-rolled mild steel separated by an air gap. The thickness of the mild steel plates used in the sandwich plate experimental work is 1.6mm and tests were conducted with varying air gap thicknesses. The same experimental techniques used for the single plates were used for the sandwich plates. The explosive used in this experimental work was Metabel. The sandwich plates tested are circular with a radius of 50mm when clamped to the test rig. The plate closest to the explosives, and hence impulsively loaded, is defined as plate A while the plate furthermost away is defined as plate B (See Figure 2-1 for the experimental sandwich plate set-up). Tests were carried out on plates with the following five different air gap sizes: 0mm, 4mm, 8mm, 12mm and 16mm. Further experiments were completed with sandwich plates consisting of three steel layers and two air gaps but these are not modelled in this work. Mid-plate deflection for plates A and B were measured as well as the diameter of the contact between the two plates. These experimental results are tabulated in Appendix A.

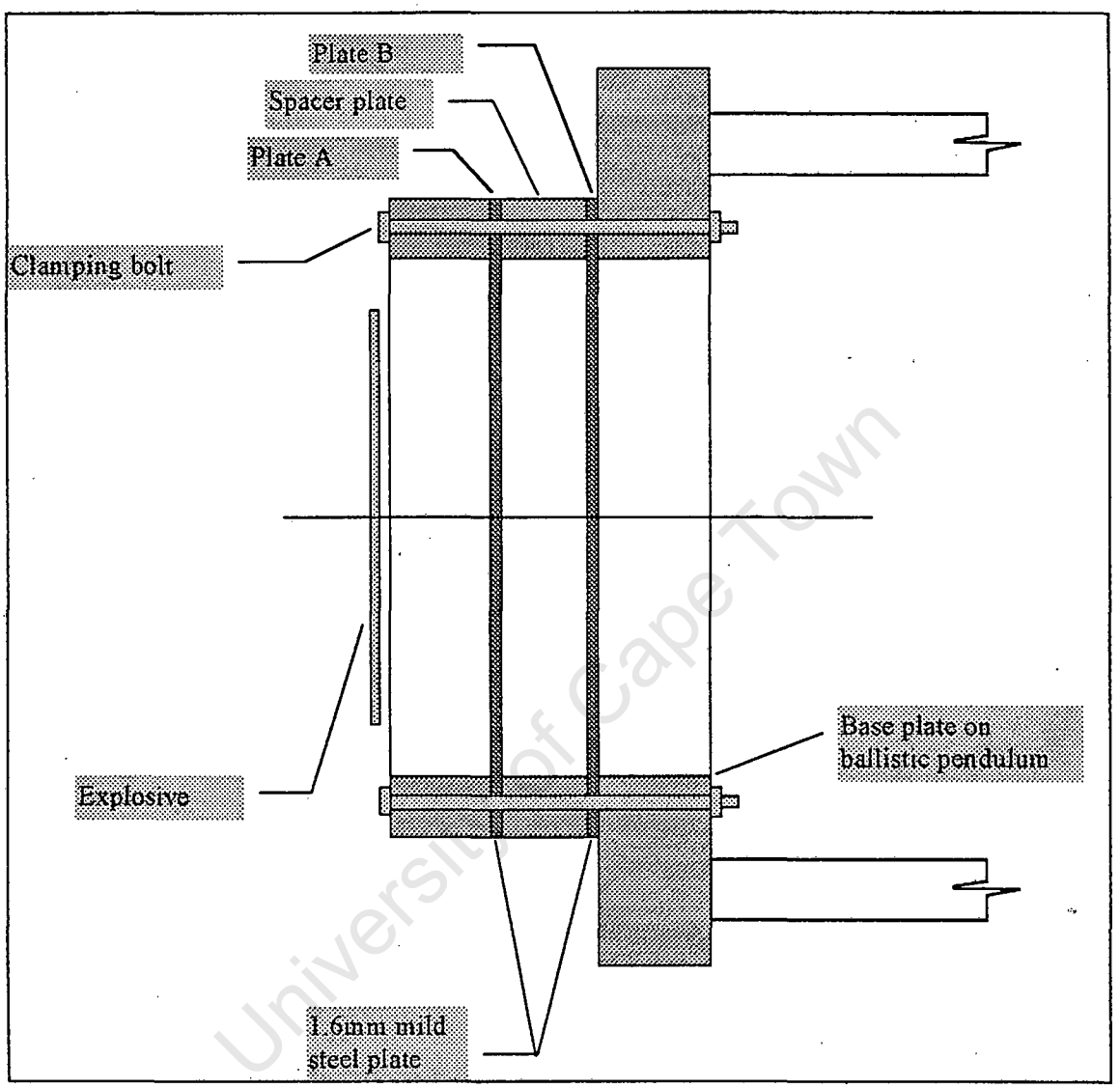

Figure 2-1 Schematic representation of the sandwich plate experimental set-up.

CHAPTER 3. ANALYSIS

3.1 Finite Element Solving Scheme

The finite element analysis was carried out with a general purpose program called ABAQUS developed by Hibbett, Karlsson & Sorenson Inc. The program is run on an IBM 560 computer. Versions 5.3 and 5.4 were used respectively for the implicit and explicit schemes.

ABAQUS offers solution techniques for both linear and non-linear problems. In the case of severely non-linear problems such as the plate deformations being modelled in this analysis, the dynamic response is obtained by direct time integration of all the degrees of freedom in the finite element model. There are two direct time integration schemes. The implicit scheme is designed to analyse the overall dynamic response of a structure while the explicit scheme is used for problems where wave propagation is dealt with on a local level.

Therefore, the explicit time integration scheme is ideally suited for the non-linear dynamic response of explosively loaded plates. In the blast loaded plates, high frequency waves are propagated through the specimen. To resolve these high frequency components, the time step in the solution scheme must be smaller than the time it takes for a dilation wave to cover the length of an element. This critical time to ensure numerical stability is estimated by $\Delta t = \frac{L_{\min}}{c_d}$ where $c_d = \sqrt{\frac{\lambda + 2\mu}{\rho}}$

is the dilation wave speed, μ and λ are Lames constants, ρ is the material density and L_{min} is the smallest characteristic length of the elements in the model. It is thus evident that no single element should have a characteristic length much smaller than any other element and therefore mesh design is critical. ABAQUS provides an automatic time step for explicit solution schemes, around $1/\sqrt{2}$ times smaller than the critical time step of the most critical element. The restriction on time increment size due to numerical stability considerations is, however, compensated for by the low cost of solving the equations due to the lumped mass matrix formulation.

The implicit scheme does not require this upper bound on a time step but solves for dynamic quantities at time $t + \Delta t$ based on these same values at times t and $t + \Delta t$. Due to this implicit technique, non-linear equations must be solved. The scheme can, however, also give acceptable solutions with the advantage of increment time steps of order 1 or 2 times the magnitude of the stability limit of the explicit scheme but the predicted response will deteriorate as the time step size increases relative to the period of the response modes. Therefore, the relative economy of the two integration techniques depends on the stability limit of the explicit scheme and the size of the time increment that can provide acceptable accuracy with the implicit scheme as well as the relative ease of solving the respective equations.

Due to errors regarding the strain rate dependence capability in the explicit scheme [14], the single plate analysis was first conducted using the implicit integration scheme. The error was subsequently corrected and the single plate analysis was recalculated using the explicit scheme. The sandwich (double plate) analysis was conducted with the explicit scheme only.

3.2 Finite Element Formulation

Two types of shell elements were used in the analysis. The SAX1 [15] axisymmetric element was used for the single plate analysis in both the implicit and explicit schemes while the S4R [15] general element was used for both single and sandwich plate analyses using the explicit solving scheme (See Appendix C for element details).

Both of these shell elements are termed 'shear flexible', i.e. they can be used to model both 'thick' and 'thin' shells. When these elements are used to model 'thick' plates, transverse shear deformation is allowed and the transverse shear stiffness is taken into account but when these elements model 'thin' plates, the transverse shear stiffness acts as a penalty function to approximately impose Kirchoff constraints. The Kirchoff constraint, which is fundamental to the classic 'thin' shell theory, is the requirement that a material line that is originally normal to the shell's reference surface will remain normal to that surface throughout deformation. The membrane and bending strain measures that are used are based on the Korte-Sanders strain theory (Budianski and Sanders [16]). The membrane, bending and transverse shear strains are calculated at one gauss point per element but at five places through the thickness at that point. Both the SAX1 and the S4R use a finite membrane strain measure and take into account shell thickness changes as a result of membrane strain (stretching).

The two element types require different mesh designs. The axisymmetric geometry of the plate makes for efficient use of the axisymmetric version of the shell elements. The cost of analysis is reduced due to fewer elements being needed to model the plate, and mesh design is simplified. Axisymmetric meshes with the number of elements ranging from 2 to 5 and 10, 20, 30 and 40 element meshes are used. A typical mesh used for the axisymmetric shell elements is shown in Figure 3-1.

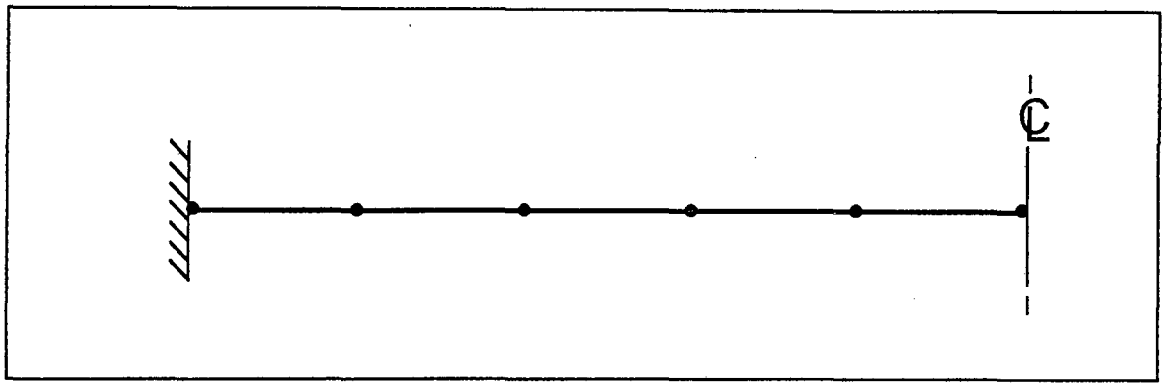

Figure 3-1 Typical axisymmetric mesh.

In contrast to the axisymmetric mesh, the mesh required for the general shell element is more complicated. It was thus necessary to code mesh generating programs in FORTRAN to simplify the task and reduce mesh errors to a minimum (See Appendices D and E). The number of elements used is reduced by using ¼ circle symmetry as shown in Figure 3-2. Four different meshes are used, the 75 element mesh having 10 unbiased elements along the radius, the 300 element mesh having 20 unbiased elements along the radius, the 507 element mesh having 26 unbiased elements along the radius and the 867 element mesh having 34 unbiased elements along the radius. A typical mesh used for the general shell elements is shown in Figure 3-2.

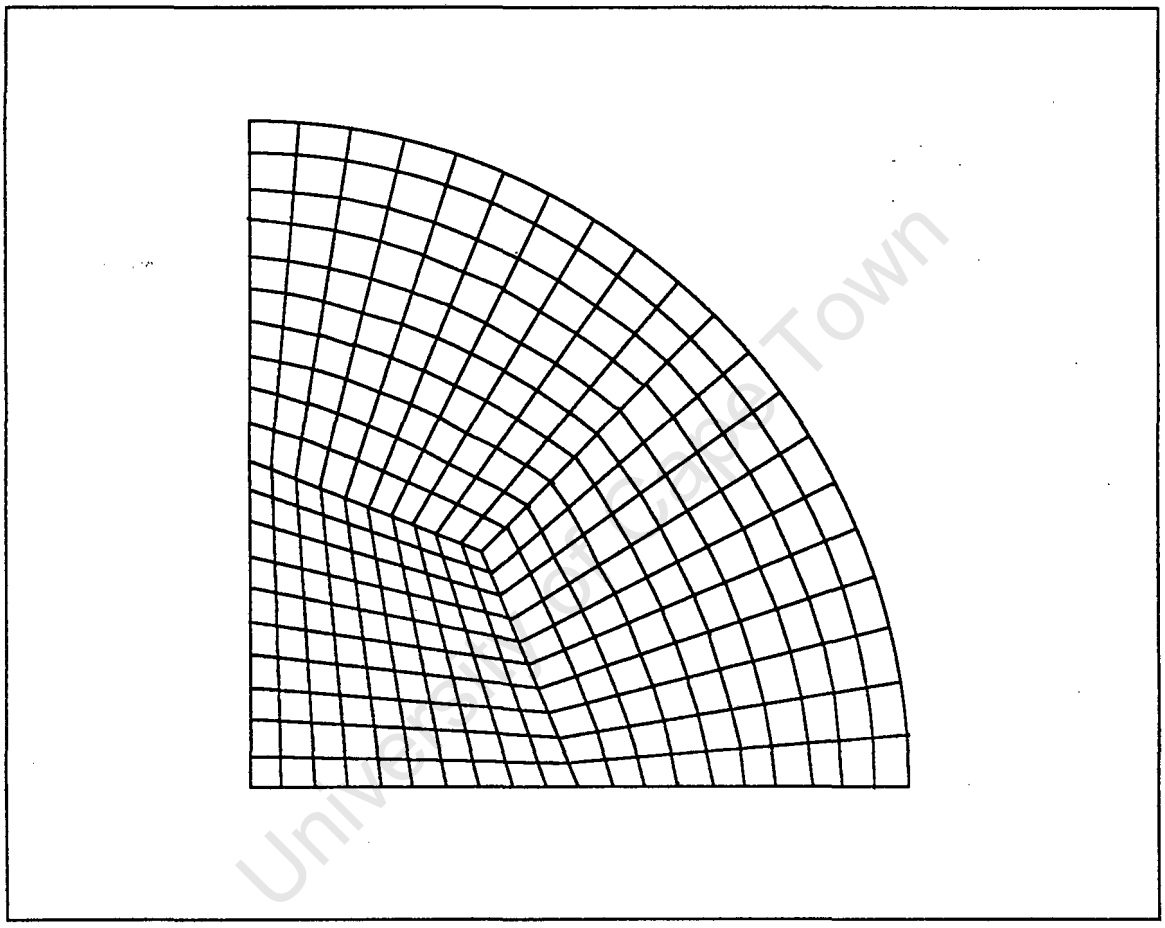

Figure 3-2 General shell element mesh (300 elements).

3.3 Material Modelling

The plates used in the experimental work are of mild steel. Typically, mild steel exhibits linear elastic and isotropic strain hardening plastic characteristics with a marked strain rate dependence in its behaviour. The Mises yield criteria with isotropic hardening and associated flow is a well suited constitutive model to describe the elasto/plastic properties of mild steel. The input requirements for ABAQUS is the stress versus plastic strain relation and a yield stress for a zero strain rate, elastic modulus and a Poisson's ratio. An assumption is made that the hardening curves are identical at different strain rates although this could be changed to include different hardening curves for specific strain rates. Temperature dependence is excluded from this analysis as the temperature changes associated with the plates have not been quantified in experimental work.

Mild steel shows a significant difference in behaviour even at relatively low strain rates of the order 10^{-2}. As strain rates sometimes exceed 10^{2} in this analysis, it is clear that strain rate dependence is of great importance. The model used to compensate for strain rate dependence of mild steel is the Cowper-Symonds relation [5]. The flow stress, σ_f, is calculated from

$$\frac{\sigma_f}{\sigma_o} = 1 + \left(\frac{\dot{\varepsilon}}{D} \right)^{\frac{1}{q}} \qquad \text{Equation (3-1)}$$

where D=40.4 s^{-1} and q=5 are strain rate material properties (as quoted in Reference [5]), σ_0 is the static yield stress and $\dot{\varepsilon}$ is the strain rate.

The physical material properties used in the analysis are as follows: elastic modulus, E=210 GPa; density, ρ=7850 kg m^{-3}; Poisson's ratio, ν=0.3; static yield stress, σ_o=290 MPa. A typical stress versus plastic strain curve for mild steel as shown in Figure 3-3 is used.

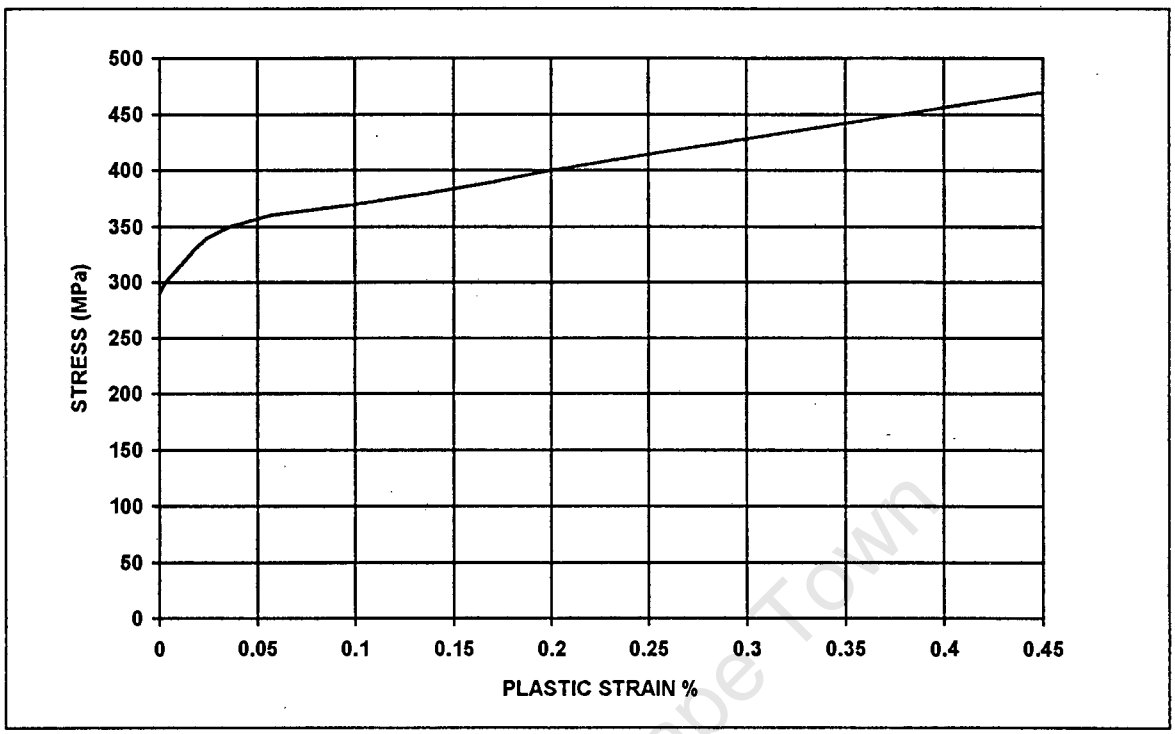

Figure 3-3 Stress versus plastic strain curve for zero strain rate.

3.4. Load Modelling

This is one of the key factors determining the overall accuracy of the finite element model. Initial velocity profiles and pressure loading are the two types of load models used in the analysis. In the past, for analytical modelling, applied initial velocity profiles were mostly used. However, in the finite element model, it is possible to use pressure loading directly to model the explosive blast. Various initial velocity profiles and pressure loading models were tested to determine which produced the most accurate model of the explosive loading conditions. The development of the loading models used are discussed below.

3.4.1 Initial velocity profiles

The general form of equation to find the velocity profile is

$$I = \int_0^R m \cdot V(r) \cdot dr \qquad \text{Equation (3-2)}$$

where V(r) is the velocity shape function, m is the radial mass of the plate and I is the total applied impulse. The velocity shape function V(r) can take numerous forms from a constant through polynomials to cosine functions.

The most simple form used is that of a constant V_0 which gives, after integration of the radial mass across the plate,

$$V_0 = \frac{I}{M}, \qquad \text{Equation (3-3)}$$

where M is the total mass of the plate. For this shape function, V_0 is applied to every node in the model at the start of the analysis. (See Figure 3-4 (a).)

The second velocity shape function used in the analysis is the linear function. The triangular initial velocity profile has a zero velocity at the circumferential nodes, velocity V_{amp} at the plate centre node and linearly interpolated velocities at all other nodes. (See

Figure 3-4 (b).) V_{amp} is calculated from equating Equation (3-2) and the shape function

$$V(r) = V_{amp} \cdot \left(1 - \frac{r}{R}\right), \qquad \text{Equation (3-4)}$$

where R is the plate radius.

The third velocity profile uses the mode approximation technique developed by Martin and Lee [17] for thin elastic-plastic plate problems. Different velocity shape functions can be used with this technique. A linearly interpolated velocity shape function was chosen. (See Figure 3-4 (b)). This shape function gives a value for V_{amp} equal to $^2/_3$ of the V_{amp} calculated for the triangular transverse profile by Equation (3-4).

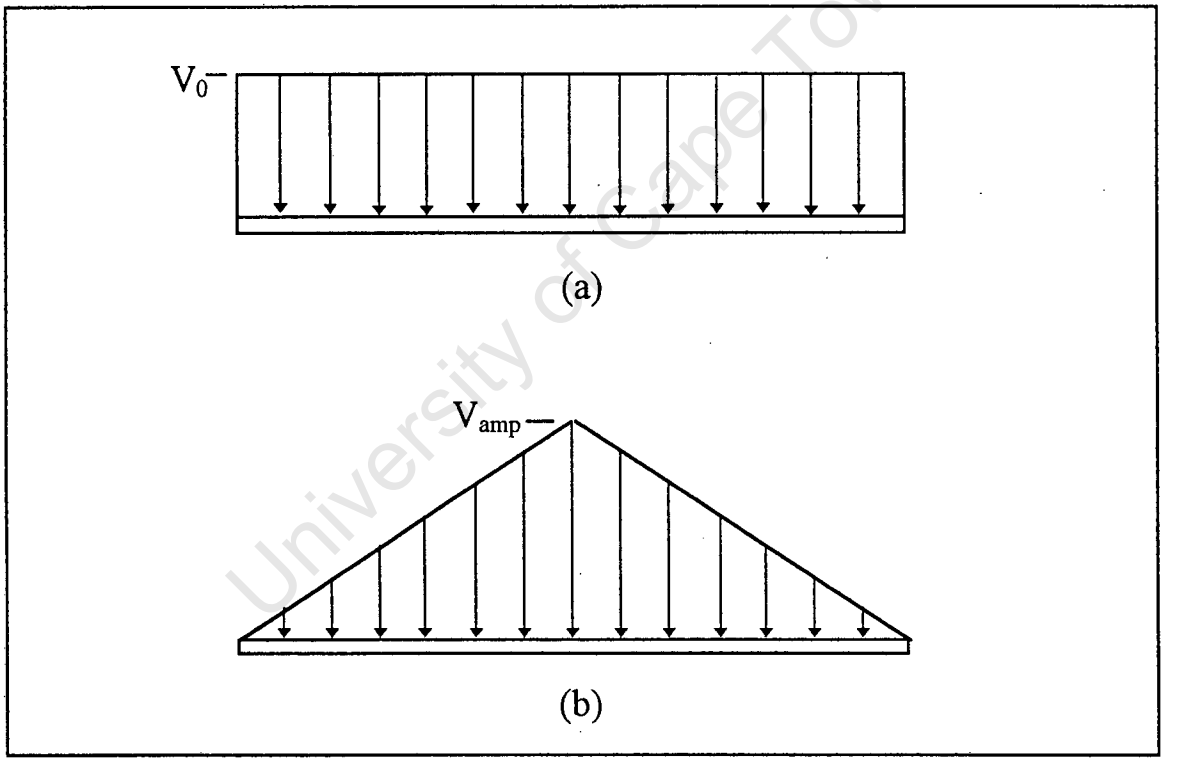

Figure 3-4 Initial velocity profiles:
(a) Uniform.
(b) Triangular and Mode approximation.

3.4.2 Pressure loading

For pressure loading, the duration of the pressure load is assumed to be that of the actual burn time t_b of the explosive and the magnitude of the pressure load is calculated by

$$P_a = \frac{I}{(t_b \cdot A)} \qquad \text{Equation (3-5)}$$

where the pressure pulse is rectangular as shown in Figure 3-5 (a); and

$$P_b = \frac{2 \cdot I}{(t_b \cdot A)} \qquad \text{Equation (3-6)}$$

where the pressure pulse is triangular as shown in Figure 3-5 (b) and A is the area of the plate.

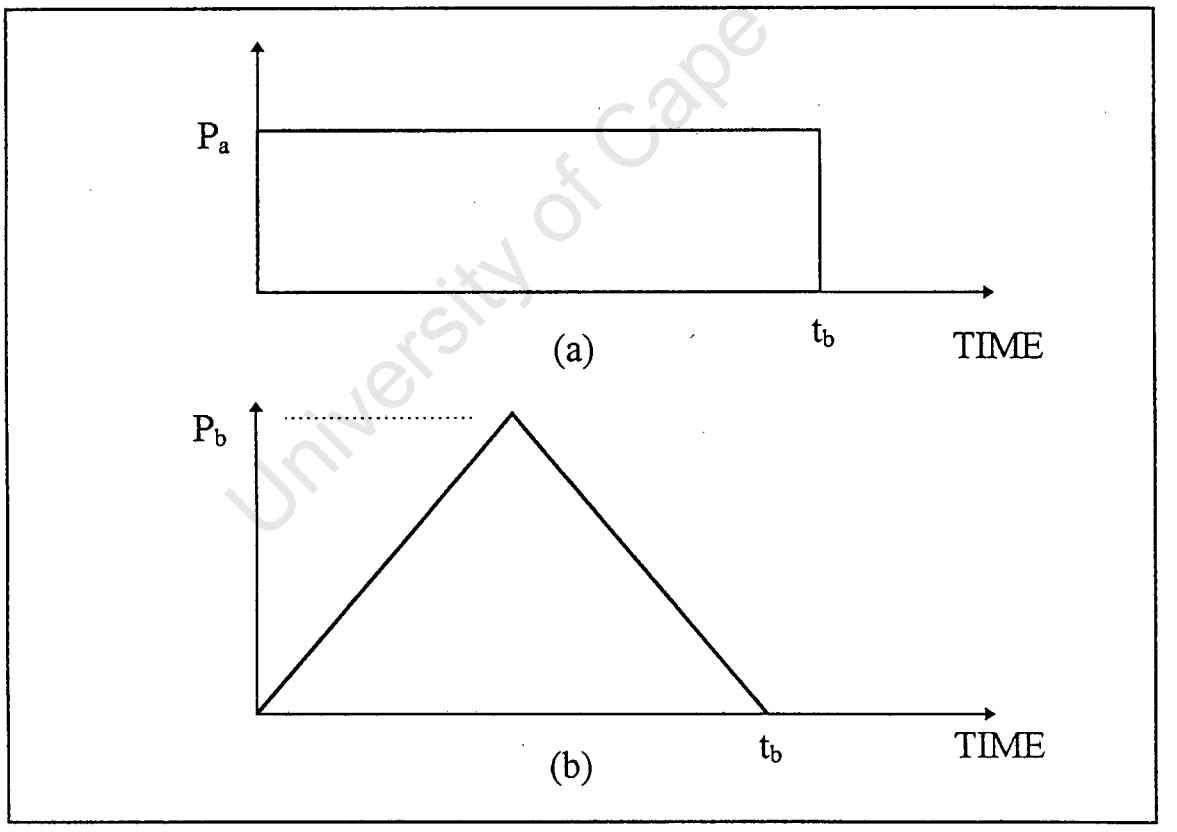

Figure 3-5 Pressure pulse profiles:
(a) Rectangular.
(b) Triangular.

The approximate burn time of the explosive is calculated to be 15μs and thus for P_a and P_b, burn time, t_b, was set at 15μs. Due to the possibility that the effect of the polystyrene buffer between the explosive and the plate is to lengthen the pressure pulse, a burn time of 30μs was also used for calculating P_a. In an attempt to establish the dependence of the results on the pulse length and shape, another burn time of 5μs was used for calculating P_b as well.

3.5 Boundary Conditions

The plate edges are modelled as integral to the plate supports. The boundary conditions needed to impose these conditions are as follows: The outer circumference of the plates are constricted in all translational and rotational degrees of freedom in the case of the quarter plate model. In the case of the axisymmetric element model, the R and Z translational and R-Z_{plane} rotational degrees of freedom of the outer boundary node are constrained. These constraints are termed natural boundary conditions. Figure 3-6 and Figure 3-7 shows the associated degrees of freedom of the two models.

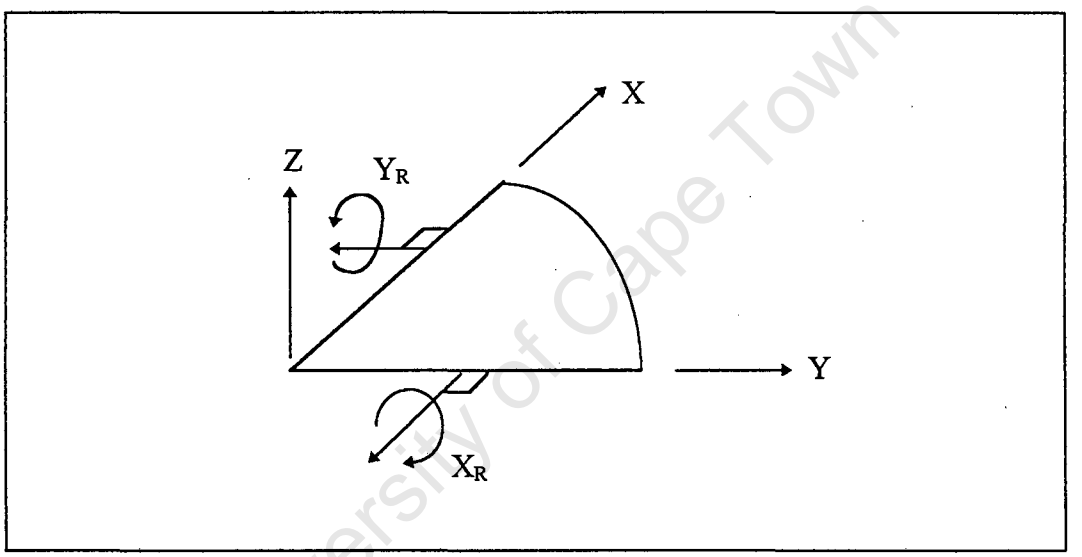

Figure 3-6 Degrees of freedom for quarter plate model.

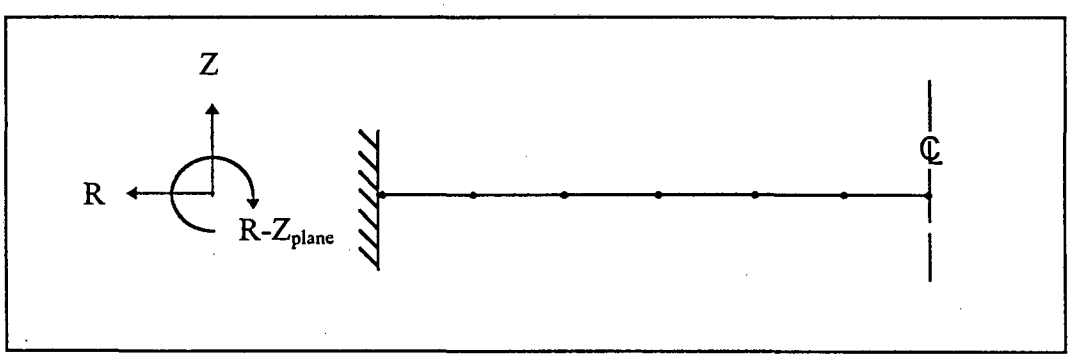

Figure 3-7 Degrees of freedom for axisymmetric model.

In both models, the plate is not modelled as a whole but symmetry is used to simplify them and for this reason artificial boundary conditions are needed to force the model to behave as if part of a full plate. The artificial boundary conditions imposed for this purpose are as follows:

The nodes on the radial edges of the quarter plate are constrained to translate only in the Z direction and rotate only about their respective perpendicular axes. That is, the nodes on the plate edge parallel to the Y axis can only rotate about the X axis and the nodes on the plate edge parallel to the X axis can only rotate about the Y axis. The numerical formulation of the nodes in the axisymmetric mesh effectively constrain them to only translate in the R and Z-direction and to rotate in the R-Z plane. (The model is two-dimensional). Therefore, only the centre plate node requires further constraining. These constraints are such that rotation in the R-Z plane and translation in the R-direction is zero.

3.6 Plate Contact

ABAQUS models contact by enforcing kinematic constraints such that the two contacting surfaces do not penetrate each other. The two type of contact models available are softened contact and hard contact.

In softened contact, the pressure between the contacting surface is dependant on the amount of overclosure, 'h', or interpenetration of the surfaces, and the amount of interpenetration can be set according to the roughness of the two surfaces.

'Hard' contact treats the interaction between the plates as being fully plastic. Pressure between the plates is independent of overclosure and is only present when contact is deemed to have occurred. Contacting points in the model instantaneously acquire the same velocity and acceleration in the direction of the impact. This plastic impact assumption is local and thus energy is absorbed by local plastic deformation. This method differs from assuming a coefficient of restitution for the impact. The contact occurring in the sandwich plate is considered as 'hard'.

On a more local level, contact between the plates is modelled, as stated above, with kinematic constraints. The overclosure, 'h', is calculated for corresponding points on the two contact surfaces. If, at a given node, $h < 0$, there is no contact and no further surface interaction calculations are needed. If $h \geq 0$, the surfaces are in contact. The constraint, $h = 0$, is enforced and contact pressure is calculated. The friction forces between the surface at that point can then be calculated.

The friction between the plates is calculated using the Coulomb friction model [15]. This model assumes that no relative motion occurs between the contacting areas if the equivalent frictional stress

$$\tau_{eq} = \sqrt{\tau_1^2 + \tau_2^2}\ , \qquad \text{Equation (3-7)}$$

is less than the critical stress, τ_{crit} where τ_1 and τ_2 are the radial and circumferential shear stresses. τ_{crit} is proportional to the contact pressure, P, and the friction coefficient, μ in the form $\tau_{crit} = \mu \times P$. Equation (3-8)

CHAPTER 4. RESULTS

4.1. Single Plate

4.1.1 Introduction

An accurate model of a single circular plate is vital in the further modelling of a sandwich plate. Thus, the plate model was tested thoroughly before proceeding to the second part of the analysis. The best loading model was chosen from the single plate analysis to be used in the sandwich plate analysis. As the single plate model was solved using both the implicit and explicit integration schemes, the advantages and disadvantages of the two schemes became evident.

Analysis is conducted over an impulse range of 4 to 24 N.s. Impulses greater than 24 N.s. have been observed to cause mode II failure [3], and as tearing of the sandwich plate was not considered for analysis, higher impulses were considered irrelevant to this work.

4.1.2 Convergence

With respect to the axisymmetric mesh, as seen in Figure 3-1, convergence of the solution for a uniform mesh takes place for small numbers of elements for both the implicit and explicit integration schemes. By nature of the required mesh, the general shell element mesh requires more elements for convergence.

Using the implicit scheme, mid-plate deflection values are converged in a four element mesh while for accurate stress and strain predictions, a finer mesh with about ten to twenty elements along the radius is needed. Mid-plate deflection results are reported for the twenty element model while stress and plastic strain results are reported for 40 element meshes.

Using the explicit scheme, it can be seen from Figure 4-1 which shows the mid-plate response for meshes with different number of elements, that convergence is adequate for a mesh with twenty elements along the radius.

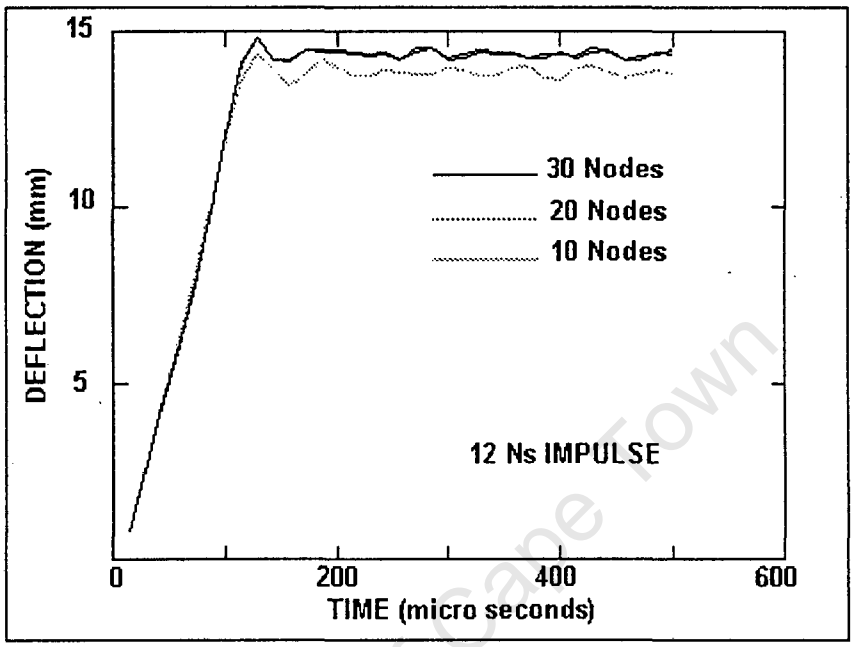

Figure 4-1 Convergence of mid-plate deflection for an axisymmetric mesh.

From analyses using the general shell element and its corresponding mesh, it was found that the 300 element mesh, as shown in Figure 3-2, is sufficient for a converged solution as far as mid-plate deflections and system energy is concerned.

4.1.3. Mid-plate Deflection

The mid-plate deflection of the plate is the most commonly used parameter for comparison of results.

4.1.3.1 Implicit scheme results

Results from the Uniform, Triangular and Mode Approximation initial velocity loading and Pressure loading models using the implicit integration scheme and the axisymmetric model are shown in Figure 4-2. Results for mid-plate deflection have been plotted as deflection-thickness ratio versus ϕ_c as proposed by Nurick and Martin [2] where

$$\phi_c = \frac{I}{\pi R H^2 \sqrt{\rho \sigma_o}}. \qquad \text{Equation (4-1)}$$

This facilitates comparison of results for plates with different geometry and material properties. The experimental results from Nurick and Martin [2] are plotted in this figure as well. The solid line is the best fit line to this experimental data and the two outer dotted lines are the associated 90% experimental confidence limits [18]. It is shown that the pressure load and uniform velocity profile models give results with the best correlation when compared with the results from Nurick and Martin [2]. The results for the triangular velocity profile although slightly overestimating the centre plate deflection are also acceptable. Deflections using the mode approximation velocity profile compare well for the lower impulse range but show significant underestimation for higher impulses.

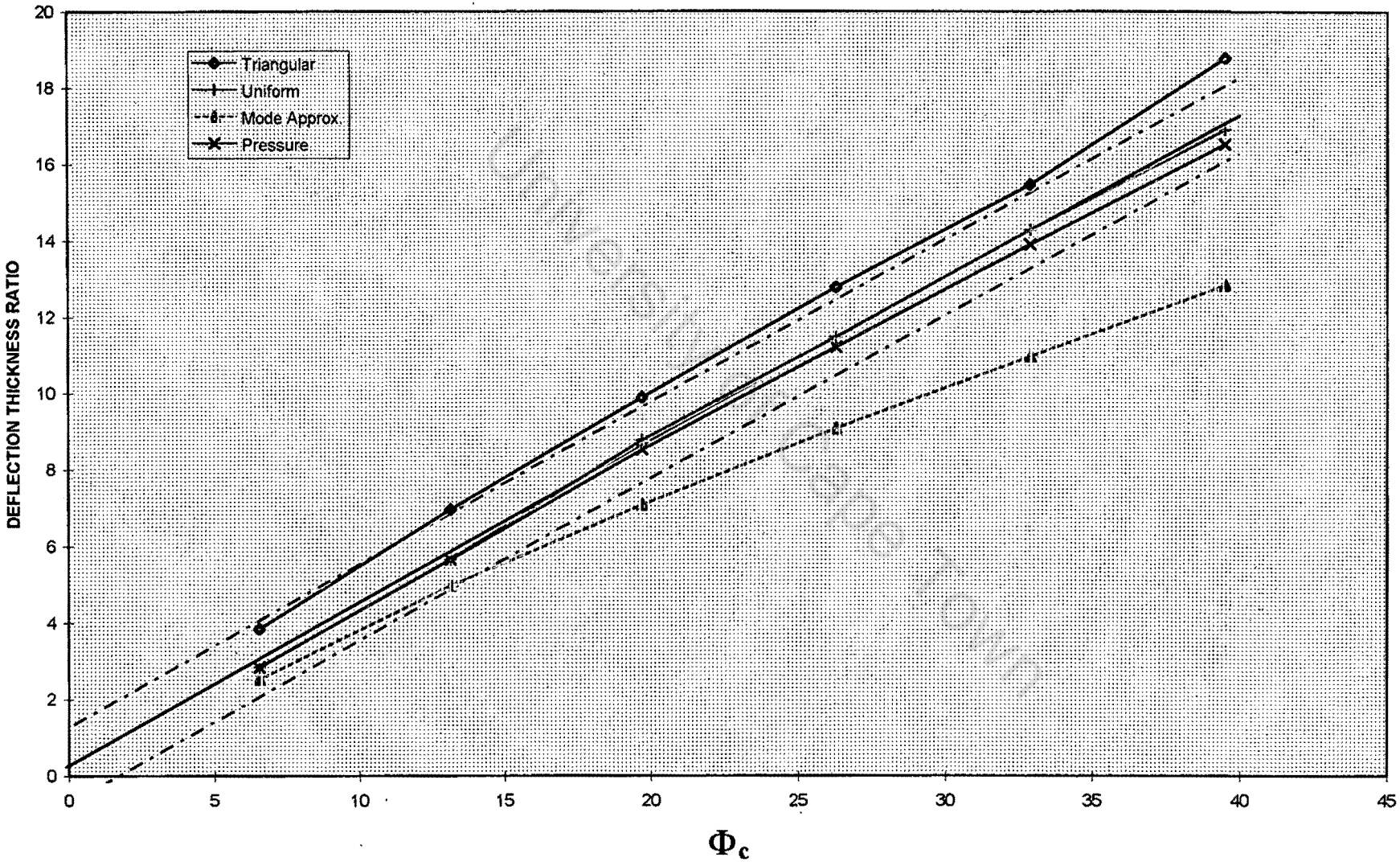

FIGURE 4-2 Deflection thickness ratio versus Phi for various loading models (Implicit scheme).

4.1.3.2 Explicit scheme results

In Figure 4-3, the explicit scheme solutions for both the axisymmetric and general shell models are plotted alongside Nurick and Martins results [2]. It is evident that both models show good correlation with the experimental data. Only the pressure loading model results are shown as the initial velocity loading models proved to be numerically unstable in the explicit scheme. The numerical stability of the solution for these models could not be guaranteed and large numerical errors often occurred.

Results for the pressure loading models using a rectangular pulse with a burn time of 15 μs and 30 μs were insignificantly different. Results of the triangular pulse with a 5 μs burn time tend to be numerically unstable unless a much finer mesh is used. From these results, it was decided to proceed with further analysis using only the Pressure loading model with a burn time of 15 μs.

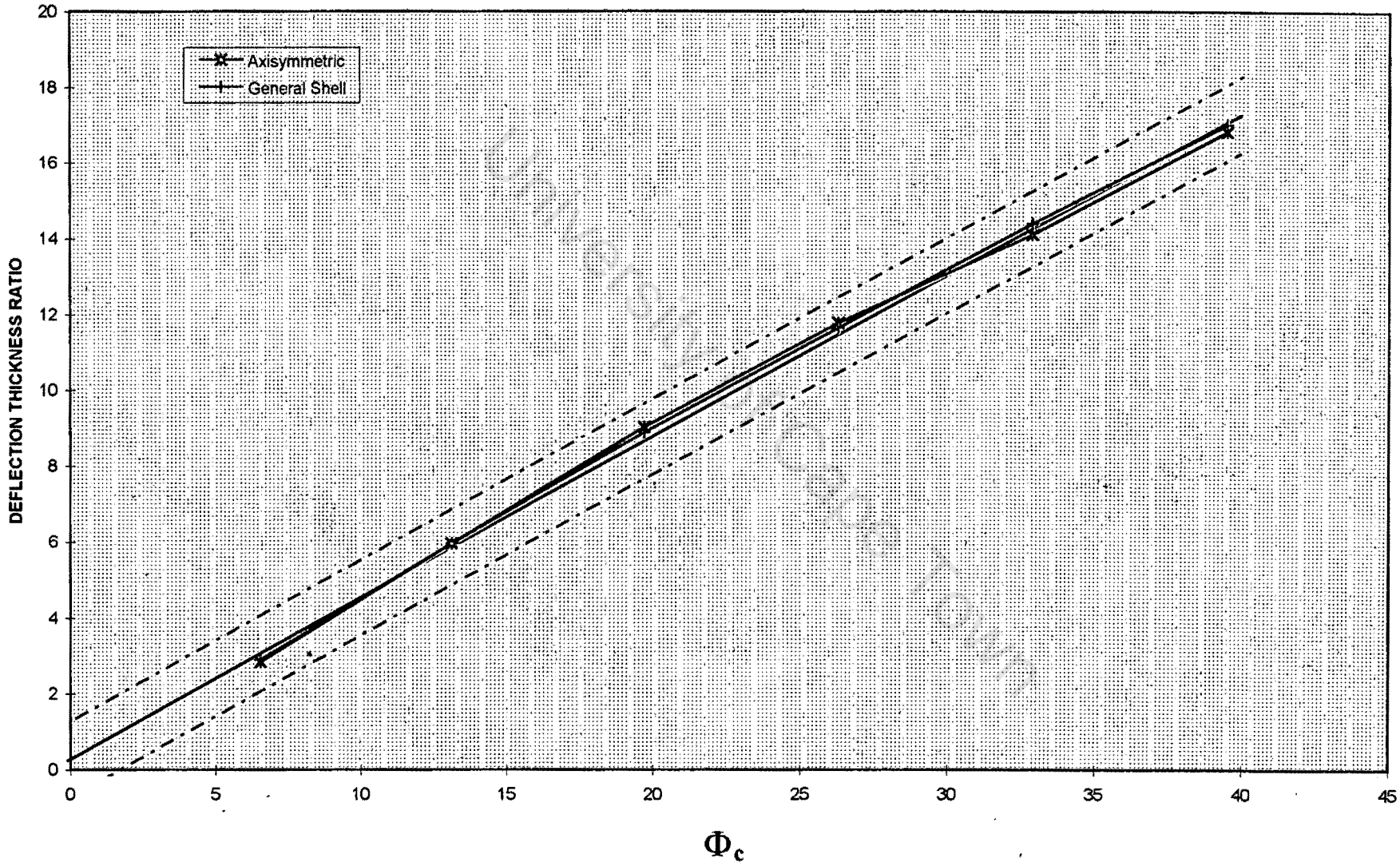

FIGURE 4-3 Deflection thickness ratio versus Phi for the axisymmetric and general shell meshes (Explicit scheme).

4.1.3.3 Comparison with previous analysis

Jones [5] predicted that the permanent mid-plate deflection for impulsively loaded clamped circular plates is

$$\frac{W_f}{H} = \left(\frac{2 \cdot \rho \cdot V_0^2 \cdot R^2}{3 \cdot n \cdot \sigma_0 \cdot H^2} \right)^{1/2} \qquad \text{Equation (4-2)}$$

where $n = 1 + \left(\frac{V_0 \cdot W_f}{3 \cdot \sqrt{2} \cdot D \cdot R^2} \right)^{1/q}$ Equation (4-3)

is the factor based on strain rate predictions of Perrone and Bhadra [19] that accounts for the strain rate dependence effects of the plate.

Symonds and Wierzbicki [20] have predicted a membrane mode solution which is written as

$$\frac{W_f}{H} = 1.0186 \times \left(\frac{2 \cdot \rho \cdot V_0^2 \cdot R^2}{3 \cdot \sigma_f \cdot H^2} \right)^{1/2} \qquad \text{Equation (4-4)}$$

where the rate dependence effect is calculated by combining the predicted average strain rate

$$\dot{\varepsilon} = \frac{I^2}{R^5 \cdot H^2 \sqrt{\sigma_f \cdot \rho^3}}, \qquad \text{Equation (4-5)}$$

and the Cowper-Symonds Equation (3-1) to get

$$\frac{I^2}{R^5 \cdot H^2 \sqrt{\sigma_f \cdot \rho^3}} = 40 \cdot \left(\frac{\sigma_f}{\sigma_0} - 1 \right)^5 \qquad \text{Equation (4-6)}$$

from which the flow stress, σ_f can be calculated using an iterative procedure. These mid-plate deflection predictions are compared with the current results in Figure 4-4 where the deflection-thickness ratio is plotted against applied impulse. Good correlation exists for the lower impulse range while for higher impulses, although the difference in the results approaches two plate thicknesses, the percentage error actually decreases.

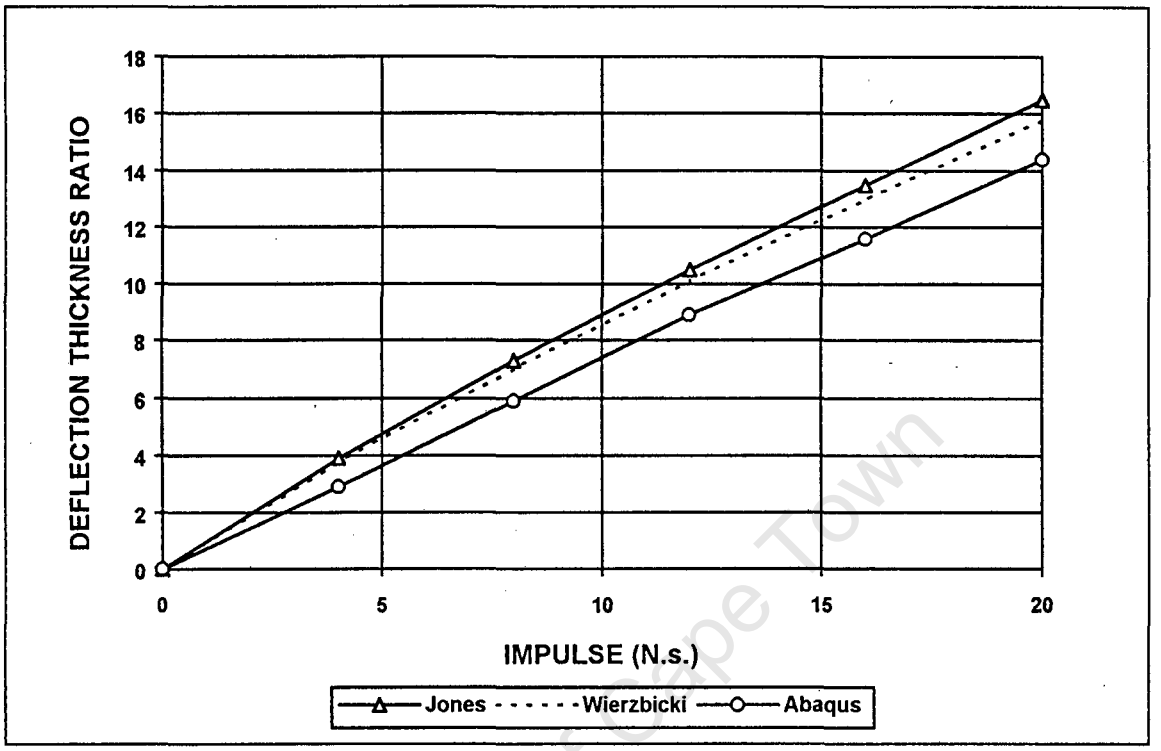

Figure 4-4 Comparison of maximum permanent displacement.

Figure 4-5 shows the transient response of the plate for times at increments of 14 microseconds. This plot is similar to plots from a finite element analysis on circular plates by Olson, Fagnan and Nurick [11]. It is seen that early in the analysis, the central region of the plate remains relatively flat while the outer regions are subjected to bending deformation. The bending region moves, with time, towards the centre until the permanent deflection is reached.

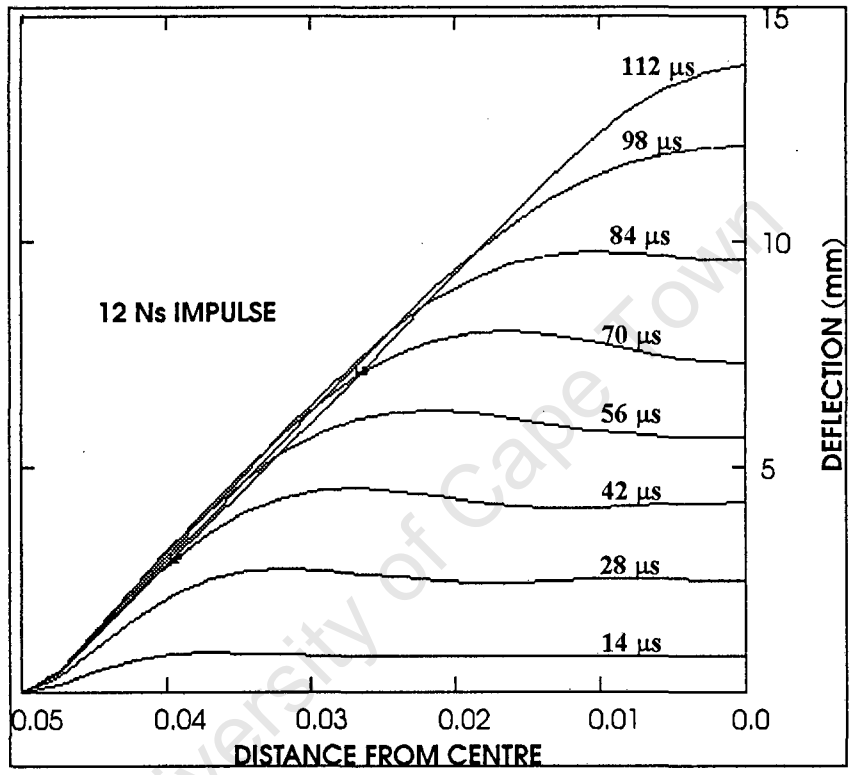

Figure 4-5 Transient plate response.

4.1.4 Strain Rate Dependence

The material strain rate sensitivity effects in a dynamic plastic response is characterised by either the mean strain rate that occurs during a response, or the average dynamic flow stress associated with the mean strain rate.

Perrone and Bhadra [19] and Symonds and Wierzbicki [20] have both predicted mean strain rates for the response of structures undergoing membrane strain in order to estimate the strain rate sensitivity influence. The mean dynamic flow stress associated with the mean strain rate is calculated by substitution of the mean strain rate into the Cowper Symonds Equation (3-1). This value is normalised with respect to the flow stress at zero strain rate by dividing by the static yield stress to give a strain rate sensitivity influence factor 'n' as used by Jones [5] and defined as

$$n = \sigma_f / \sigma_0 \quad . \qquad \text{Equation (4-7)}$$

In the current analysis, the strain rate, $\dot{\varepsilon}$, varies from point to point across the plate and with time. Thus a measure of strain rate is needed to characterise the response of the plate as modelled in the presented analysis. This is done as follows:
The maximum flow stress occurring during the response is calculated at regularly spaced points along the radius of the plate. These maximum flow stress values are weighted according to the circumference of their radial co-ordinate and are averaged to give the averaged maximum flow stress of the plate. This value is substituted into the Cowper Symonds Equation (3-1) to give the maximum strain rate, $\dot{\varepsilon}$, of the response. This is halved (as done by Perrone and Bhadra [19]) to give a characteristic mean strain rate of the response that corresponds to the mean strain rate predictions of Symonds and Wierzbiki, and Perrone and Bhadra.

The average flow stress and 'n' are calculated, as described above, by substitution of the average strain rate into the Cowper Symonds Equation (3-1) and normalising.

In Table 4-1 the current predicted ABAQUS values of 'n' are compared with the values of 'n' calculated from the analytically predicted strain rates of Perrone and Bhadra [19] and

Symonds and Wierzbicki [20]. The analytically predicted 'n' values are also tabulated as a percentage of the corresponding ABAQUS values.

IMPULSE	PERRONE and BHADRA		SYMONDS and WIERZBICKI		ABAQUS
(N.s.)	n	%	n	%	n
0	1	100	1	100	1
2	1.69	106	1.84	115	1.6
4	1.9	90	2.09	99	2.11
8	2.17	83	2.43	92	2.63
12	2.37	77	2.66	87	3.06
16	2.53	75	2.85	85	3.37
20	2.66	74	3.02	84	3.58

Table 4-1 Comparison of 'n' values showing rate dependence influences.

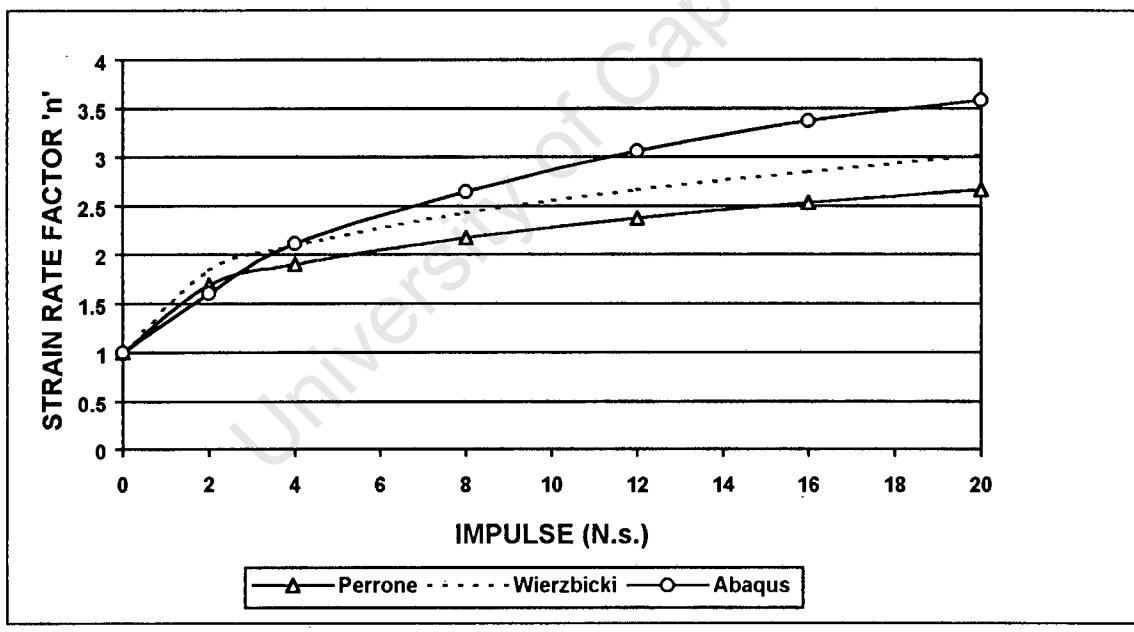

Figure 4-6 Plot of 'n' values derived from Table 4.1.

From Figure 4-6, it is evident that in the lower impulse range of 0-6 N.s, there is little difference in the predicted strain rate sensitivity influence compared to Perrone and Bhadra's and Symonds and Wierzbicki's predictions. For impulses higher than 6 N.s., however, the current 'n' values indicate a larger strain rate sensitivity influence.

While Symonds and Wierzbicki's analytical predictions of mid-plate deflections incorporating their strain rate dependence factor, and Jones' mid-plate predictions incorporating Perrone and Bhadra's strain rate dependence factor correlated well with the experimental data when published [5], the impulse range for which the experimental data was collected is from 3 to 7 N.s. It appears that Symonds and Wierzbicki's and Perrone and Bhadra's mean strain rate estimates are valid for this impulse range but do not account for the strain rates at higher impulses. In the impulse range of 10 to 20 N.s., Jones' deflection Equation (4-2) and Symonds and Wierzbicki's deflection Equation (4-4) give results that correlate favourably to deflection results of Nurick and Martin [2] when the strain rate influence factor calculated in the present work is incorporated.

It is evident from these strain rate factors that the strain rate dependence of mild steel has a large effect on the yield stress. A comparison of the deflection-time history of a model with the strain rate effects included and excluded is shown in Figure 4-7. The permanent deflection reduction in the case of a 12 N.s. impulse is in the order of 45%. This deflection reduction has also been shown by Olson et al [10,11].

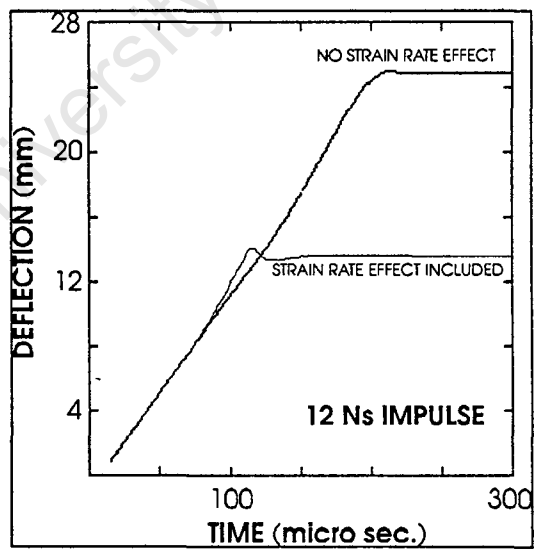

Figure 4-7 Mid-plate displacement response.

4.1.5 Strain Predictions

The radial and hoop strains are calculated for each of five points through the plate thickness at each element (gauss point). These strains are shown in Figure 4-8 and Figure 4-9 respectively where the bottom of the plate is the side of the plate exposed to the applied impulse. It is evident from these plots that the maximum strain is present at the top surface of the plate centre. The plot of the equivalent plastic strain [15] in Figure 4-10 confirms this trend.

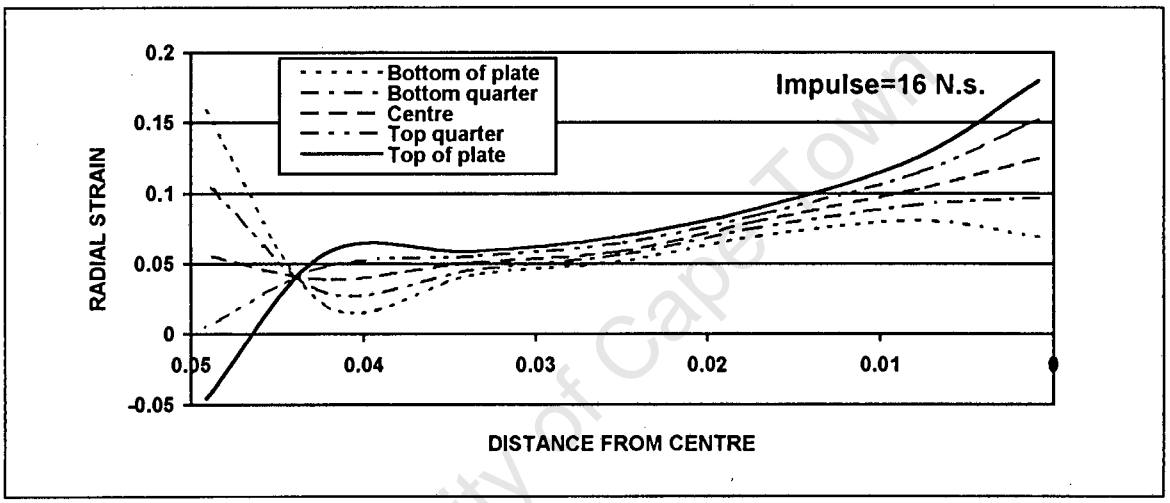

Figure 4-8 Radial strain distribution.

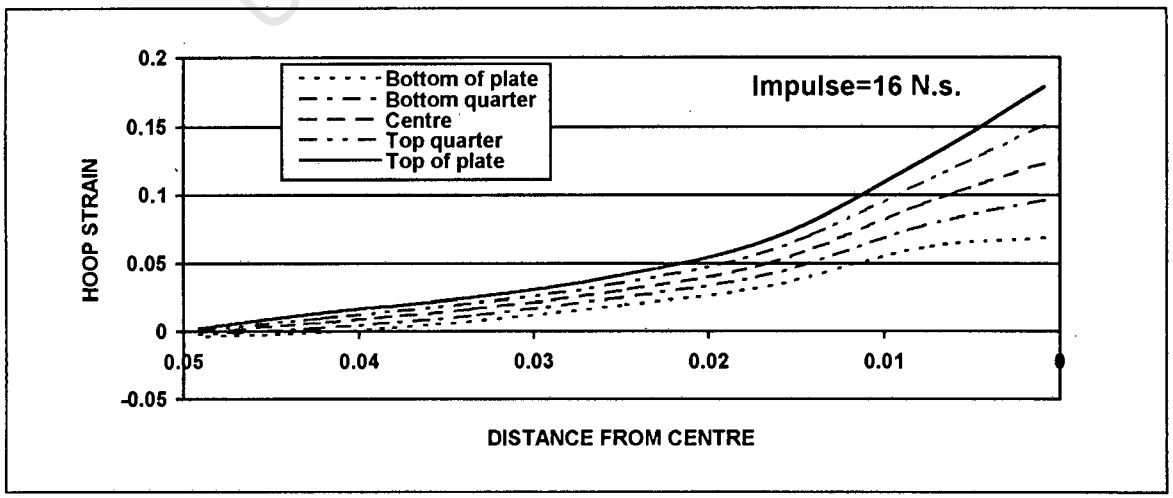

Figure 4-9 Hoop strain distribution.

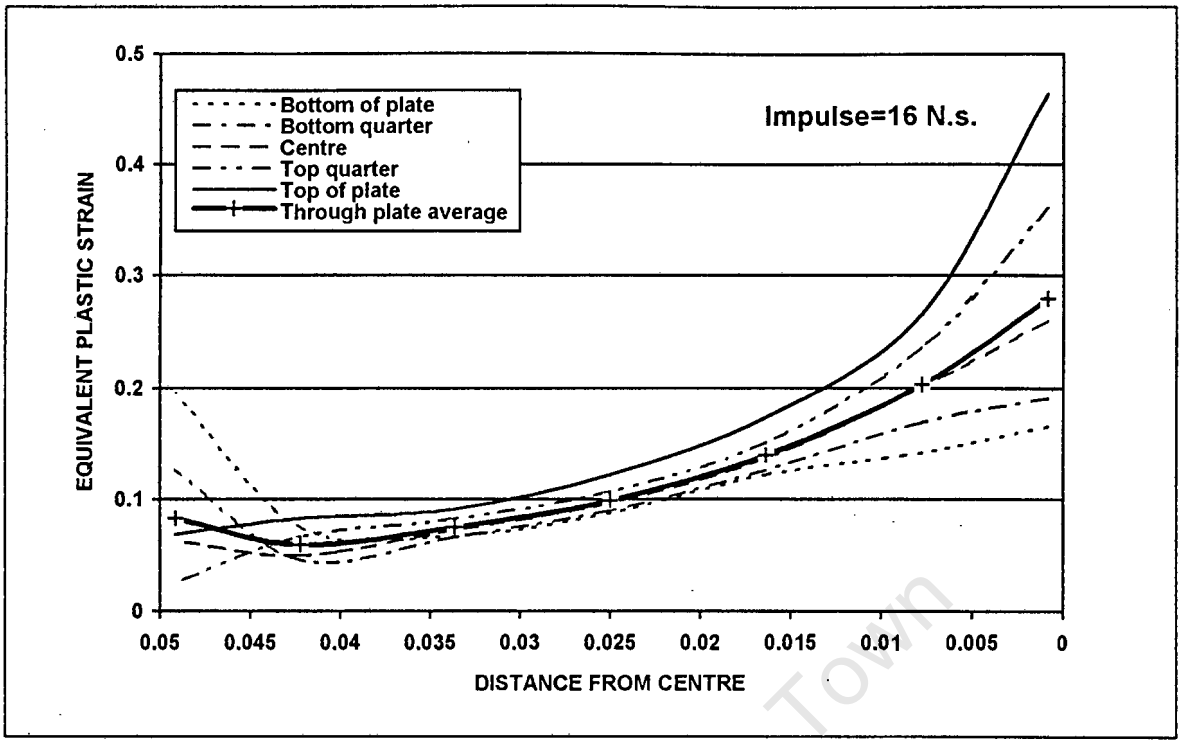

Figure 4-10 Equivalent plastic strain distribution.

Mode II failure by tearing has been shown to occur at the outer boundary [3]. A widely used failure criteria uses a maximum equivalent plastic strain measure to indicate failure. Using this criteria in the presented case, failure would occur at the plate centre which is inconsistent with the experimental evidence. More work is needed with respect to failure criteria and the study of stress concentrations at the boundary to predict failure in the present numerical model. As the prediction of Mode II failure is not in the scope of the presented analysis, however, no further work was done regarding failure.

4.1.6 Plate thinning

Figure 4-11 shows a typical contoured plot of the predicted plate thickness after impulse. It is interesting to note that the predicted thinnest section is at the centre of the plate and not at the boundary.

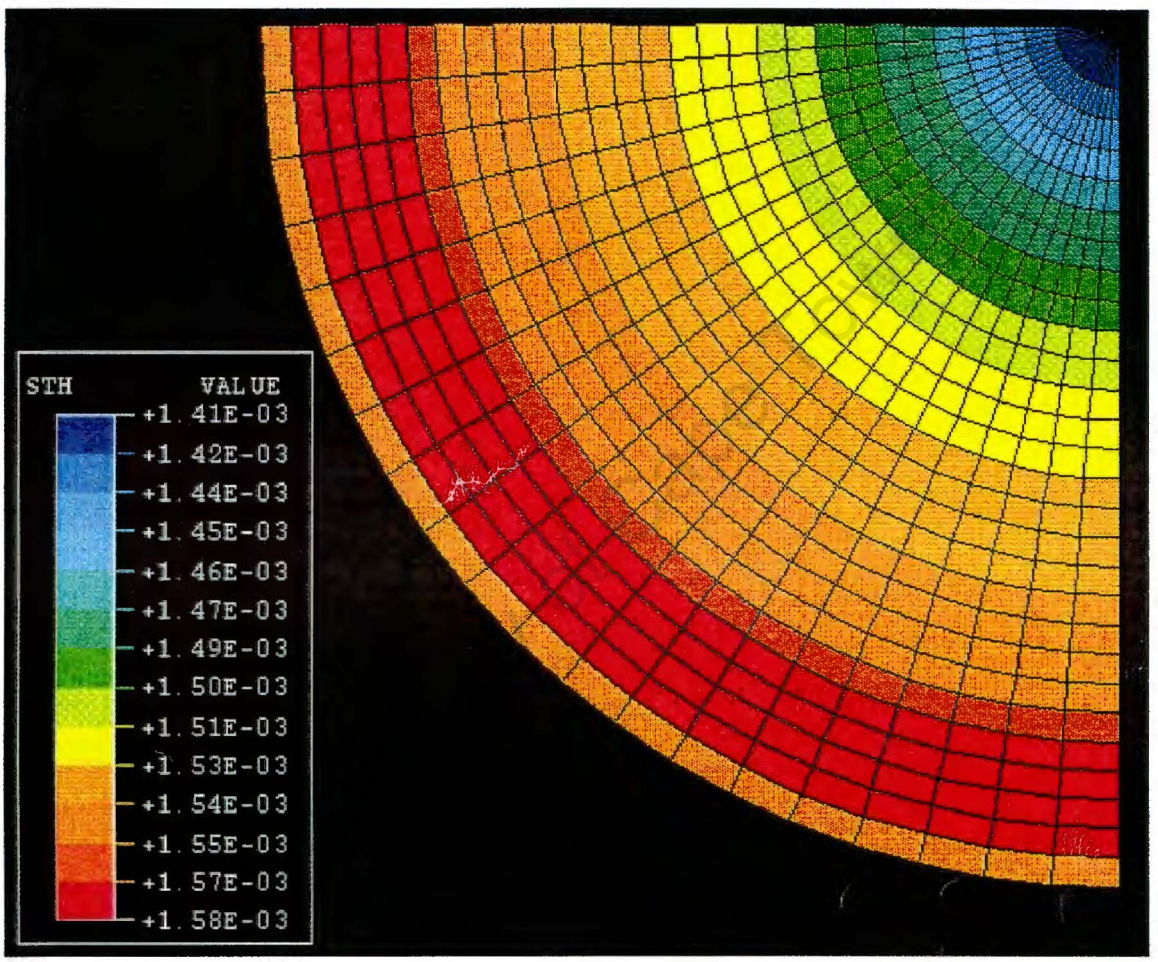

Figure 4-11 Contour plot of the resultant thickness of a plate subjected to an 11 N.s. impulse.

The thickness of built-in plates subjected to a 11.22 N.s and a 14.83 N.s. impulse from experimental work by Thomas [4] were measured by mechanical means for comparison with predictions from ABAQUS. These values are plotted in Figure 4-12. The experimental results are for plates that are thicker than the plate modelled in ABAQUS and thus the thickness values are not the same. However, it is shown that the trends for

the experimentally determined and numerically predicted plate thickness correlate well. The plate thinning predictions are consistent with equivalent plastic strain predictions as described in Chapter 4.1.5 as the thickest area of the plate corresponds to the area that has the least equivalent plastic strain.

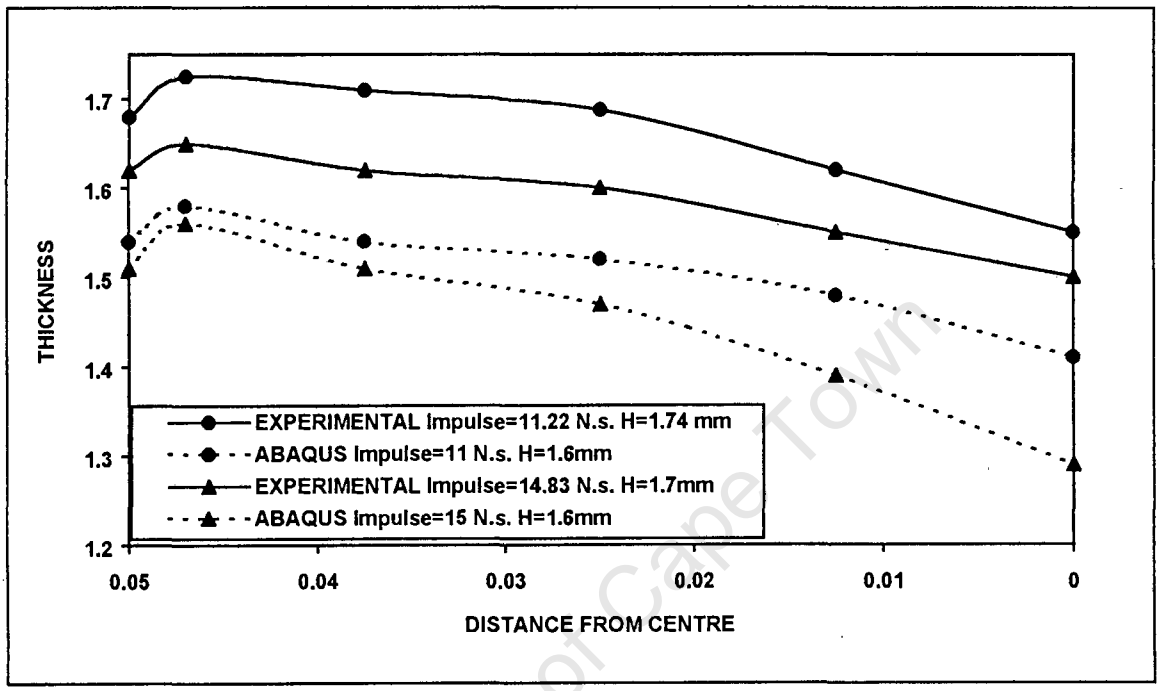

Figure 4-12 Comparison of plate thickness results.

4.1.7 Deformed Plate Shape

The final deformed shapes resulting from the applied load of 12 N.s. are shown in Figure 4-13. The shape for the Mode approximation velocity profile is the same as that of the triangular velocity profile. This is because the initial velocity profiles are the same for these two models. The deformed shapes of the two pressure loading models and the uniform initial velocity profile model are essentially the same but are distinctly different to the deformed shape of triangular and Mode approximation velocity profile loading models.

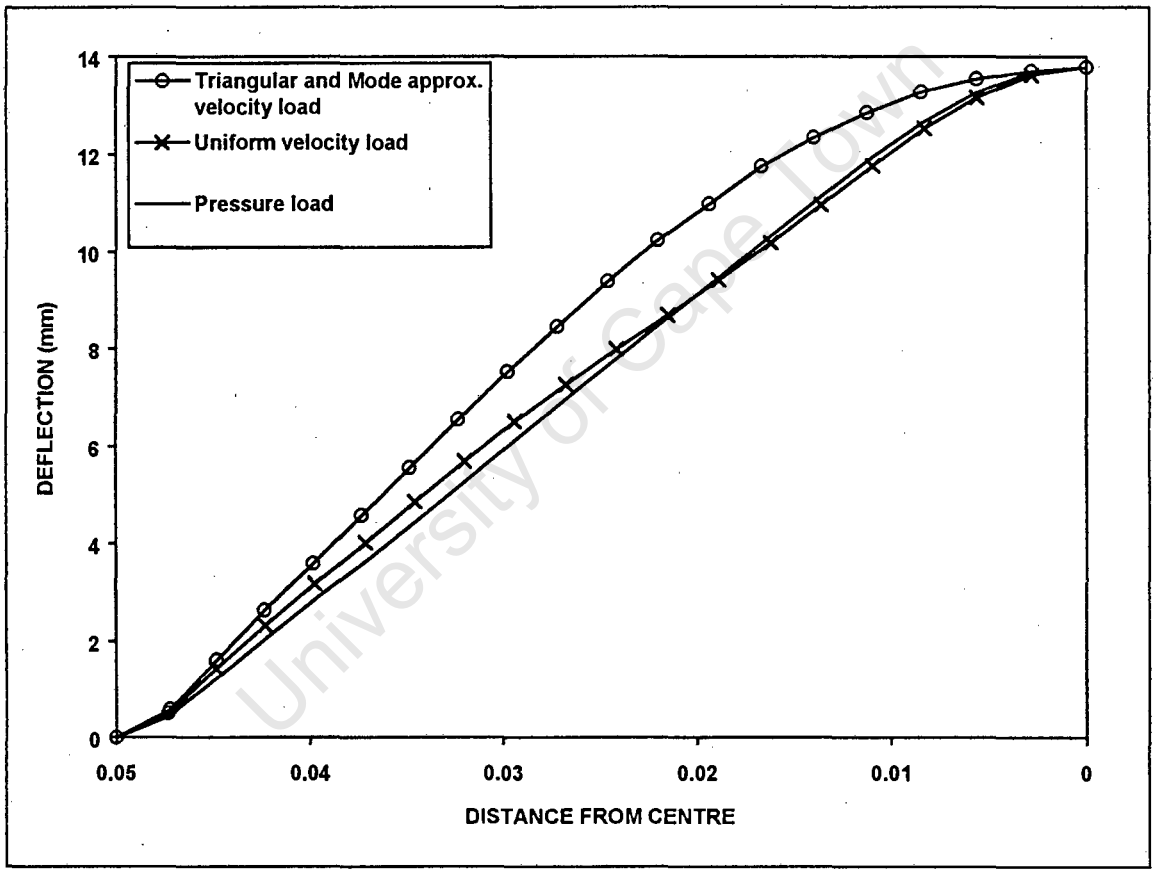

Figure 4-13 Deformed plate shapes for a 12 N.s. impulse.

In Figure 4-14, the final deformed shape for the triangular velocity model is compared with three analytically derived plate deformation shape functions namely, Duffey [21], Westine and Baker [22], and Teeling-Smith and Nurick [23]. Teeling-Smith found that the modified Stirling formula for the shape profile compared well with the experiments. It is shown in Figure 4-14 that the ABAQUS predicted deformed shape also compares well with this shape. Thus the correlation between the experimental and presented triangular velocity load deformation shape is good.

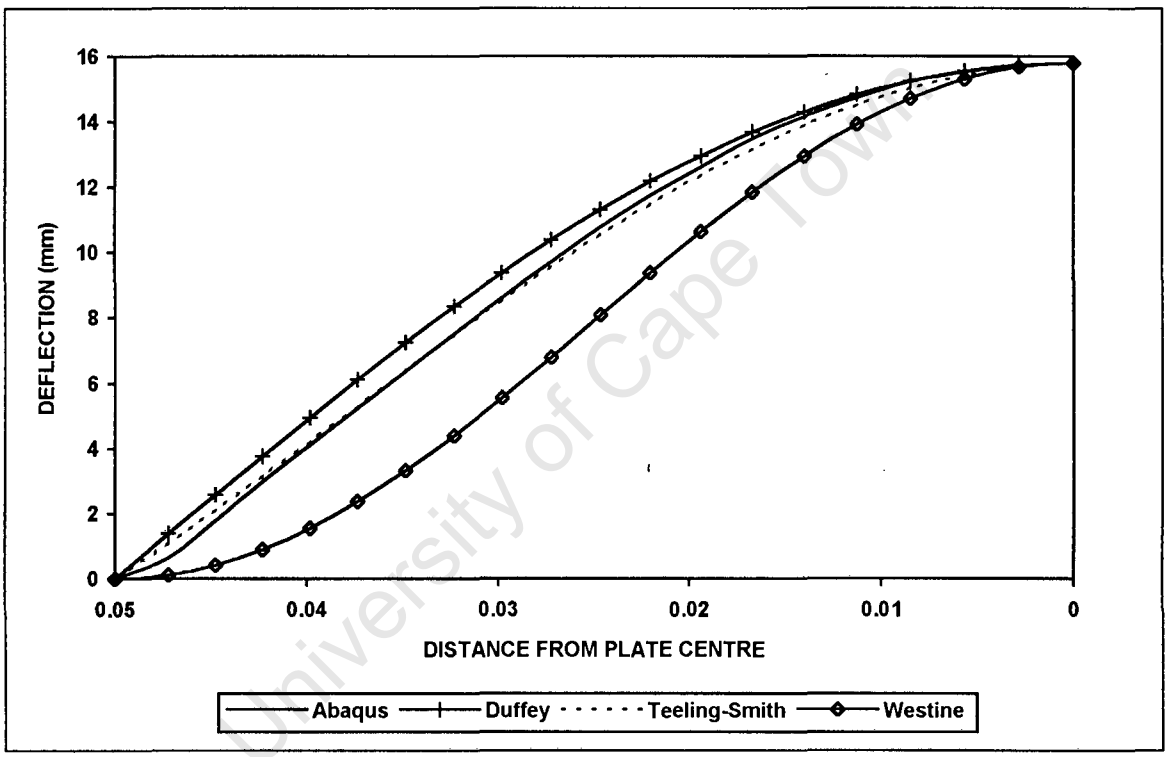

Figure 4-14 Comparison of analytical shape functions with Triangular velocity profile shape.

The main difference in the predicted shapes occur at the boundary where ABAQUS fails to model the pronounced rotation which occurs. The plate is modelled with an integral boundary compared to the experimental work in which the plates are clamped. Nurick and Teeling-Smith [13] found experimentally that the edge effects due to clamping result in local necking and thus thinning of the plate for impulses larger than 12 - 13 N.s. Further work by Thomas [4] has shown experimentally that in the case of integral plates, the curve

of the bend of plates start at the boundary, while in the case of clamped plates, the curve extends into the clamped region. These two observations might account for the unpredicted rotation at the boundary in the case of the experimental results.

4.1.8 Response Time

The response time of the single plates vary with applied impulse. Figure 4-15 shows that for a 4 N.s. impulse, the response time is approximately 125 μs while for a 20 N.s. impulse, a response time of 115 μs is predicted. There is a linear change in the response times for impulses within the range of 4 N.s. and 20 N.s. Nurick [24] observed from experimental work that for impulses in this range, the plate response times are scattered in the range of 140 to 170 μs with no significant trend evident. Predictions from other numerical models [24], however, predict response times in the order of 100 to 120 μs.

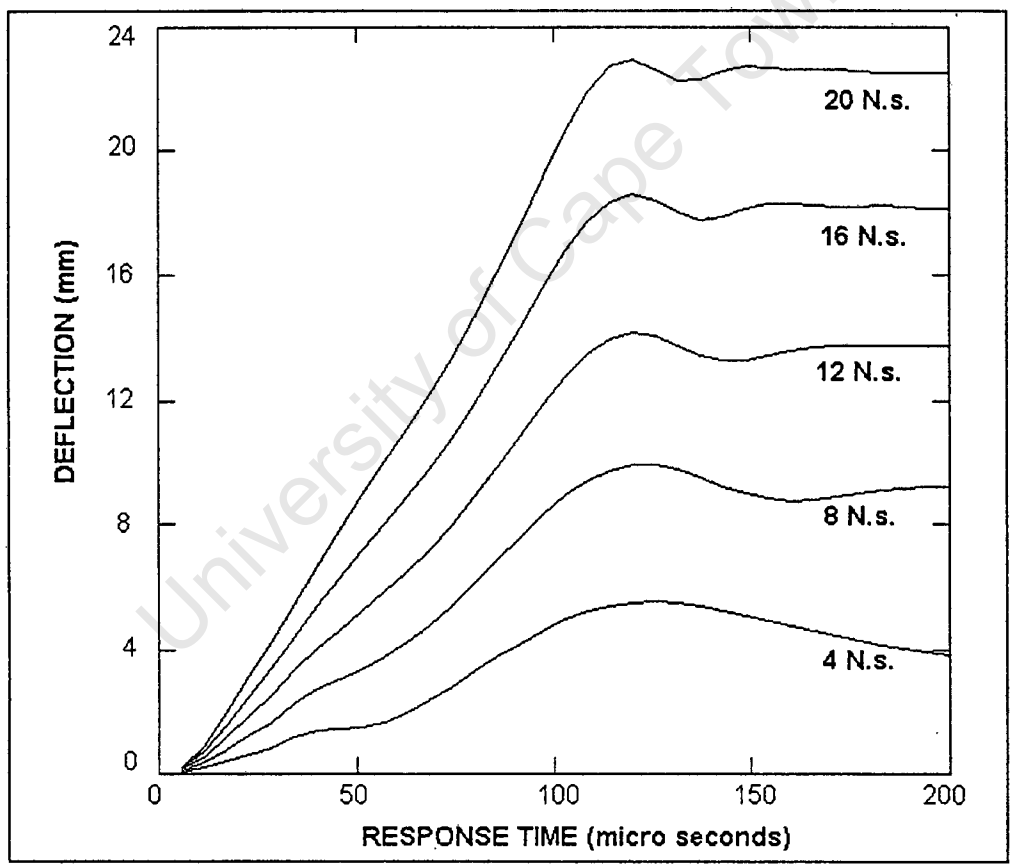

Figure 4-15 Response times of the plate under 4, 8, 12, 16 and 20 N.s. impulses.

4.2. Sandwich Plate

4.2.1 Introduction

The model for the sandwich plate is twice as large as the equivalent single plate model and hence computational costs are higher. The axisymmetric model of the sandwich plate did not run for a mesh of over 20 elements and thus convergence of the solution was not possible. Hence, only the computationally costly general shell element mesh could be used. For these two reasons and that the explicit scheme is the more suited scheme for dynamic analyses, it was decided to use only the explicit scheme in the sandwich plate analysis. Due to reasons discussed in Chapter 4.1.3, only a pressure load model with a burn time of 15 μs is used for the sandwich plate.

Analysis was conducted over the same range of impulses as for the experimental work. Further analysis has been conducted outside of the impulse range of the experimental data (in the case of the 8mm and 12mm air gap plates) in an attempt to study the behaviour of the plate at and around the impulse that just causes contact between the plates.

4.2.2 Convergence

Convergence of the mid-plate deflection for the general shell element mesh is, as in the case of a single plate, sufficient with a 300 element mesh and a further refinement of the mesh does not have an accuracy advantage to offset the additional computational cost. All further analyses use, unless specified, a 300 element per plate mesh. Table 4-2 shows the convergence of the permanent mid-plate deflections of an 8mm air gap sandwich plate subjected to a 12 N.s. impulse for different mesh refinements.

NO. OF ELEMENTS PER PLATE	PLATE A DEFLECTION (mm)	PLATE B DEFLECTION (mm)
75	10.2	3.5
300	10.5	4
507	10.65	4
867	10.7	4

Table 4-2 Convergence of mid-plate deflection.

4.2.3 Mid-plate Deflections

Results of mid-plate deflection versus impulse for the four air gap sizes are plotted with the corresponding experimental data in Figures 4-16 to 4-19. It is shown that the current results over predict in the range analysed although the trends are similar. This may be due to variations in material properties, and simplification of the boundary conditions.

Analyses were conducted for certain sandwich plates with different coefficients of friction to asses the influence of the coefficient on the results. The air gap sizes and impulse loads used for comparison in the analyses were chosen to maximise the contact areas and the contact pressure involved in the response. The resultant mid-plate deflections of the 4mm air gap plate subjected to a 34 N.s. impulse changed from 19.0mm to 19.2mm for plate B while plate A did not change in deflection when the coefficient was changed from 0.4 to 0.0. The 8mm air gap plate when loaded with a 34 N.s. impulse, resulted in plate A deflections of 21.8mm and 21.85mm and plate B deflections of 17.6mm and 18.1mm respectively for coefficients of 0.4 and 0.0. The largest difference involved is 2.8 percent while the average difference for the mid-plate deflection values is 1 percent. The friction coefficient appears to have little effect on the response of the sandwich plates.

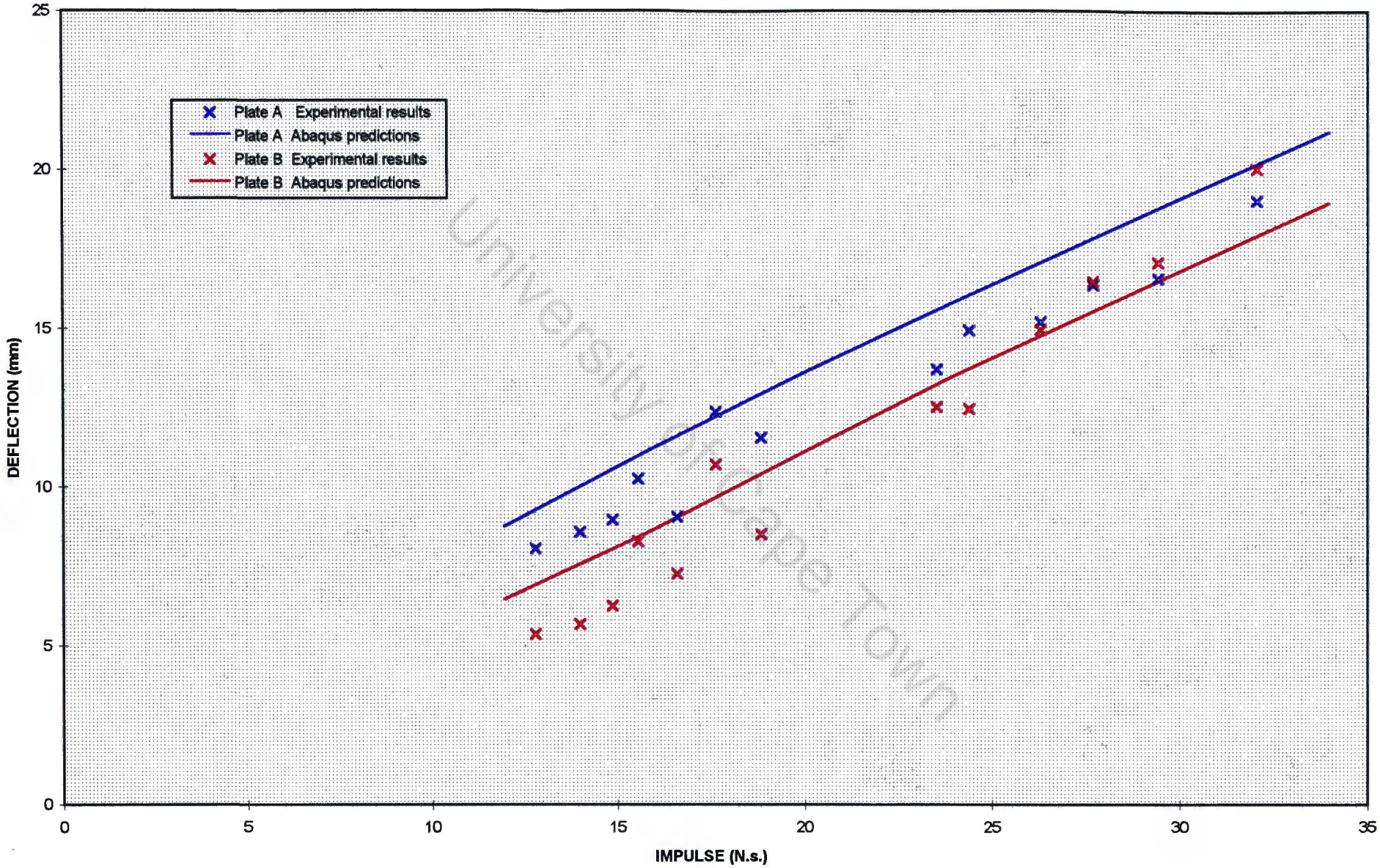

Figure 4-16 Mid-plate deflections of the 4mm air gap sandwich plate.

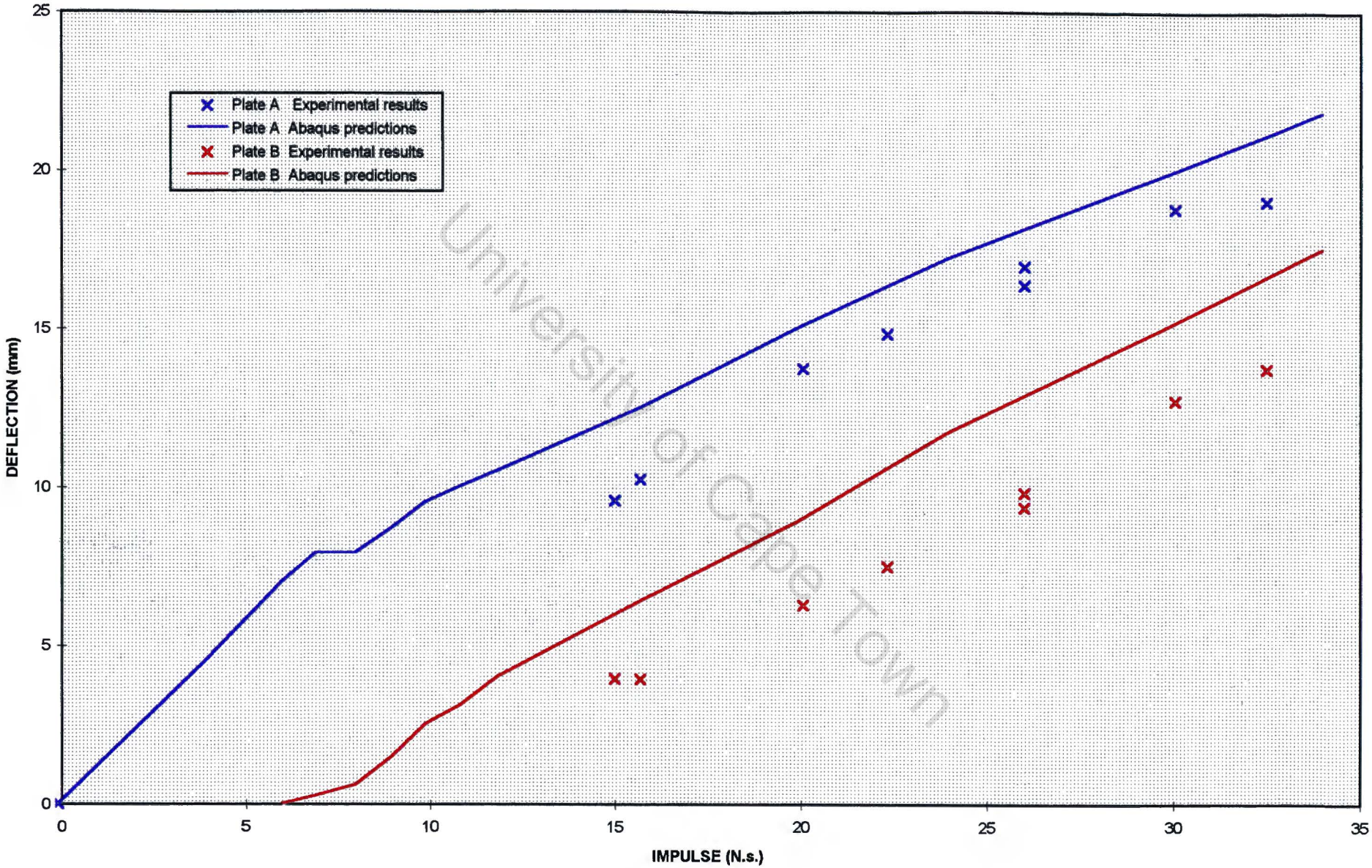

Figure 4-17 Mid-plate deflections of the 8mm air gap sandwich plate.

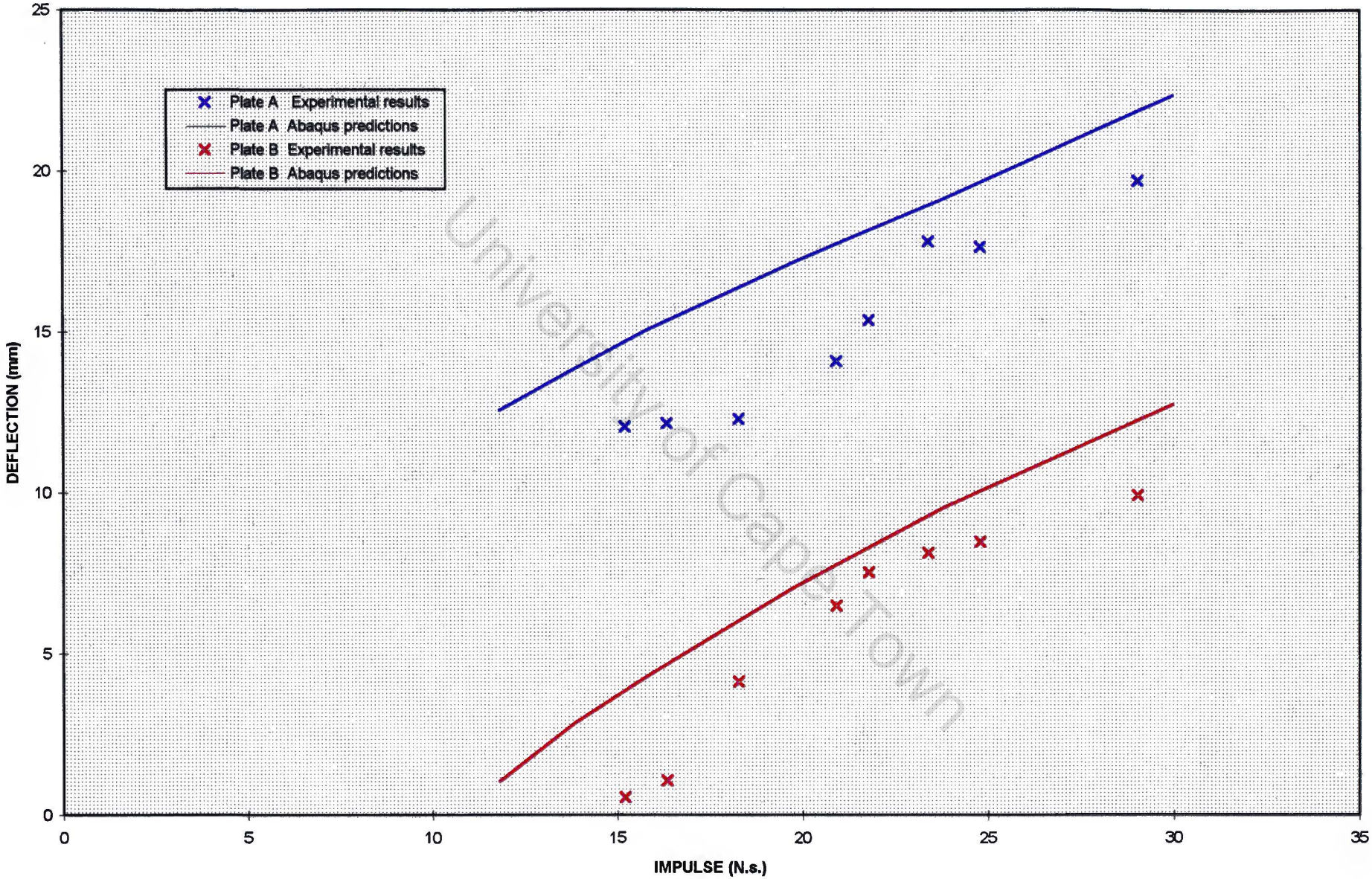

Figure 4-18 Mid-plate deflections of the 12mm air gap sandwich plate.

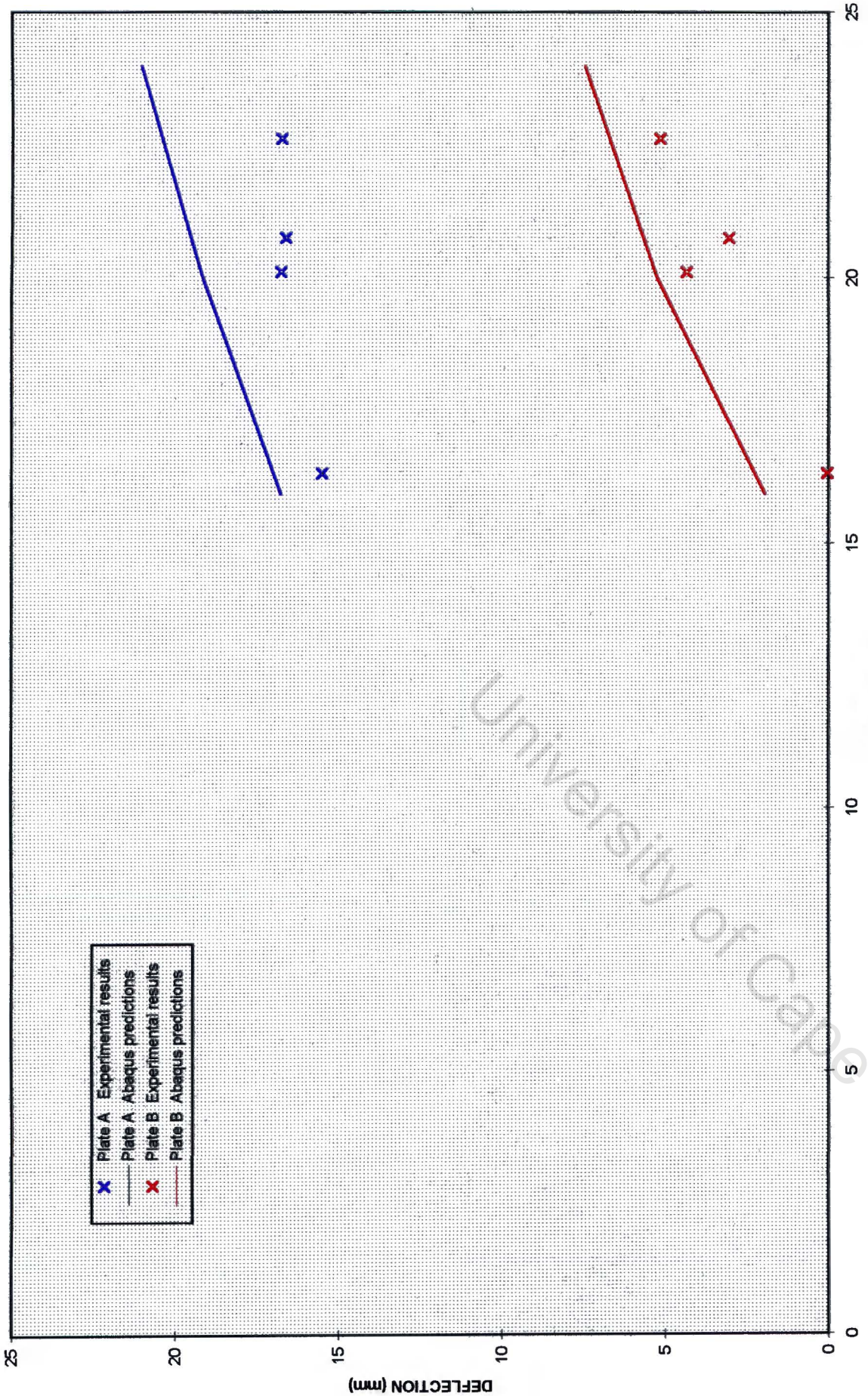

Figure 4-19 Mid-plate deflections of the 16mm air gap sandwich plate.

It was found from the experimental data [1] that three phases exist in the deformation of plate A.

Phase I is characterised by the deformation of plate A with no interaction between the two plates and hence no deformation of plate B. Phase II is characterised by contact between plate A and plate B whereby plate A flattens at contact without its deflection increasing significantly, while plate B deforms. Phase III occurs for higher impulses than Phase II. During this phase, plate A no longer flattens but, like plate B, continues to deform. These distinct phases are shown schematically in Figure 4-20.

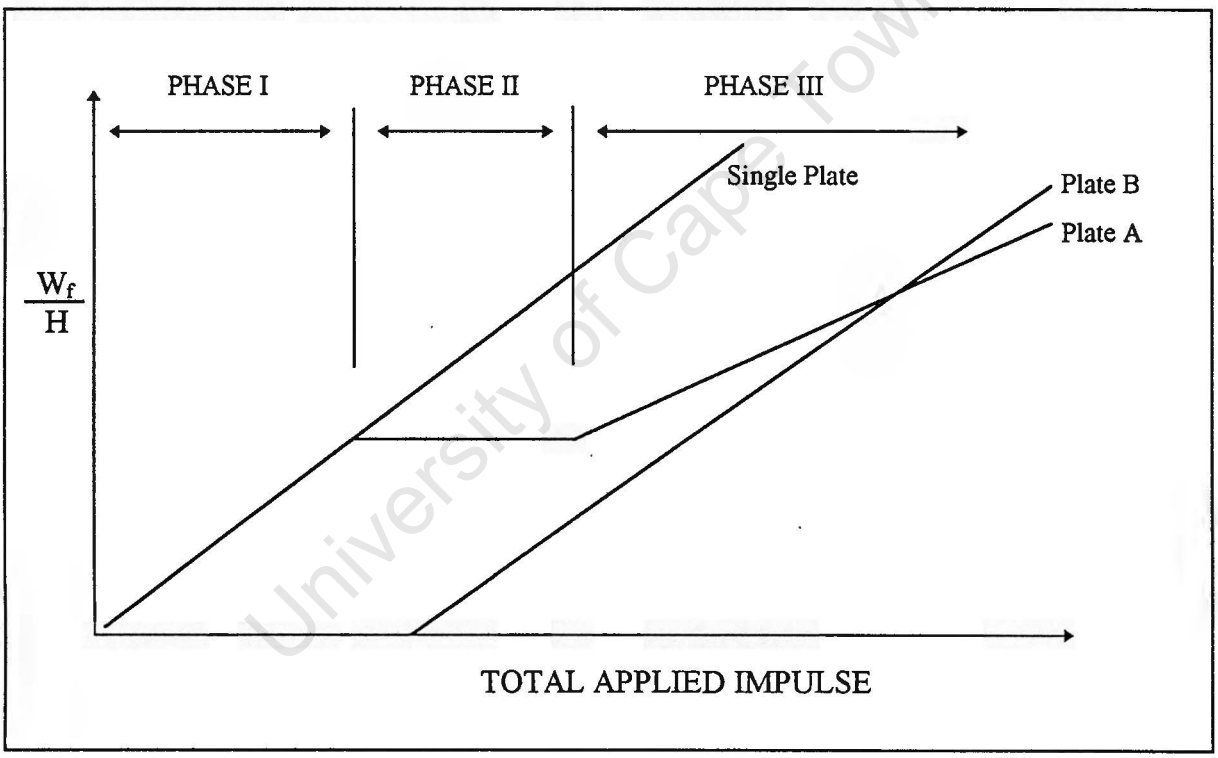

Figure 4-20 Phases of sandwich plate deformation.

It is not evident from the experimental work, however, at which impulse the transition between phases II and III actually takes place. An attempt was made to analyse these phases using the 8mm and 12 mm air gap plates. The reason for not analysing the 4mm air gap plate is that phase II was thought to be very small with phase III dominating. For the 16mm air gap plates, phase II is thought to be very large and all the experimental data available is in phase II and thus no clear transition would be observed.

Figure 4-21 and Figure 4-22 show smoothed predicted curves of plate A deflection versus plate B deflection as well as the experimental data points for the 8mm and 12mm air gap plates. It appears from these plots that the finite element model does not predict phase II at all. It must be noted, however, that for impulses that would cause phase II deformations, large elastic vibrations are predicted in plate A. These vibrations occur for a long time relative to the plate response time and thus predicted values of permanent mid-plate deflections are not exact for this impulse range.

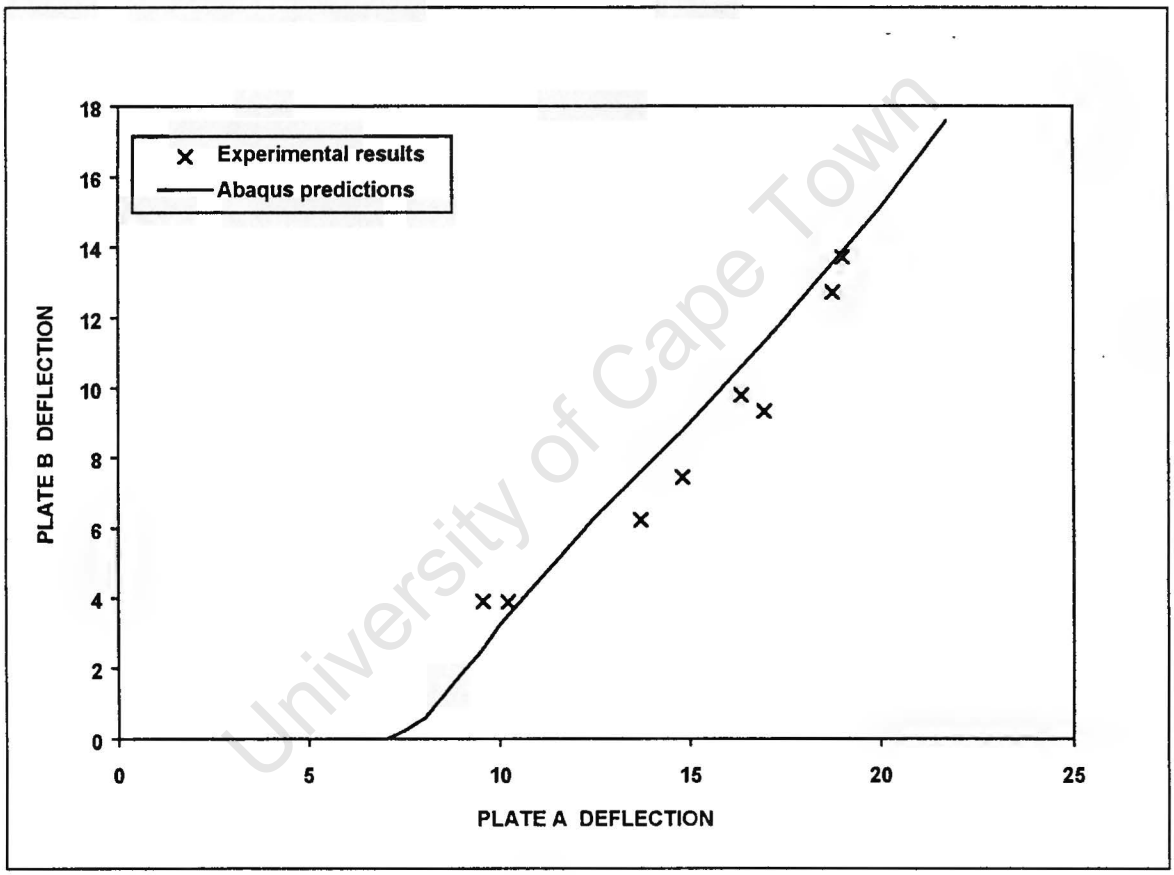

Figure 4-21 Plate A deflection versus Plate B deflection of the 8mm air gap sandwich plate.

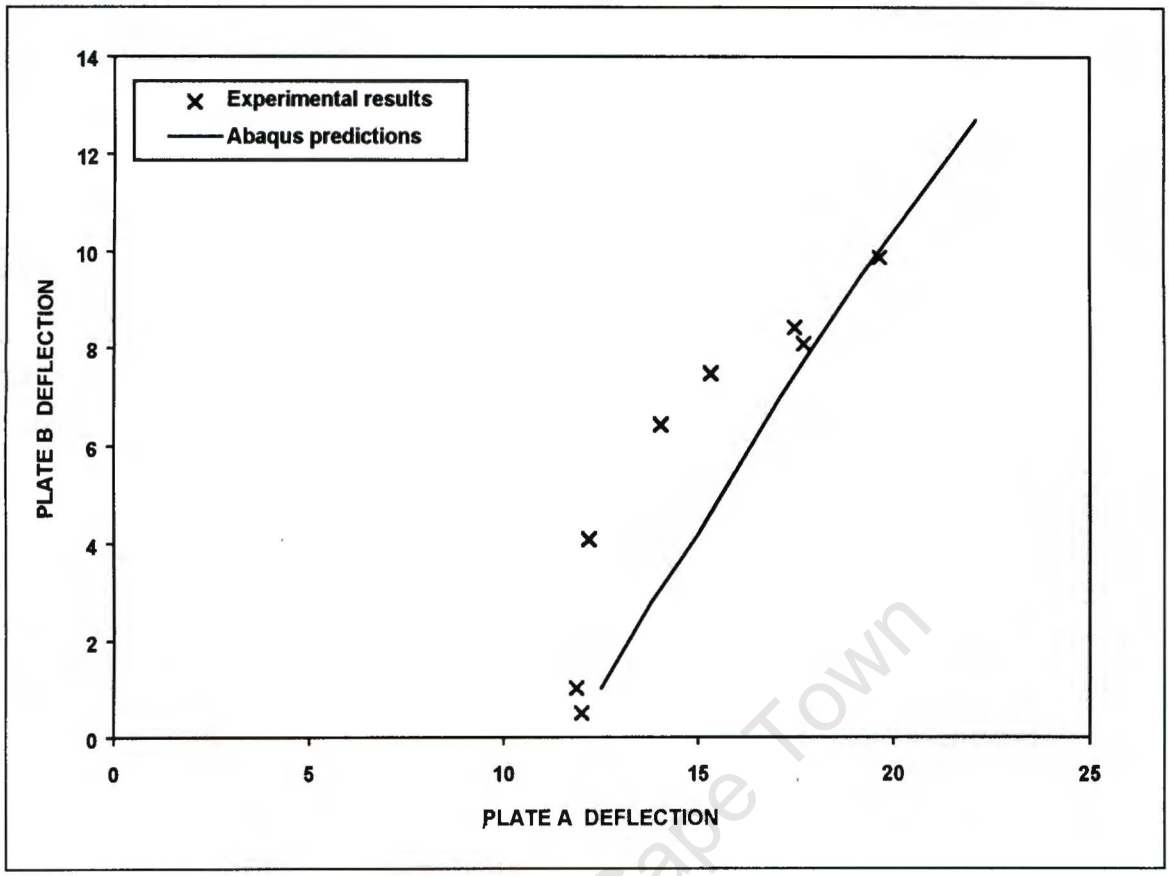

Figure 4-22 Plate A deflection versus Plate B deflection of the 12mm air gap sandwich plate.

Over page in Figure 4-23 is a quarter plate general shell element mesh final deformation plot of an 8mm air gap plate after being exposed to a 12Ns impulse (deflection of plate A =9.6mm and deflection of plate B=3.6mm).

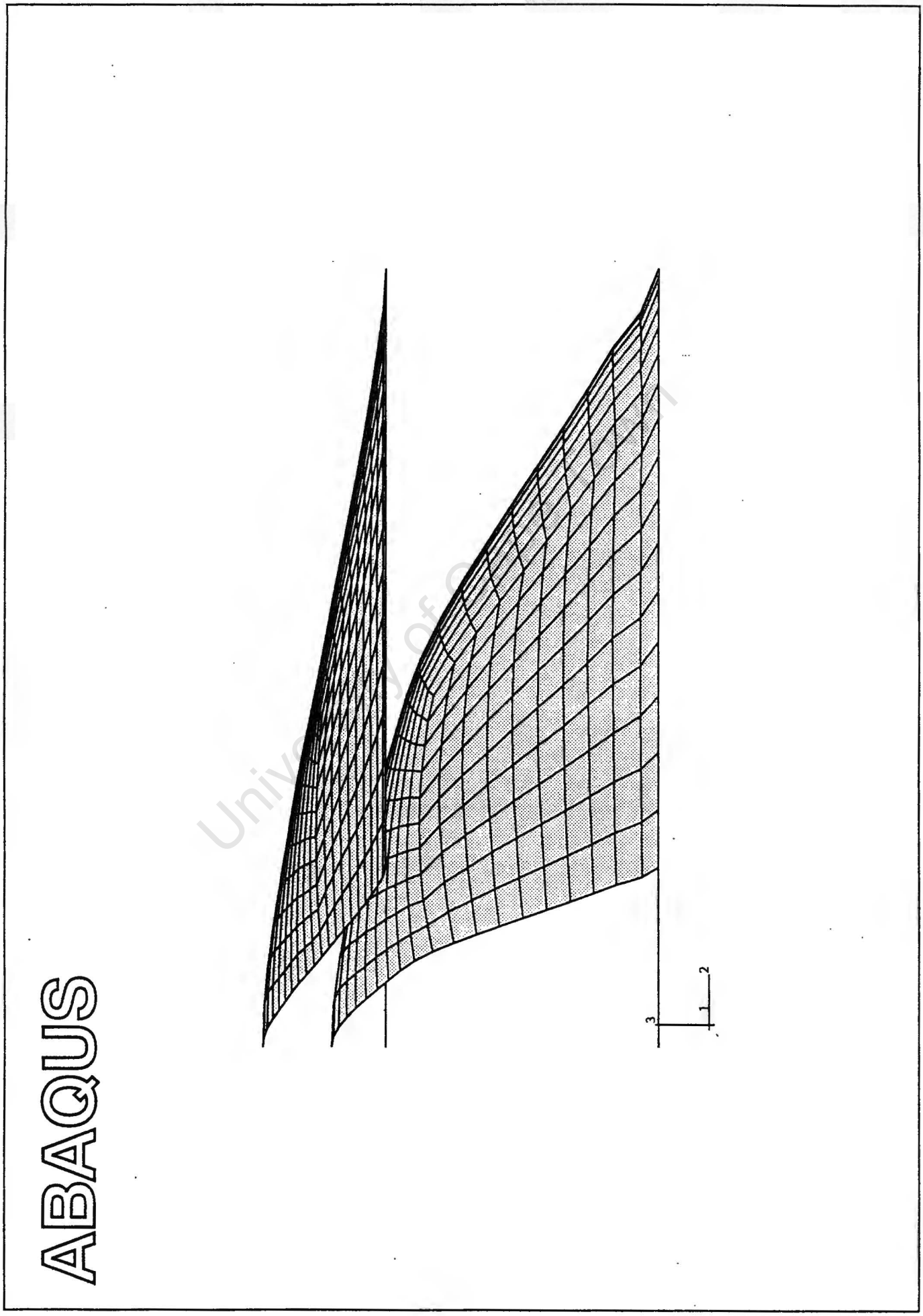
ABAQUS
3
1
2

4.2.4 Contact Diameter

The contact diameter is the maximum diameter of the area of contact between the two plates in the sandwich plate set-up during the analysis. Experimentally the diameter is measured from the markings on the metal. It is calculated in this analysis by measuring and plotting the distance between corresponding points on the two plates at all points along a radial line at the time of contact. As there is a practical limit to how many restarts can be saved, interpolation of the plot is needed in order to get an accurate value for the contact diameter. An example of such a plot is shown in Figure 4-24.

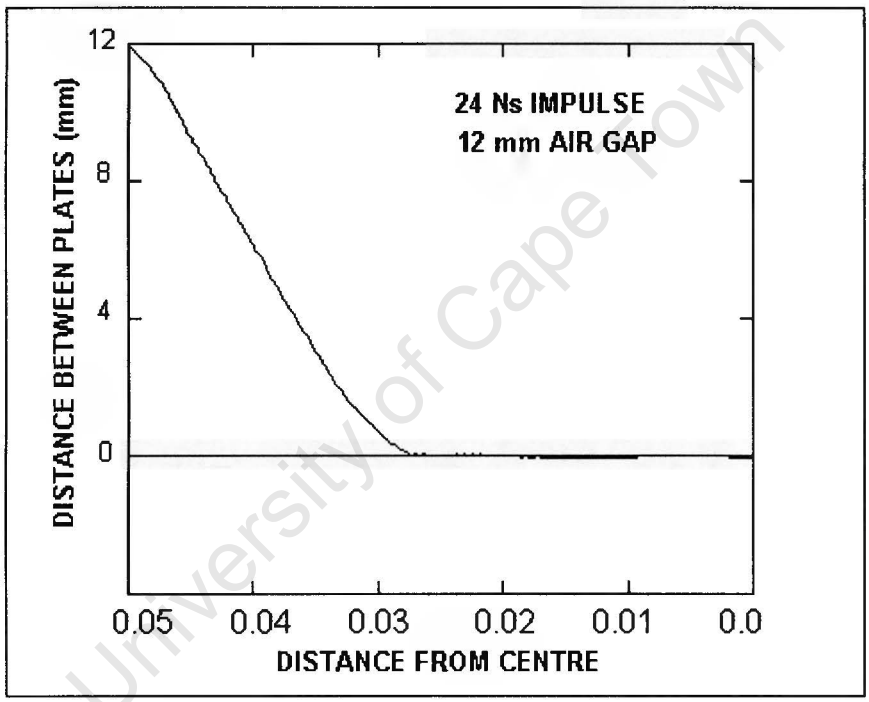

Figure 0-24 Graph of relative distance between plates A and B at contact.

Another means of measuring the contact diameter is to plot the contact pressure at the time of contact. Due to the inability to interpolate these plots for accurate values of diameter, this method was not used but an example of the contact pressure plot corresponding to the graph in Figure 4-24 is shown in Figure 4-25.

Over page in Figure 4-25 is a typical plot of contact pressure between plates A and B.

ABAQUS

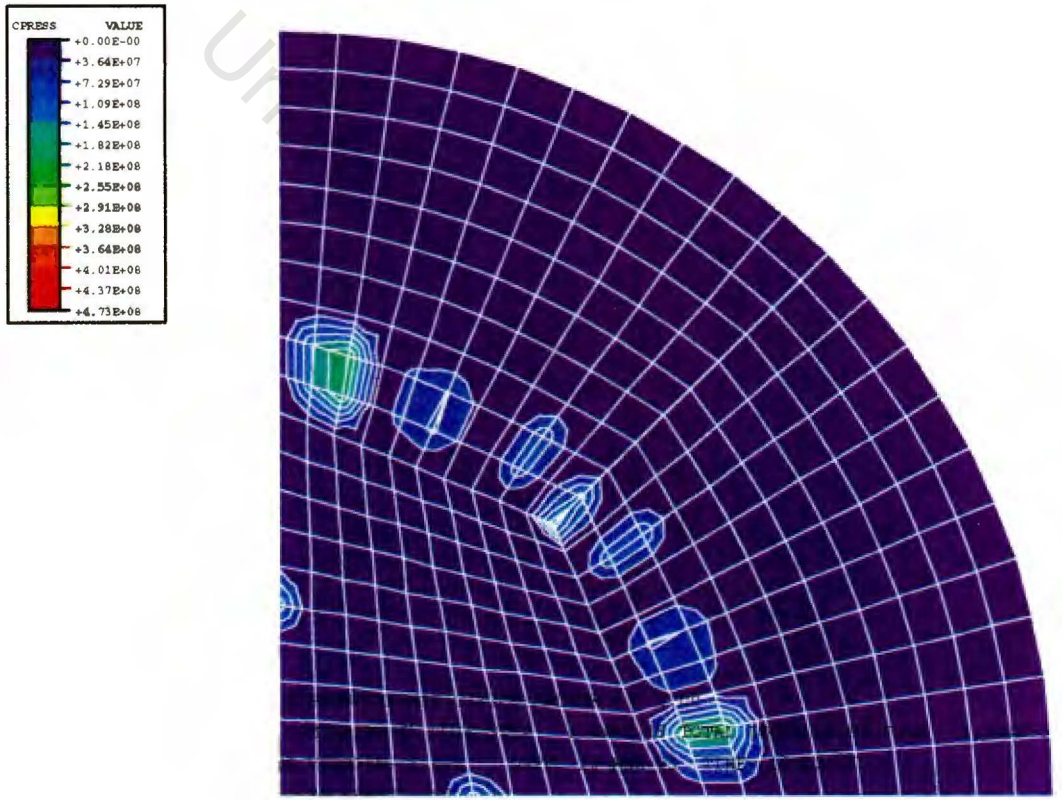
CPRESS
VALUE
+0.00E-00
+3.64E+07
+7.29E+07
+1.09E+08
+1.45E+08
+1.82E+08
+2.18E+08
+2.55E+08
+2.91E+08
+3.28E+08
+3.64E+08
+4.01E+08
+4.37E+08
+4.73E+08

The predicted contact diameters are shown together with the experimentally observed data in Figure 4-26 to Figure 4-29. Trends are correct but the over prediction of mid-plate deflection is again evident, especially in the plot of the 16mm air gap plate as there is contact predicted for a 16 N.s. impulse where, according to the experimental data, contact should not occur.

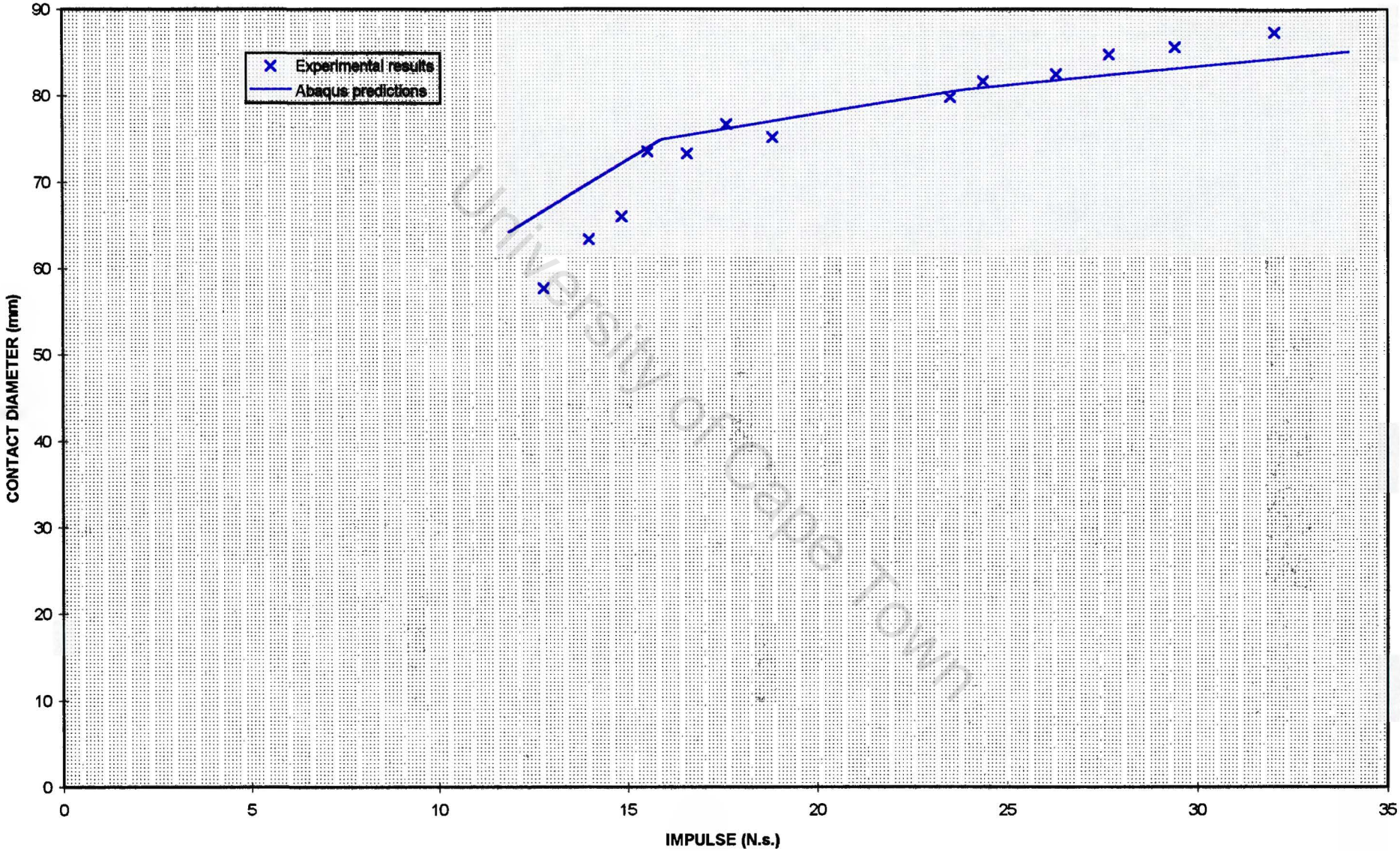

Figure 4-26 Contact diameters of the 4mm air gap sandwich plate.

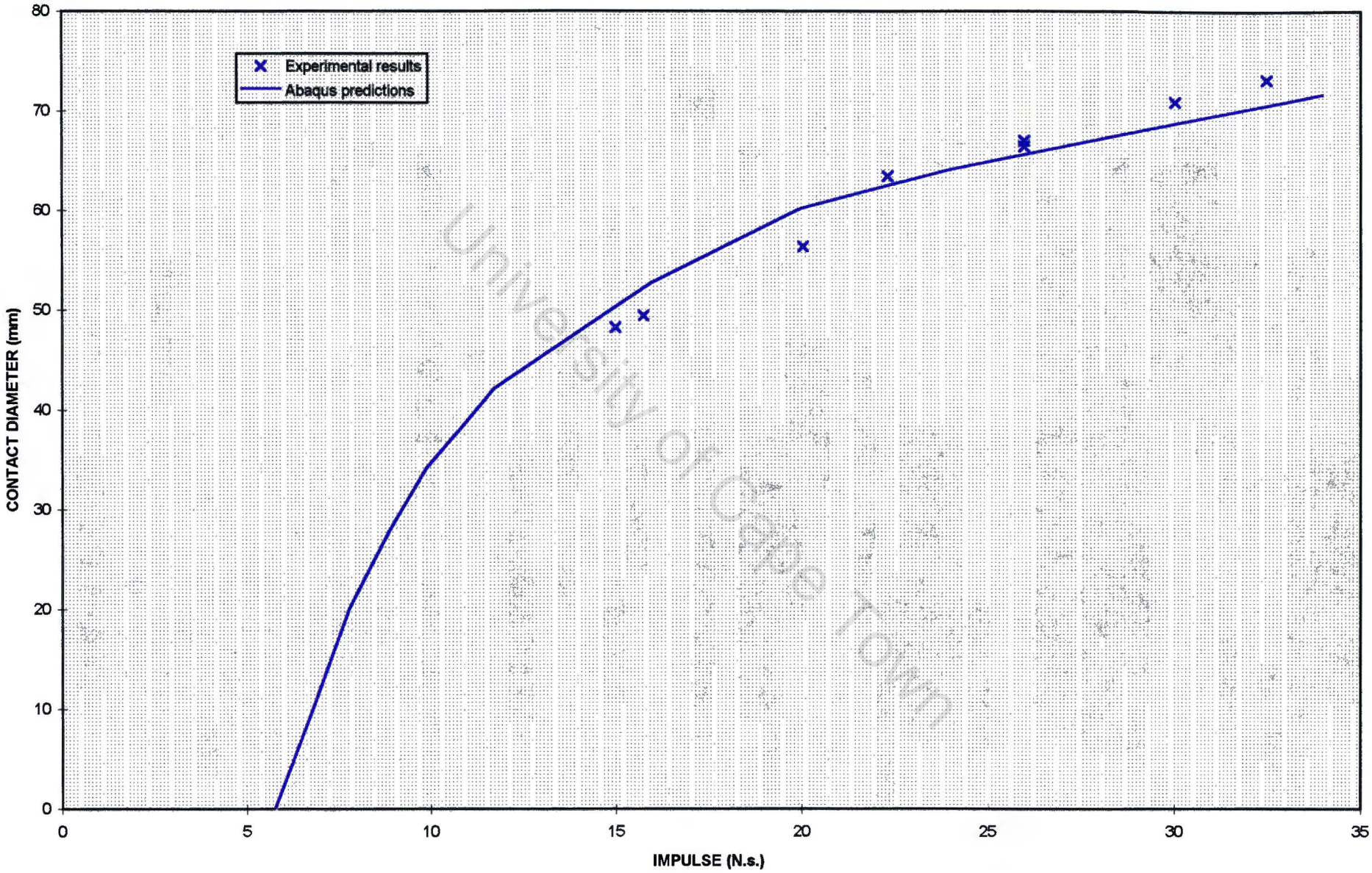

Figure 4-27 Contact diameters of the 8mm air gap sandwich plates.

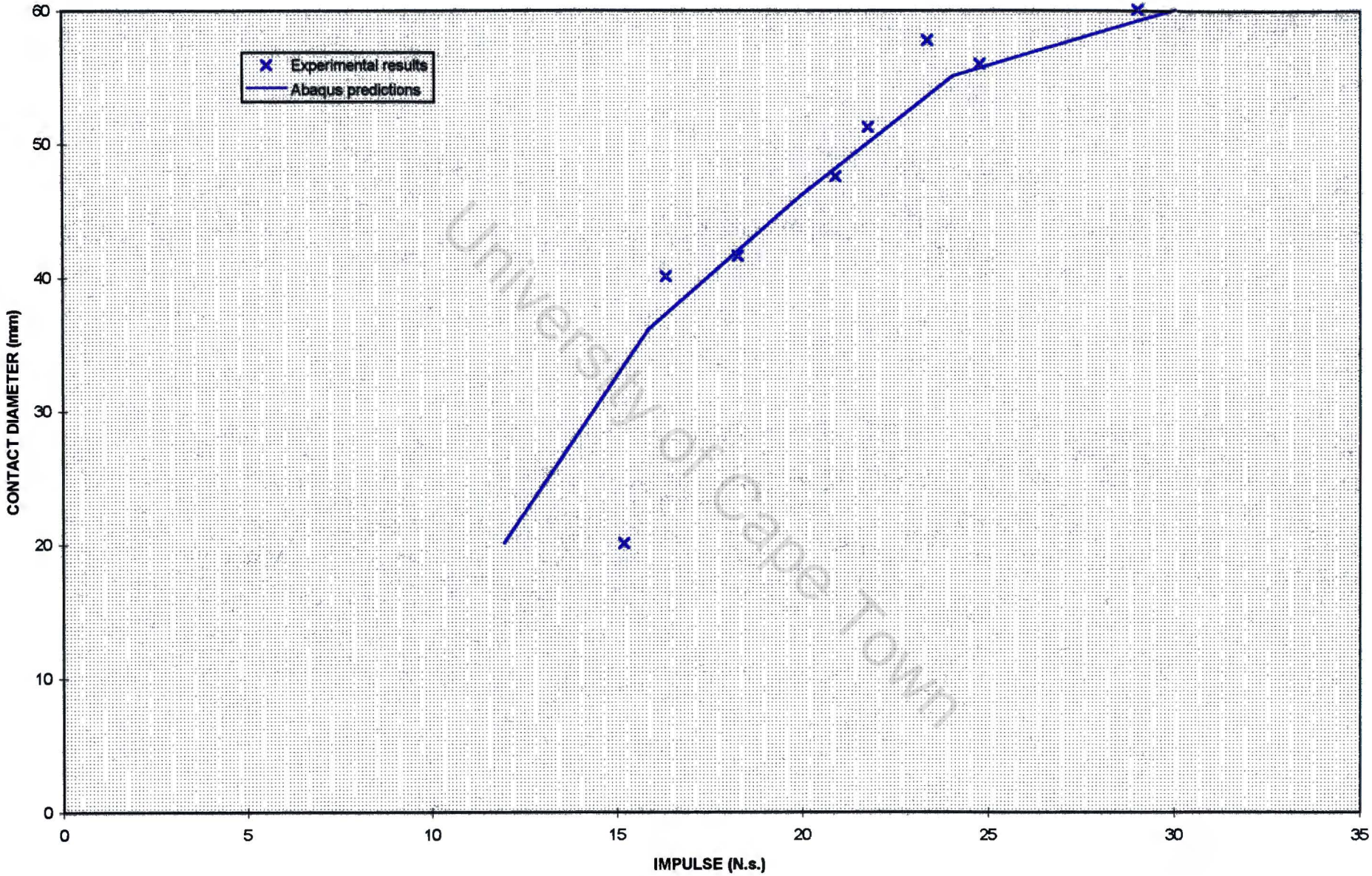

Figure 4-28 Contact diameters of the 12mm air gap sandwich plate.

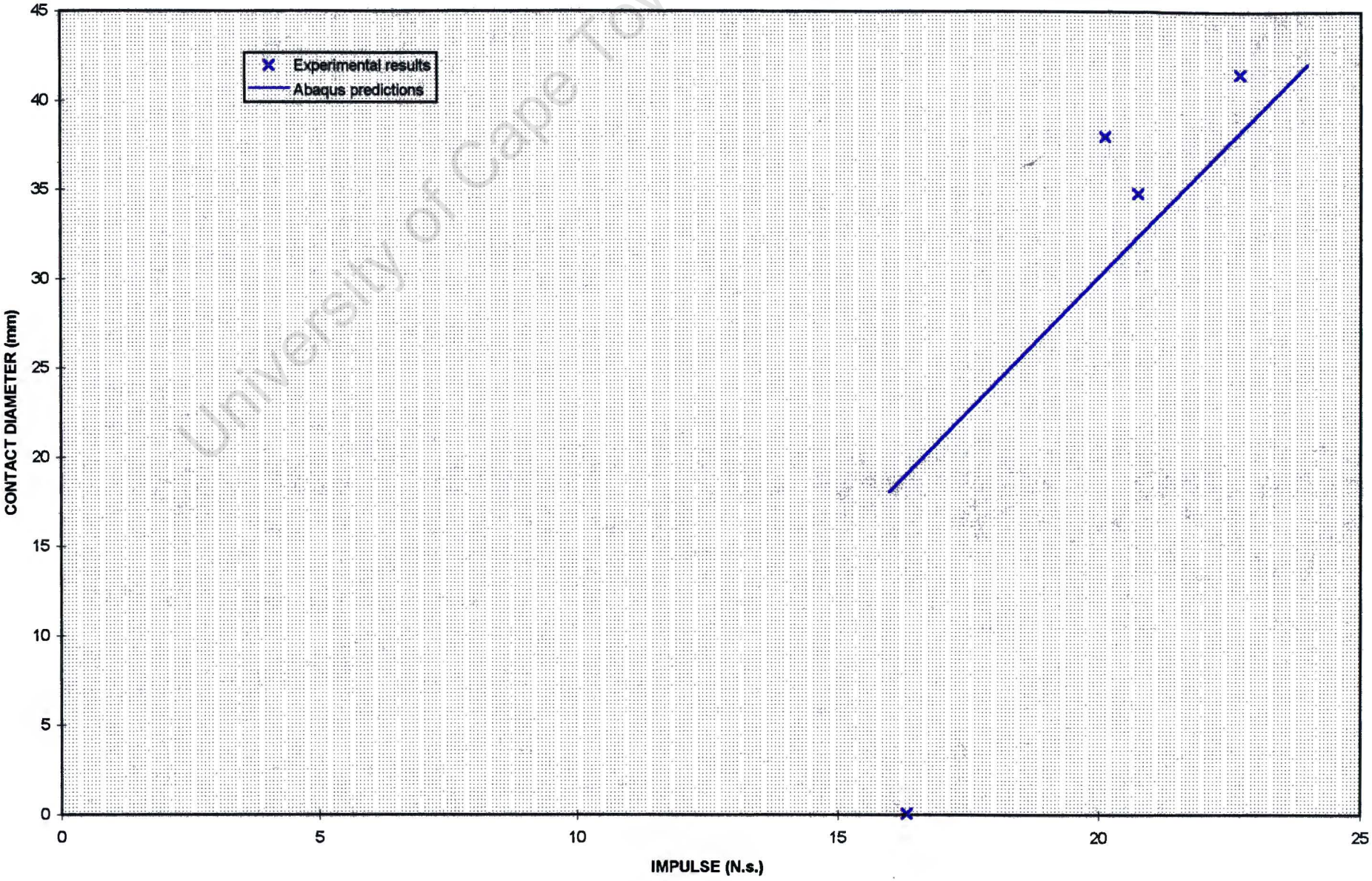

Figure 4-29 Contact diameters of the 16mm air gap sandwich plate.

4.2.5 Plate Energy

Numerical instability is usually easy to detect in linear problems because the solution grows without limit. In non-linear problems, as in the case of the plates of elastic-plastic energy dissipating mild steel, extra energy introduced into the system by numerical instability may be dissipated by plastic work or some other irreversible mechanism such that the instability is arrested. This is often difficult to detect as errors of 10% to 50% or even more might appear reasonable. Even numerical damping in the model can sometimes 'create' or 'dissipate' energy which, if too large, can invalidate the solution. It is thus usually advisable to perform an energy balance check to assure stable and accurate computation. Ideally, the energy of the system at any time should satisfy the equation

$$K_e + E_e + P_e + C_e = W_e \qquad \text{Equation (4-8)}$$

where K_e is the kinetic energy of the system, E_e is the stored elastic strain energy, P_e is the stored plastic strain energy, C_e is the energy lost to contact and friction, and W_e is the work done on the system by external loads.

In the presented problem, the work input is of short duration at the beginning of the analysis, and thus it is easy to establish whether a solution is correct by using the above equation, where the left hand side is summed at the end of the analysis and compared to the value of W_e at the end of the pressure pulse.

It must be noted, however, that the exact solving of structural problems requires that both force and moment equilibrium be maintained at all times over any arbitrary volume of the body. The displacement finite element method is based on approximating this requirement by replacing it with a weaker requirement, which is that the equilibrium must be maintained in an average sense over a finite number of divisions of the body. This equilibrium statement is written in a virtual work form and thus the summation of the plate energies do not always equate to W_e calculated from

$$W_e = \frac{1}{2}\int_0^R m \cdot V(r)^2 \, dr \qquad \text{Equation (4-9)}$$

in the case of the initial velocity loading model where m is the radial mass and v(r) the velocity function across the radius. It is evident, however, that as the mesh is refined, these values approximate each other more closely.

The energies associated with the deformations of each plate have thus been predicted in order to verify the results of the analyses, as well as to calculate the energy losses involved with the contact and friction between plate A and plate B. All analyses done with the explicit integration scheme on the sandwich plate model were correct in terms of the energy balance Equation (4-8) and thus can be presumed to be numerically stable and correct.

The energy losses due to contact are significant with respect to the energy of the applied impulse, especially for the higher impulse range, as there is a high degree of plate interaction. The strain energy of the system can, in the sandwich plate model, be separated into that of plate A and plate B. As the strain energy densities are calculated at five points through the thickness of each element, the Newton-Cotes integration technique is used to calculate the average energy density of each element before the overall strain energy per plate is calculated. The breakdown of the input energy for the sandwich plates are plotted in Figure 4-30 to Figure 4-33. The energy lost to contact is the same as the strain energy of plate B for impulses that cause first contact i.e. zero, but increases more quickly as the impulse and hence, contact, increases. For impulses relatively high compared to initial contact impulse, the contact loss energy is of the order of the energy associated with strain in plate A. In Figure 4-34, which shows the percentage breakdown of energy for the 8mm air gap sandwich plate, the increase in the contact energy relative to the input energy is evident as the impulse increases. It is clear that the contact absorbs a large proportion of energy and can be seen as an energy absorber with similar capabilities to that of a plate.

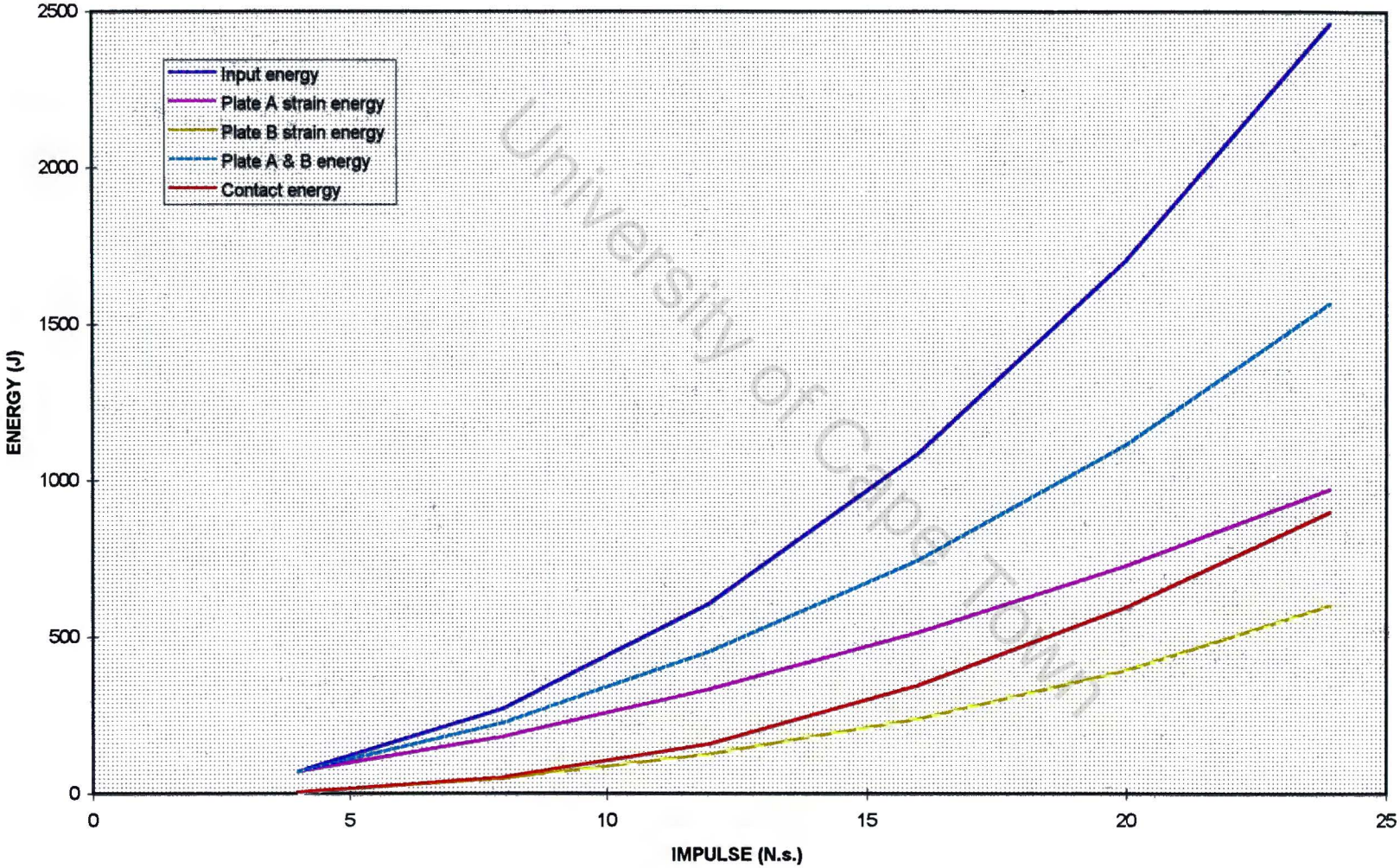

Figure 4-30 Energy breakdown of the 4mm air gap sandwich plate.

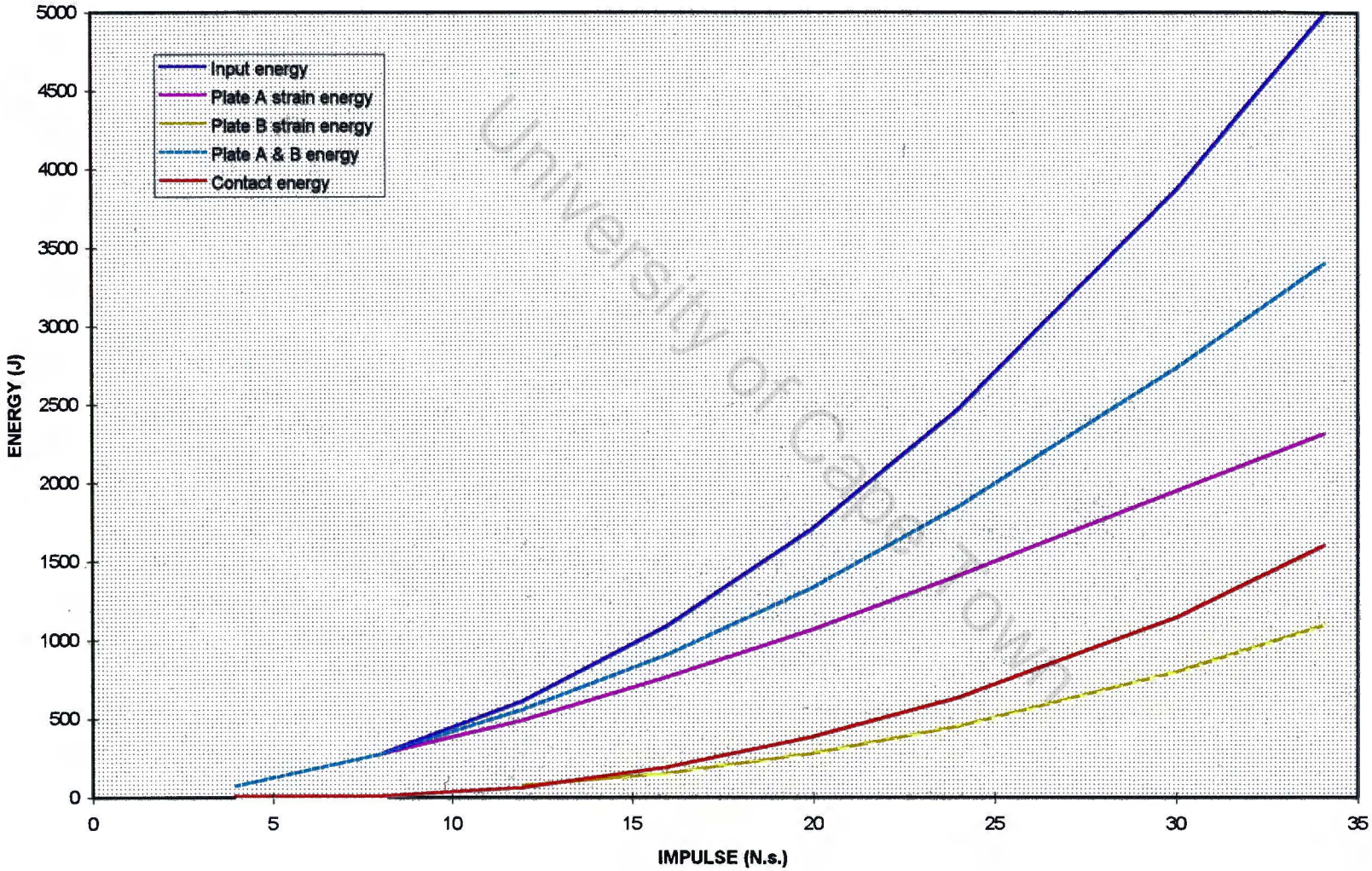

Figure 4-31 Energy breakdown of the 8mm air gap sandwich plate.

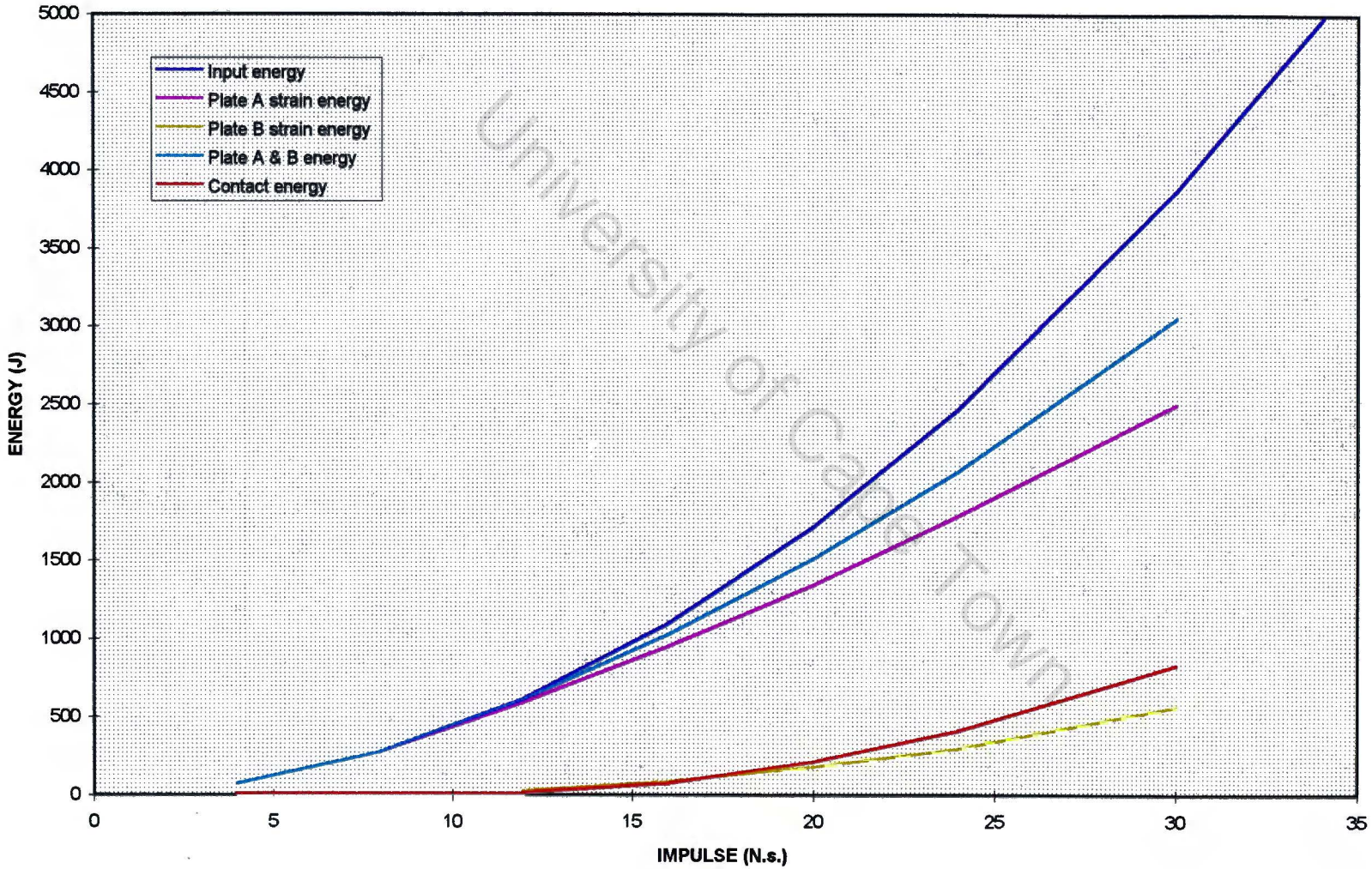

Figure 4-32 Energy breakdown of the 12mm air gap sandwich plate.

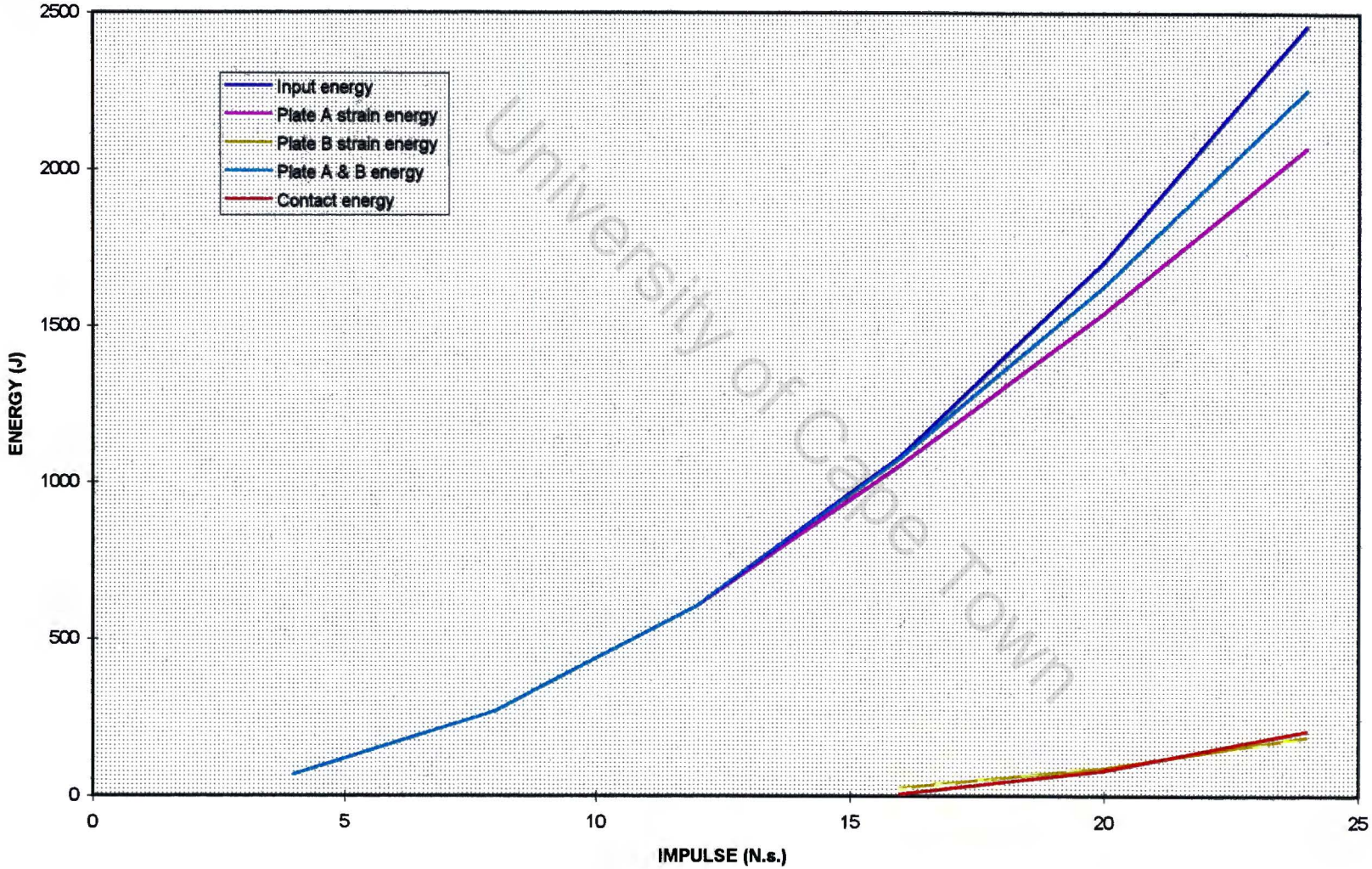

Figure 4-33 Energy breakdown of the 16mm air gap sandwich plate.

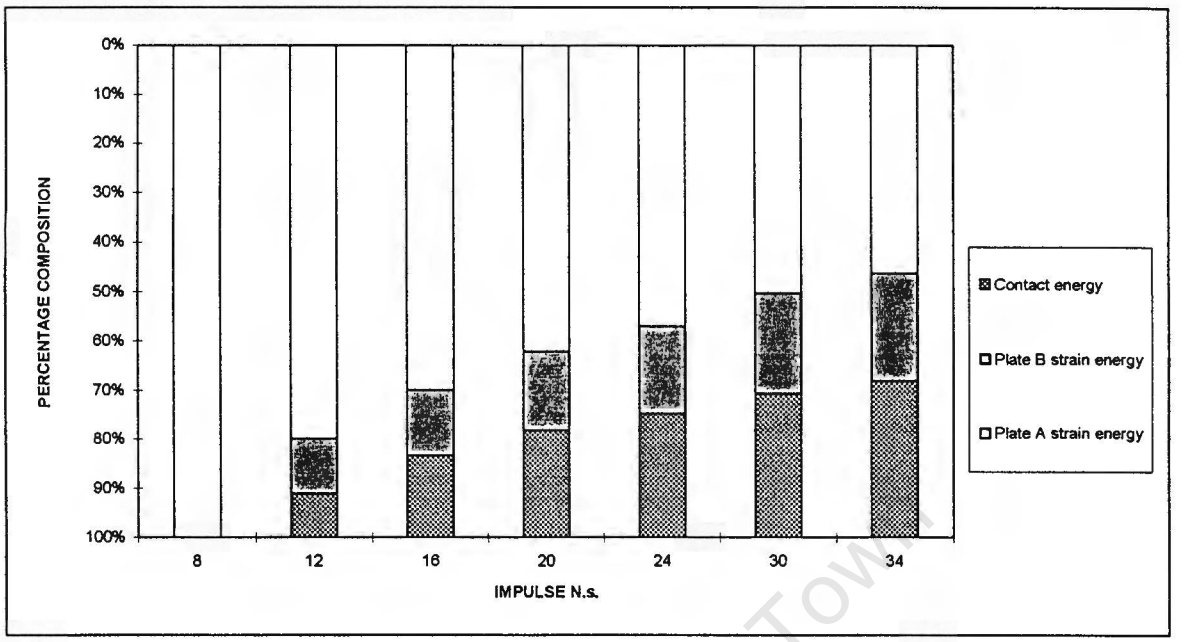

Figure 4-34 Percentage breakdown of input energy in an 8mm air gap sandwich plate.

Mid-plate deflections are plotted against absorbed strain energy for plate A of the 8, 12 and 16mm plates in Figure 4-35 and for plate B of the 8 and 12mm plates in Figure 4-36. Data for plate A is excluded for the 4mm air gap as is data for plate B for the 4 and 8mm air gaps. This is due to the fact that contact energies for these cases are insignificantly small. The mid-plate deflections versus absorbed strain energy for a single impulsively loaded plate is also plotted. It is evident that more strain energy is required for the plates in the sandwich plate set-up than for the same deflection of an impulsively loaded single plate. This extra energy requirement is due to the different deformed shapes which the sandwich plates assume when compared to the single plate.

In the case of plate A, this change in plate shape from the shape of a single plate is due to the impact between plate A and plate B.

In the case of plate B, however, the deformed shape is equivalent to the shape function of a single plate which has a loading area that is smaller than the total plate area. This area of loading is dependent on the contact diameter between plate A and plate B.

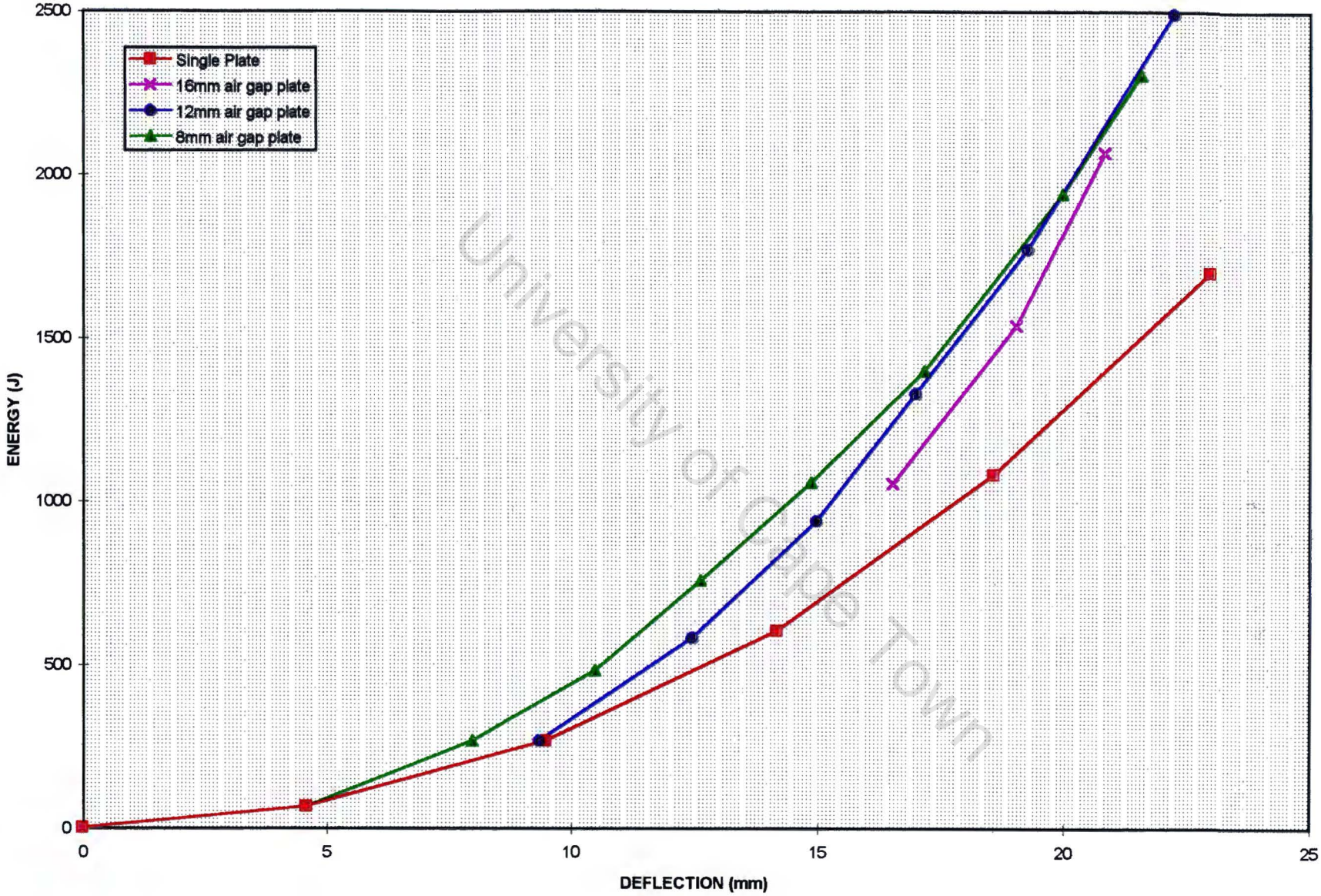

Figure 4-35 Mid-plate deflection versus absorbed strain energy for plate A.

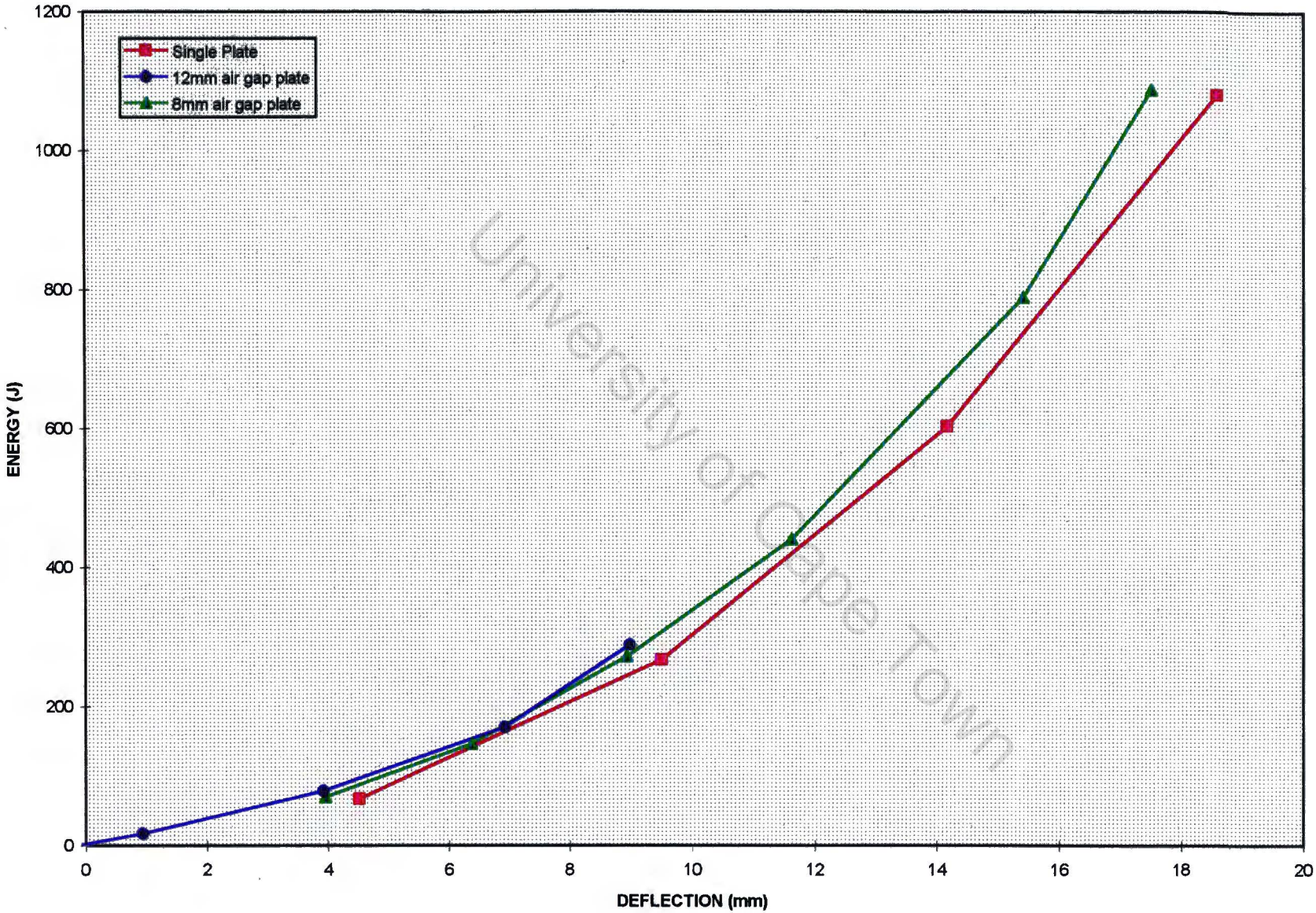

Figure 4-36 Mid-plate deflection versus absorbed strain energy for plate B.

4.2.6 Response time

The plots in Figure 4-37 show mid-plate deflection responses of plate A and plate B of the sandwich plate for the 4mm, 8mm, 12mm and 16mm air gap sizes. The impulses for which the responses are plotted are as follows: 8N.s. and 24 N.s. for the 4mm air gap plate, 8 N.s. and 34 N.s. for the 8mm air gap plate, 12 N.s. and 30 N.s. for the 12mm air gap plate and 16 N.s. and 24 N.s for the 16mm air gap plate. All the response times are in the region of 120 μs to 130 μs. There is no obvious trend evident in the plots concerning the response times between sandwich plates of different thickness'. From the responses plotted in Figure 4-37 , it can be seen how the impact between the plates affects the displacement response of Plate A. The large elastic vibrations that occur in Plate A, for impulses that just cause contact (as discussed in Chapter 4.2.3), are also visible in the lower impulse loading response of each sandwich plate.

Over page in Figure 4-37 are the plots of response times of plates A and B of the sandwich plate.

ABAQUS

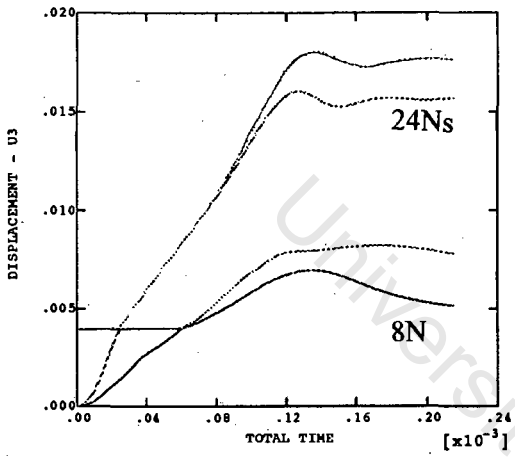

4mm AIR GAP PLATE

ABAQUS

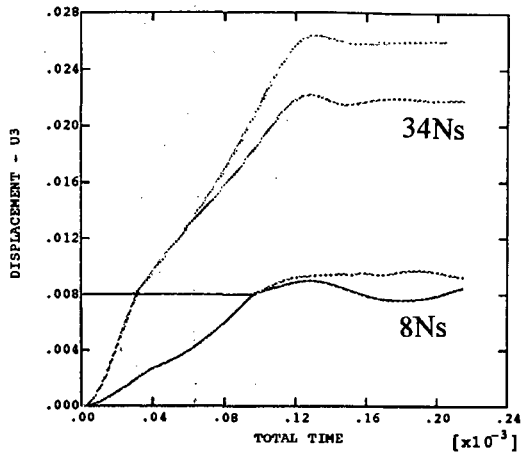

8mm AIR GAP PLATE

ABAQUS

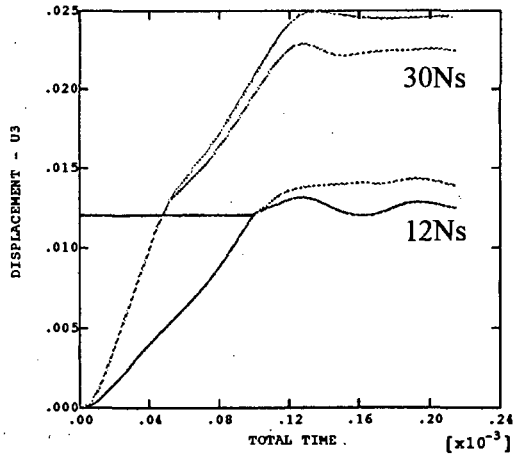

12mm AIR GAP PLATE

ABAQUS

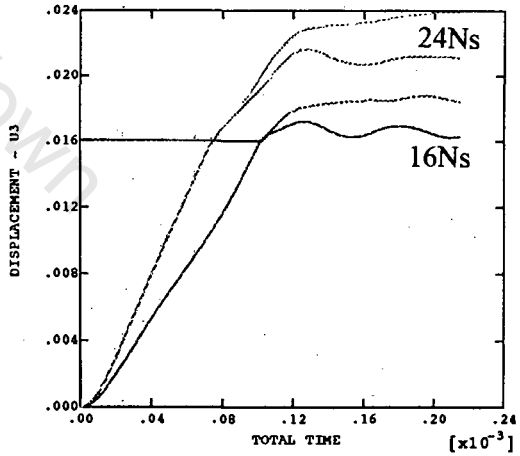

16mm AIR GAP PLATE

CHAPTER 5. DISCUSSION AND CONCLUSIONS

This thesis presents an investigation into the response of sandwich plates to impact loading. The numerical tool used in this analysis is the ABAQUS finite element package. This discussion includes comments on the single and sandwich plate responses as well as on the finite element method and its incorporated models.

The explicit integration scheme holds certain advantages and disadvantages over the implicit scheme. The disadvantages are mesh and stability related. It has been found that the explicit scheme requires a more refined mesh for the same level of convergence as the implicit scheme. The numerical stability of the solution is often reduced in the case of the explicit scheme. The stability is effected by mesh design in that it is important that the mesh is not biased so that certain elements are too 'critical' compared to the mesh as a whole. From these observations it is clear that mesh design is more important when using the explicit scheme. Due to numerical instabilities associated with the explicit solution scheme and the fact that numerical errors are not obvious in the results, checks must be done on the energy values of the system to ensure valid solutions while in the implicit scheme, instabilities are easily detected.

The advantage regarding the explicit scheme lies in the reduced cost of computation compared to the implicit scheme while still giving accurate converged solutions. The CPU time for an explicit scheme run can be in the order of ten times less than an equivalent model running under the implicit scheme. This factor is, however, not as important in the research field as in commercial applications.

Element choice is important with regard to time saving and to a lesser extent, accuracy. As element choice is often dictated by the type and symmetry of the structure being analysed it does not allow much scope for time saving and accuracy in general. Solutions from the SAX1 and the S4R element are nominally the same but the CPU time associated with their respective meshes are very different as the axisymmetric mesh out performed the quarter plate mesh with regards to time.

The material model is an area that requires research and attention. ABAQUS has the capability to allow modifications to the constitutive model of the material. Simple modifications can made to the stress versus plastic strain curve to exactly match the mild steel being modelled and a modification could be made to the assumption of isotropy as the mild steel used is in fact cold rolled. These differences are thought to be marginal, however.

The type of loading model was found to be not very important for Mode I failure. In the case of the pressure loading model, the burn times of 15μs and 30μs resulted in similar results. A burn time of around 5μs, however, resulted in reduction of the stability of the solution and hence inaccurate results. It was found that by refining the mesh, the shorter burn time of 5μs could yield stable results. The reason for the insensitivity to the burn time is that the burn times used are short compared with the response time of Mode I failure, but in Mode II and Mode III failure the response time is smaller and thus the burn time might prove to be critical. In general the pressure loading model produces stable solutions that show good correlation with the experimental data.

The velocity loading models give reasonable results but also tend to reduce the stability of the analysis. The transverse initial velocity profiles are more difficult to model than the uniform initial velocity profile especially in the case of the general shell model where velocities must be calculated for up to 954 nodes in the case of the 867 element mesh. Of the velocity load models, the uniform initial velocity profile gave the best correlation to experimental data. This model would be correct for a true impulsive load where the impulse is only applied at time t=0 but as the impulsive loading is modelled experimentally by applying an explosive blast and does not happen instantaneously, the pressure loading model is a more accurate model..

Mid-plate predictions for single plates compare favourably to a wide range of experimental work conducted. A difference exists between the current results and the analytical predictions of Jones and Wierzbicki. While the current analysis appears to correlate more closely to the experimental work of Nurick and Martin [2] than these analytical

predictions, it must be noted that these analytical predictions were presented only when experimental data in the range of impulses below 7 N.s. was available.

The plate deformation shape do not exactly predict the plate shapes from experimental work. It is thought that this is due to the simplification of regarding the boundary condition of the outer circumference as being built in. In the experimental work used for comparison, there is draw-through and local thinning at the circumference which would cause a larger rotation of the plate near the boundary. Comparison of the predicted plate deformation shapes with experimental data of built in plates might show this to be true. Comparison of plate thickness predictions to experimental data of plates with built in boundaries showed good correlation, while the response time of the plates compared well with experimentally and analytically determined values.

Within the sandwich plate analysis, the contact model is the most critical component. There are not many contact modelling options in the explicit scheme and thus the contact solution is dependent almost entirely on the accuracy of the explicit contact algorithm. From analysis of the contact between the plates, it appears that the duration of the contact is very short. Due to this short contact time, the energy lost to friction is assumed to be small. This is confirmed by the fact that by varying the coefficient of friction, only very small differences are predicted in the mid-plate deflections. The energy lost through contact is proportional to the area of contact.

The results for the contact diameter exhibit good correlation with the experimental data. The results of mid-plate deflection for the sandwich plates do not correlate with the experimental data as well as in the case of the single plate but are, however, acceptable in that the predicted trends show good correlation with the experimental data. The over estimate of the mid-plate deflection results could be due to numerous reasons. The contact algorithm might not be modelling the actual contact very accurately, while the experimental data to which the present work is compared is not expansive and experimental variation is possible. In conclusion, models for blast loaded single and sandwich plates have been found which correlate well with experimental data.

CHAPTER 6. RECOMMENDATIONS

The research on impulsively loaded circular plates should be continued to include Mode II and Mode III failure. Of importance in this work would be the failure criteria used to predict the material failure of the plate. As failure of the plate occurs at the boundary, the boundary conditions would have to be studied to acquire a full understanding of the effects the boundary conditions have on the material failure. This work should be conducted for both circular and square plates.

An experimental study of thinning and residual stresses in impulsively loaded plates could be compared to predictions of a finite element analysis.

An experimental study of impact between plates would be beneficial in that it could be compared to ABAQUS results in an attempt to verify the contact model within the code.

REFERENCES

1. D. MILBURN-PYLE, *Investigation into the response of sandwich plates subjected to impulsive loading*, Final year thesis, University of Cape Town (1989).
2. G. N. NURICK and J. B. MARTIN, Deformation of thin plates subjected to impulsive loading-A review: Part I - Theoretical Consideration and Part II - Experimental studies. *Int. J. Impact Engng.* **8,** 159-186 (1989).
3. R. G. TEELING-SMITH, *An investigation into the deformation and tearing of thin circular plates subjected to impulsive loads*, M.Sc., University of Cape Town (1989).
4. B. M. THOMAS, *The effect of boundary conditions on the failure of thin plates subjected to impulsive loading*, M.Sc., University of Cape Town (1995)
5. N. JONES, *Structural impact. Cambridge University Press,* Cambridge (1989).
6. T. WIERZBICKI and A. L. FLORENCE, A theoretical and experimental investigation of impulsively loaded clamped circular viscoplastic plates, *Int. J. Solids Struct.* **6,** 553-568 (1970).
7. G. N. NURICK, H. T. PEARCE and J. B. MARTIN, The deformation of thin plates subjected to impulsive loading. In *Inelastic behaviour of plates and shells* (ed. L. BEILACQUA). Springer-Verlag, Berlin (1986).
8. G. N. NURICK, H. T. PEARCE and J. B. MARTIN, Prediction of transverse deflections and in-plane strains in impulsively loaded thin plates. *Int. J. of Mech. Sci.* **29**, 435-442 (1987).
9. W. G. SHEN and N. JONES, Dynamic response and failure of fully clamped circular plates under impulsive loading. *Int. J. Impact. Engng.* **13**(1), 259-278 (1993).
10. M. D. OLSON, G. N. NURICK and J. R. FAGNAN, Deformation and rupture of blast loaded square plates-predictions and experiments. *Int. J. Impact Engng.* **2,** 279-291 (1993).
11. M. D. OLSON, J. R. FAGNAN and G. N. NURICK, Analysis of the deformation and tearing of blast loaded circular plates. (Submitted Nov. 1994) *Int. J. Impact Engng.*
12. S. B. MENKES and H. J. OPAT, Tearing and shear failures in explosively loaded clamped beams, *Exp. Mech.*, **13**, 480-486 (1973).

13. G. N. NURICK and R. G. TEELING-SMITH, Predicting the onset of necking and hence rupture of thin plates loaded impulsively- An experimental view, *In Structures Under Shock and Impact II*, (ed. P. S. BULSON). Thomas Telford, London (1992).
14. HIBBITT, KARLSSON & SORENSEN, INC, Status of Abaqus/Explicit ver. 5.3 as of 12-Oct-1994, in *Abaqus status file, Status_explicit.info.*
15. HIBBITT, KARLSSON & SORENSEN, INC, *Abaqus user manual.* (1993).
16. B. BUDIANSKI and J. L. SANDERS, *On the 'Best' first order linear shell theory*, Progress in Applied Mechanics, The Prager Anniversary Volume, Macmillan, London, 129-140 (1963).
17. J. B. MARTIN and L. S.-S. LEE, Approximate solutions for impulsively loaded elastic-plastic beams. *J. App. Mech.* **Dec,** 803-809 (1968).
18. G. N. NURICK, An empirical solution for predicting maximum central deflections of impulsively loaded plates, *Proc. 4th Int. Conf. On Mechanical Properties of Material at High Rates of Strain*, Institute of Physics Publishing, Bristol (1989).
19. N. PERRONE and P. BHADRA, A simplified method to account for plastic rate sensitivity with large deformations, *J. App. Mech*, **46**, 811-816 (1979).
20. P. S. SYMONDS and T. WIERZBICKI, Membrane mode solutions for impulsively loaded circular plates. *J. App. Mech.* **46,** 58-64 (1979).
21. T. A. DUFFEY, *The large deflection dynamic response of clamped circulator plates subjected to explosive loading*. Sandia Laboratories Research Report, SC-RR-67-532.
22. P. S. WESTINE and W. E. BAKER, *Energy solutions for predicting deformation in blast loaded structures*, Proc. 16th Explosive Safety Seminar, Hollywood Beach, Florida, USA, 849-879.
23. R. G. TEELING-SMITH and G. N. NURICK, The deformation and tearing of thin circular plates subjected to impulsive loads. *Int. J. Impact Engng.* **11,** 77-91 (1991).
24. G. N. NURICK, *Large deformations of thin plate subjected to impulse loading,* Ph.D., University of Cape Town (1987).
25. R. COOK, *Concepts and applications of Finite element analysis. John Wiley & Sons,* Singapore (1989).
26. G. N. NORVALL, *Impact Analysis: Modelling the deformation of thin plates and beams subjected to impulsive loading with the finite element programme ABAQUS/Explicit*, Final year thesis, University of Cape Town (1993).

APPENDIX A

Experimental Results of Sandwich Plates

TEST NO	GAP	IMPULSE	DEFLECTION		CONTACT DIAMETER	NOTES
			PLATE A	PLATE B		
	(mm)	(N.s.)	(mm)	(mm)	(mm)	
121001	4.0	24.41	14.88	12.40	81.5	
121002	4.0	incomplete explosive detonation				
121003	4.0	26.32	15.14	14.90	82.3	
121004	4.0	27.71	16.30	16.40	84.6	
161001	4.0	29.45	16.50	17.00	85.5	
161002	4.0	32.07	18.96	19.96	87.2	
171001	4.0	23.54	13.65	12.46	79.7	
171002	4.0	17.66	12.30	10.64	76.5	
171003	4.0	18.87	11.48	8.44	75.0	
171004	4.0	15.59	10.20	8.22	73.3	
171005	4.0	16.63	9.00	7.20	73.1	
171006	4.0	12.84	8.00	5.30	57.7	
171007	4.0	14.90	8.90	6.20	65.8	
171008	4.0	14.04	8.52	5.62	63.2	
171009	4.0	36.45				tearing
171010	4.0	38.74				tearing
241001	8.0	15.03	9.54	3.92	48.1	flat
241002	8.0	15.72	9.84	3.90	49.3	flat
241003	8.0	20.07	13.70	6.24	56.2	
241004	8.0	22.34	14.80	7.46	63.3	
241005	8.0	26.01	16.94	9.32	66.9	
241006	8.0	26.01	16.32	9.78	66.3	
241007	8.0	30.05	18.74	12.70	70.7	
241008	8.0	32.51	19.00	13.70	73.0	
251001	12.0	15.24	12.00	0.50	20.0	flat
251002	12.0	16.38	12.10	1.02	40.0	flat
251003	12.0	18.31	12.24	4.08	41.7	flat
251004	12.0	20.94	14.04	6.38	47.5	
251005	12.0	21.82	15.40	7.48	51.2	
251006	12.0	24.82	17.66	8.42	57.7	
251007	12.0	23.41	17.76	8.08	55.9	
251008	12.0	29.06	19.64	9.88	60.0	
261001	16.0	16.34	15.44	0.00	0.0	
261002	16.0	22.71	16.68	5.10	41.4	flat
261003	16.0	28.59				tearing
261004	16.0	20.23	16.70	4.46	37.9	flat
261005	16.0	20.76	16.56	3.16	34.7	flat

APPENDIX B

Presented Numerical Results of Sandwich Plates

IMPULSE	GAP	NO. OF	DEFLECTION		CONTACT	ENERGY		
		ELEMENT	PLATE A	PLATE B	DIAMETER	PLATE A	PLATE B	INPUT
	(mm)	(N.s.)	(mm)	(mm)	(mm)			
8	4.0	300	6.0	3.0		44.1	10.8	64.6
12	4.0	300	8.7	6.4	64.0	81.7	30.3	150.3
16	4.0	300	11.1	8.4	75.0	126.9	58.0	269.7
20	4.0	300	13.5	11.0		180.4	96.7	424.3
24	4.0	300	15.6	13.6	81.0	241.5	148.8	613.9
34	4.0	300	21.2	19.0	85.0	Friction coefficient = 0.4		
34	4.0	300	21.2	19.2		Friction coefficient = 0.0		
6	8.0	300	7.0	0.0	0.0			
7	8.0	300	7.9	0.25				
8	8.0	300	8.0	0.75	20.0			
9	8.0	300	8.7	1.5				
10	8.0	300	9.5	2.5	34.0			
11	8.0	300	10.0	3.4				
12	8.0	75	10.2	3.5				
12	8.0	300	10.5	4.0	42	120	17	150.3
12	8.0	507	10.6	4.0				
12	8.0	867	10.8	4.0				
16	8.0	300	12.5	6.5	53.0	188.6	36.1	269.7
20	8.0	300	15.0	9.0	60.0	263.6	67.6	424.3
24	8.0	300	17.2	11.7	64.0	349.2	109.6	613.9
30	8.0	300	20.0	15.1		485.1	196.9	965.7
34	8.0	300	21.8	17.6	72.0	585.9	271.5	1245.0
34	8.0	300	21.85	18.1		Friction coefficient = 0.0		
12	12.0	75	12.0	0.7				
12	12.0	300	12.5	1.0	20.0	145.0	4.0	150.7
12	12.0	587	12.6	1.0				
14	12.0	300	13.8	2.9				
16	12.0	300	15.0	4.0	38.0	234.2	19.2	269.7
20	12.0	300	17.1	7.0	44.0	331.6	42.2	
24	12.0	300	19.2	9.5	55.0	442.8	71.7	613.9
30	12.0	300	22.3	12.7	60.0	622.7	138.5	965.7
8	16.0	300	9.4	0.0	0.0	64.6	0.0	64.6
12	16.0	300	14.2	0.0	0.0	150.3	0.0	150.3
16	16.0	300	16.7	1.9	18.0	262.96	5.82	269.7
20	16.0	300	19.1	5.0	30.0	383.9	21.41	424.3
24	16.0	300	21.0	7.5	42.0	516.5	46.20	613.9

APPENDIX C

SAX1 and S4R Element Descriptions

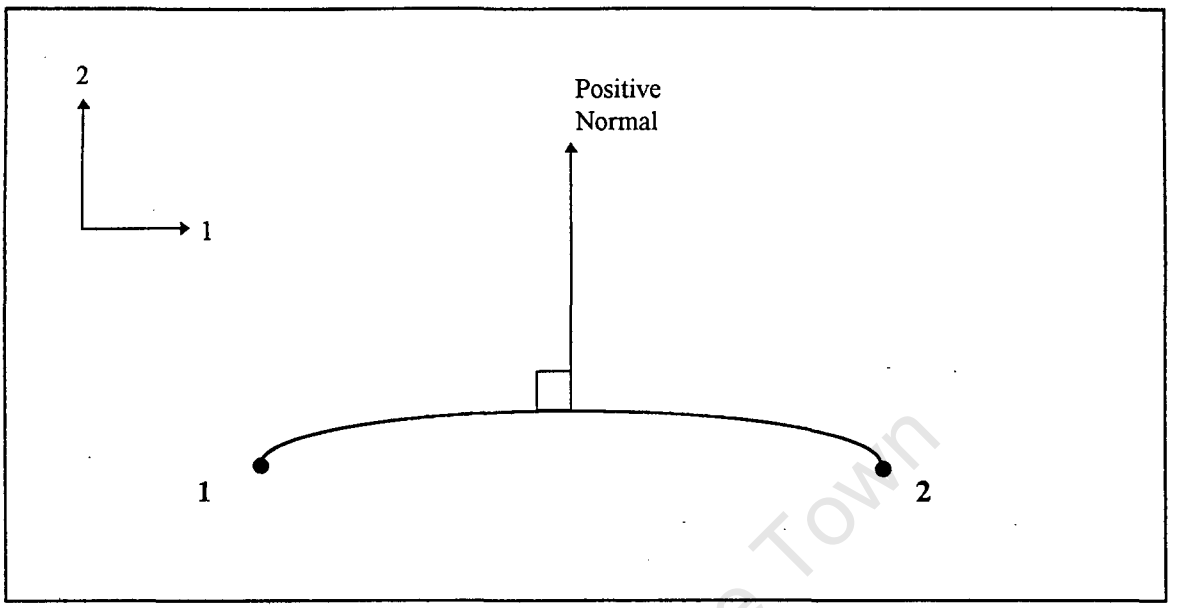

SAX1 Axisymmetric Shell Element

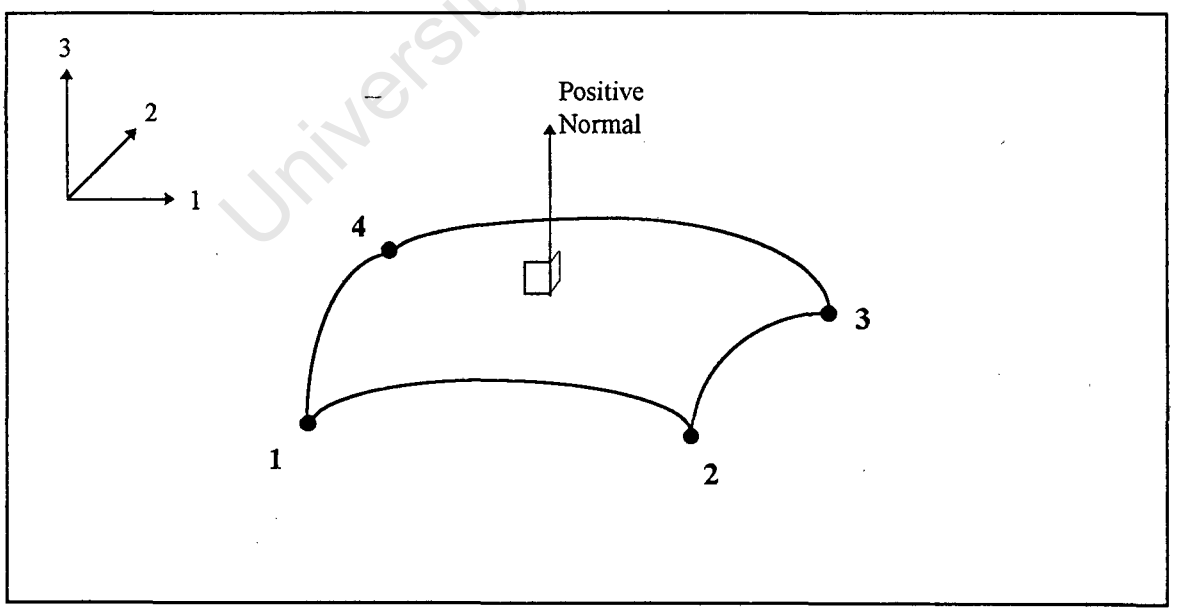

S4R General Shell Element

APPENDIX D

FORTRAN coding for generating the ABAQUS input deck of a single plate under a transverse initial velocity load.

```
      PROGRAM MESH
c*************************************************************************
c     SINGLE  PLATE WITH GENERAL SHELL ELEMENTS
c     AND A TRANSVERSE INITIAL VELOCITY LOAD MODEL.
c*************************************************************************
      INTEGER  n, J, K, M, NODE
      REAL     JJ, nn, A, VEL, X, Y, V, X1, X2
c****Input deck file name
     OPEN (UNIT=1,FILE='SCV20I12.INP')
c****Number of elements along radius
      n=20
c****Velocity Function Amplitude in m.s-1
      VEL=81.1
c****Z co-ordinate of plate
      Z=0.

100    FORMAT(I3,', ',1F5.4,', ',1F5.4,', ',1F5.4)
200    FORMAT(I3,',  ',I3,',  ',I3,',  ',I3,',  ',I3)
300    FORMAT(I3,',  ',I3,',  ',I3,',  ',I3,',  ',I3,',  ',I3,',  ',I3)
400    FORMAT(I3,',  ',I3,',  ',I3)
500    FORMAT(I3,',  3,  ',F7.2)

      WRITE(1,*)    '**************************************************'
      WRITE(1,*)    '*HEADING'
      WRITE(1,*)    'SCV20I04.INP   '
      WRITE(1,*)    '**S4R ELEMENTS,  CIRCULAR PLATE'
      WRITE(1,*)    '**20 NON-BIASED ELEMENTS ALONG THE RADIUS'
      WRITE(1,*)    '**12 N.s IMPULSIVE LOAD'
      WRITE(1,*)    '**************************************************'
      WRITE(1,*)    '**********************NODE'
      WRITE(1,*)    '*NODE'

      DO 20 J = 0, (n/2)
        DO 10 K = 0, (n/2)
          X= (.025-(.025-.0177)*J*2/n)*K*2/n
          Y= (.025-(.025-.0177)*K*2/n)*J*2/n
          NODE= (n/2+1)*J+K+1
          WRITE(1,100)  NODE,X,Y,Z
10      CONTINUE
20    CONTINUE
```

```
      DO 40 K = 1, (n/2)
       DO 30 J = 0, n
        nn = FLOAT(n)
        JJ = FLOAT(J)
        A  = JJ/nn

        IF (J.LE.(n/2)) THEN
        X1 = .025-(.025-.0177)*J*2/n
        X2 = COS(1.5708*A)*.05
        X  = ((X2-X1)*K*2/n+X1)
        Y  = X*TAN(1.5708*A)

        ELSE
        Y1 = .0177+(.025-.0177)*(J-n/2)*2/n
        Y2 = SIN(1.5708*A)*.05
        Y  = ((Y2-Y1)*K*2/n+Y1)
        X  = Y*TAN(1.5708*(1-A))

        END IF

        NODE = (J+1)+(n/2+1)**2+(K-1)*(n+1)
        WRITE(1,100)  NODE,X,Y,Z
30      CONTINUE
40     CONTINUE

      WRITE(1,*)     '*NSET,NSET=NSETA,GENERATE'
      WRITE(1,400)  1, (n/2+1)**2+1+(n/2-1)*(n+1)+n, 1
      WRITE(1,*)     '**********************ELEMENTS'
      WRITE(1,*)     '*ELEMENT,TYPE=S4R'
      WRITE(1,200)  1, 1, 2, (n/2+3), (n/2+2)
      WRITE(1,200)  (n/2)**2+1+n, (n/2+1)**2+1, (n/2+1)**2+2+n,
     &               (n/2+1)**2+3+n, (n/2+1)**2+2
      WRITE(1,*)     '**'

     DO 50 m = 1, n
       IF (M.LE.(n/2)) THEN
       WRITE(1,200)  (n/2)**2+m,(n/2+1)*m,(n/2+1)**2+m,
     &               (n/2+1)**2+1+m,(n/2+1)*(m+1)
       ELSE
       WRITE(1,200)  (n/2)**2+m,(n/2+1)**2-(m-n/2)+1,(n/2+1)**2+m,
     &               (n/2+1)**2+1+m,(n/2+1)**2-(m-n/2)
       END IF
50    CONTINUE
```

```
WRITE(1,*)    '**'
WRITE(1,*)    '*ELGEN'
WRITE(1,300)  1,  (n/2),1,1,  (n/2),(n/2+1),(n/2)
WRITE(1,300)  (n/2)**2+1+n,  (n/2-1),(n+1),1,  n,1,(n/2-1)
WRITE(1,*)    '*ELSET,ELSET=MODEL,GENERATE'
WRITE(1,400)  1, (n/2)**2+n/2*n, 1
WRITE(1,*)    '********NAME NODE SETS'
WRITE(1,*)    '*NSET,NSET=OA,GENERATE'
WRITE(1,400)  (n/2+1)**2+(n/2-1)*(n+1)+1,(n/2+1)**2+(n/2)*(n+1),1
WRITE(1,*)    '*NSET,NSET=XA,GENERATE'
WRITE(1,400)  1,(n/2+1),1
WRITE(1,400)  (n/2+1)**2+1,(n/2+1)**2+1+(n/2-1)*(n+1),(n+1)
WRITE(1,*)    '*NSET,NSET=YA,GENERATE'
WRITE(1,400)  1,(n/2+1)**2-n/2,(n/2+1)
WRITE(1,400)  (n/2+1)**2+1+n,(n/2+1)**2+1+(n/2-1)*(n+1)+n,(n+1)
WRITE(1,*)    '**********************BOUNDARY CONDITIONS*****'
WRITE(1,*)    '*BOUNDARY'
WRITE(1,*)    'OA,ENCASTRE'
WRITE(1,*)    'XA,YSYMM'
WRITE(1,*)    'YA,XSYMM'
WRITE(1,*)    '************************MATERIAL DEFENITION*****'
WRITE(1,*)    '*SHELL SECTION,ELSET=MODEL,MATERIAL=STEEL'
WRITE(1,*)    '.0016'
WRITE(1,*)    '*MATERIAL,NAME=STEEL'
WRITE(1,*)    '*ELASTIC'
WRITE(1,*)    '210.E9,0.29'
WRITE(1,*)    '*PLASTIC'
WRITE(1,*)    '290E6,0.00'
WRITE(1,*)    '300E6,0.003'
WRITE(1,*)    '310E6,0.008'
WRITE(1,*)    '320E6,0.013'
WRITE(1,*)    '330E6,0.018'
WRITE(1,*)    '340E6,0.024'
WRITE(1,*)    '350E6,0.035'
WRITE(1,*)    '360E6,0.056'
WRITE(1,*)    '370E6,0.10'
WRITE(1,*)    '380E6,0.137'
WRITE(1,*)    '390E6,0.171'
WRITE(1,*)    '400E6,0.20'
WRITE(1,*)    '470.E6,0.403'
WRITE(1,*)    '*DENSITY'
WRITE(1,*)    '7850.'
WRITE(1,*)    '*RATE DEPENDENT'
WRITE(1,*)    '40.,5.'
WRITE(1,*)    '************************************************'
```

```
      WRITE(1,*)     '*INITIAL CONDITIONS,TYPE=VELOCITY'

      DO 70 J = 0, (n/2)
       DO 60 K = 0, (n/2)
        X = (.025-(.025-.0177)*J*2/n)*K*2/n
        Y = (.025-(.025-.0177)*K*2/n)*J*2/n
        V = (.05-(X**2+Y**2)**.5)/.05*VEL
        NODE = (n/2+1)*J+K+1
        WRITE(1,500)  NODE,V
60     CONTINUE
70    CONTINUE

      DO 90 K = 1, (n/2)
       DO 80 J = 0, (n)
        nn = FLOAT(n)
        JJ = FLOAT(J)
        A  = JJ/nn
        IF (J.LE.(n/2)) THEN
        X1 = .025-(.025-.0177)*J*2/n
        X2 = COS(1.5708*A)*.05
        X  = ((X2-X1)*K*2/n+X1)
        Y  = X*TAN(1.5708*A)

        ELSE
        Y1 = .0177+(.025-.0177)*(J-n/2)*2/n
        Y2 = SIN(1.5708*A)*.05
        Y  = ((Y2-Y1)*K*2/n+Y1)
        X  = Y*TAN(1.5708*(1-A))

        END IF

        V = (.05-(X**2+Y**2)**.5)/.05*VEL
        NODE = (J+1)+(n/2+1)**2+(K-1)*(n+1)
        WRITE(1,500)  NODE,V
80     CONTINUE
90    CONTINUE

      WRITE(1,*)     '*RESTART,WRITE,NUMBER INTERVAL=30'
      WRITE(1,*)     '**********************************************'
      WRITE(1,*)     '**********************HISTORY*****************'
      WRITE(1,*)     '*STEP'
      WRITE(1,*)     '*DYNAMIC,EXPLICIT'
      WRITE(1,*)     ',.01'
      WRITE(1,*)     '*FILE OUTPUT,NUMBER INTERVAL=1'
      WRITE(1,*)     '*NODE FILE'
```

```
WRITE(1,*)    'U,V'
WRITE(1,*)    '*MONITOR,NODE=1,DOF=3'
WRITE(1,*)    '*EL FILE'
WRITE(1,*)    'PEEQ,MISES '
WRITE(1,*)    '*ENERGY FILE'
WRITE(1,*)    '*END STEP'
END
```

APPENDIX E

FORTRAN coding for generating the ABAQUS input deck of a sandwich plate under a pressure load.

```
      PROGRAM MESH
c*****************************************************************
c      SANDWICH  PLATE WITH GENERAL SHELL ELEMENTS
c      AND A PRESSURE  LOADING MODEL.
c*****************************************************************
      INTEGER n, J, K, M, NODE
      REAL      JJ, nn, A, X, Y, X1, X2, Z1, Z2, PRES

c****Input deck file name
     OPEN (UNIT=1,FILE='DC820I12.INP')
c****Number of elements along radius
      n=20
c****Applied pressure load in MPa
      PRES=101.9
c****Z co-ordinate of plate A
      Z2=0.0056
c****Z co-ordinate of plate B
      Z1=0.0

      WRITE(1,*)    '************************************************'
      WRITE(1,*)    '*HEADING'
      WRITE(1,*)    'DC810I12.INP    '
      WRITE(1,*)    '**QUARTER CIRCLE'
      WRITE(1,*)    '**S4F  ELEMENTS,  DOUBLE PLATE'
      WRITE(1,*)    '**20 NON-BIASED ELEMENTS ALONG THE RADIUS'
      WRITE(1,*)    '**12 N.s IMPULSIVE LOAD'
100    FORMAT(I4,', ',1F5.4,', ',1F5.4,', ',1F5.4)
200    FORMAT(I4,',  ',I4,',  ',I4,',  ',I4,',  ',I4)
300    FORMAT(I4,',  ',I4,',  ',I4,',  ',I4,',  ',I4,',  ',I4,',  ',I4)
400    FORMAT(I4,',  ',I4,',  ',I4)
500    FORMAT('PLATEA,P,'  ,1F7.2,'E6')

      WRITE(1,*)    '**********************PLATE A******************'
      WRITE(1,*)    '**********************NODE'
      WRITE(1,*)    '*NODE'
      DO 20 J = 0 , (n/2)
       DO 10 K = 0 , (n/2)
         X= (.025-(.025-.0177)*J*2/n)*K*2/n
         Y= (.025-(.025-.0177)*K*2/n)*J*2/n
         NODE= (n/2+1)*J+K+1
```

```
      WRITE(1,100  NODE,X,Y,Z1
10    CONTINUE
20   CONTINUE

     DO 40 K = 1, (n/2)
      DO 30 J = 0 , n
       nn = FLOAT(n)
       JJ = FLOAT(J)
       A  = JJ/nn

       IF (J.LE.(n/2)) THEN
       X1 = .025-(.025-.0177)*J*2/n
       X2 = COS(1.5708*A)*.05
       X  = ((X2-X1)*K*2/n+X1)
       Y  = X*TAN(1.5708*A)

       ELSE
       Y1 = .0177+(.025-.0177)*(J-n/2)*2/n
       Y2 = SIN(1.5708*A)*.05
       Y  = ((Y2-Y1)*K*2/n+Y1)
       X  = Y*TAN(1.5708*(1-A))

       END IF

       NODE= (J+1)+(n/2+1)**2+(K-1)*(n+1)
       WRITE(1,100)  NODE,X,Y,Z1
30     CONTINUE
40   CONTINUE

     WRITE(1,*)     '*NSET,NSET=NSETA,GENERATE'
     WRITE(1,400)  1, (n/2+1)**2+1+(n/2-1)*(n+1)+n, 1

     WRITE(1,*)  '**********************ELEMENTS'
     WRITE(1,*)     '*ELEMENT,TYPE=S4R'
     WRITE(1,200)  1, 1, 2, (n/2+3), (n/2+2)
     WRITE(1,200)  (n/2)**2+1+n, (n/2+1)**2+1, (n/2+1)**2+2+n,
    &              (n/2+1)**2+3+n, (n/2+1)**2+2
     WRITE(1,*)     '**'

    DO 50 m = 1 , n
      IF (M.LE.(n/2)) THEN
      WRITE(1,200)  (n/2)**2+m,(n/2+1)*m,(n/2+1)**2+m,
    &               (n/2+1)**2+1+m,(n/2+1)*(m+1)
      ELSE
      WRITE(1,200  (n/2)**2+m,(n/2+1)**2-(m-n/2)+1,(n/2+1)**2+m,
```

```
   &                (n/2+1)**2+1+m,(n/2+1)**2-(m-n/2)
      END IF
50   CONTINUE

      WRITE(1,*)     '**'
      WRITE(1,*)     '*ELGEN'
      WRITE(1,300)  1,   (n/2),1,1,   (n/2),(n/2+1),(n/2)
      WRITE(1,300)  (n/2)**2+1+n,   (n/2-1),(n+1),1,   n,1,(n/2-1)
      WRITE(1,*)     '*ELSET,ELSET=PLATEA,GENERATE'
      WRITE(1,400)  1, (n/2)**2+n/2*n, 1
      WRITE(1,*)     '********NAME NODE SETS'
      WRITE(1,*)     '*NSET,NSET=OA,GENERATE'
      WRITE(1,400)  (n/2+1)**2+(n/2-1)*(n+1)+1,(n/2+1)**2+(n/2)*(n+1),1
      WRITE(1,*)     '*NSET,NSET=XA,GENERATE'
      WRITE(1,400)  1,(n/2+1),1
      WRITE(1,400)  (n/2+1)**2+1,(n/2+1)**2+1+(n/2-1)*(n+1),(n+1)
      WRITE(1,*)     '*NSET,NSET=YA,GENERATE'
      WRITE(1,400)  1,(n/2+1)**2-n/2,(n/2+1)
      WRITE(1,400)  (n/2+1)**2+1+n,(n/2+1)**2+1+(n/2-1)*(n+1)+n,(n+1)

      WRITE(1,*)     '**********************PLATE B*****************'
      WRITE(1,*)     '**********************NODE'
      WRITE(1,*)     '*NODE'
      DO 1020 J = 0 , (n/2)
       DO 1010 K = 0 , (n/2)
        X= (.025-(.025-.0177)*J*2/n)*K*2/n
        Y= (.025-(.025-.0177)*K*2/n)*J*2/n
        NODE = (n/2+1)*J+K+1+1000
        WRITE(1,100)  NODE,X,Y,Z2
1010    CONTINUE
1020  CONTINUE

      DO 1040 K = 1 , (n/2)
       DO 1030 J = 0 , n
        nn= FLOAT(n)
        JJ= FLOAT(J)
        A = JJ/nn

        IF (J.LE.(n/2)) THEN
        X1 = .025-(.025-.0177)*J*2/n
        X2 = COS(1.5708*A)*.05
        X  = ((X2-X1)*K*2/n+X1)
        Y  = X*TAN(1.5708*A)

        ELSE
```

```
        Y1 = .0177+(.025-.0177)*(J-n/2)*2/n
        Y2 = SIN(1.5708*A)*.05
        Y  = ((Y2-Y1)*K*2/n+Y1)
        X  = Y*TAN(1.5708*(1-A))

        END IF

        NODE = 1000+(J+1)+(n/2+1)**2+(K-1)*(n+1)
        WRITE(1,100)  NODE,X,Y,Z2
1030    CONTINUE
1040   CONTINUE

      WRITE(1,*)     '*NSET,NSET=NSETB,GENERATE'
      WRITE(1,400)  1001, 1000+(n/2+1)**2+1+(n/2-1)*(n+1)+n, 1



      WRITE(1,*)     '**********************ELEMENTS'
      WRITE(1,*)     '*ELEMENT,TYPE=S4R'
      WRITE(1,200)  1000+1,1001,1002,1000+(n/2+3),1000+(n/2+2)
      WRITE(1,200)  1000+(n/2)**2+1+n, 1000+(n/2+1)**2+1,
     &              1000+(n/2+1)**2+2+n,1000+(n/2+1)**2+3+n,
     &              1000+(n/2+1)**2+2
      WRITE(1,*)     '**'

     DO 1050 m = 1 , n
        IF (M.LE.(n/2)) THEN
        WRITE(1,200)  1000+(n/2)**2+m,1000+(n/2+1)*m,
     &               1000+(n/2+1)**2+m,
     &               1000+(n/2+1)**2+1+m,1000+(n/2+1)*(m+1)
        ELSE
        WRITE(1,200)  1000+(n/2)**2+m,1000+(n/2+1)**2-(m-n/2)+1,
     &               1000+(n/2+1)**2+m,
     &               1000+(n/2+1)**2+1+m,1000+(n/2+1)**2-(m-n/2)
        END IF
1050  CONTINUE

      WRITE(1,*)     '**'
      WRITE(1,*)     '*ELGEN'
      WRITE(1,300)  1000+1,   (n/2),1,1,   (n/2),(n/2+1),(n/2)
      WRITE(1,300)  1000+(n/2)**2+1+n, (n/2-1),(n+1),1, n,1,(n/2-1)
      WRITE(1,*)     '*ELSET,ELSET=PLATEB,GENERATE'
      WRITE(1,400)  1000+1, 1000+(n/2)**2+n/2*n, 1
      WRITE(1,*)     '******NAME NODE SETS'
      WRITE(1,*)     '*NSET,NSET=OB,GENERATE'
```

```
      WRITE(1,400)  1000+(n/2+1)**2+(n/2-1)*(n+1)+1,
     &              1000+(n/2+1)**2+(n/2)*(n+1),1
      WRITE(1,*)     '*NSET,NSET=XB,GENERATE'
      WRITE(1,400)  1000+1,1000+(n/2+1),1
      WRITE(1,400)  1000+(n/2+1)**2+1,
     &              1000+(n/2+1)**2+1+(n/2-1)*(n+1),(n+1)
      WRITE(1,*)     '*NSET,NSET=YB,GENERATE'
      WRITE(1,400)  1000+1,1000+(n/2+1)**2-n/2,(n/2+1)
      WRITE(1,400)  1000+(n/2+1)**2+1+n,
     &              1000+(n/2+1)**2+1+(n/2-1)*(n+1)+n,(n+1)
      WRITE(1,*)  '*ELSET,ELSET=MODEL'
      WRITE(1,*)  'PLATEA,PLATEB'
      WRITE(1,*)  '**********************BOUNDARY CONDITIONS*****'
      WRITE(1,*)  '*BOUNDARY'
      WRITE(1,*)  'OA,ENCASTRE'
      WRITE(1,*)  'XA,YSYMM'
      WRITE(1,*)  'YA,XSYMM'
      WRITE(1,*)  'OB,ENCASTRE'
      WRITE(1,*)  'XB,YSYMM'
      WRITE(1,*)  'YB,XSYMM'
      WRITE(1,*)  '**********************MATERIAL DEFENITION*****'
      WRITE(1,*)  '*SHELL SECTION,ELSET=MODEL,MATERIAL=STEEL'
      WRITE(1,*)  '.0016'
      WRITE(1,*)  '*MATERIAL,NAME=STEEL'
      WRITE(1,*)  '*ELASTIC'
      WRITE(1,*)  '210.E9,0.29'
      WRITE(1,*)  '*PLASTIC'
      WRITE(1,*)  '290E6,0.00'
      WRITE(1,*)  '300E6,0.003'
      WRITE(1,*)  '310E6,0.008'
      WRITE(1,*)  '320E6,0.013'
      WRITE(1,*)  '330E6,0.018'
      WRITE(1,*)  '340E6,0.024'
      WRITE(1,*)  '350E6,0.035'
      WRITE(1,*)  '360E6,0.056'
      WRITE(1,*)  '370E6,0.10'
      WRITE(1,*)  '380E6,0.137'
      WRITE(1,*)  '390E6,0.171'
      WRITE(1,*)  '400E6,0.20'
      WRITE(1,*)  '470.E6,0.403'
      WRITE(1,*)  '*DENSITY'
      WRITE(1,*)  '7850.'
      WRITE(1,*)  '*RATE DEPENDENT'
      WRITE(1,*)  '40.,5.'
      WRITE(1,*)  '**************************************************'
```

```
WRITE(1,*) '*RESTART,WRITE,NUMBER INTERVAL=15'
WRITE(1,*) '**********************************************'
WRITE(1,*) '**********************HISTORY*****************'
WRITE(1,*) '*STEP'
WRITE(1,*) '*DYNAMIC,EXPLICIT'
WRITE(1,*) ',0.000015'
WRITE(1,*) '*SURFACE DEFINITION,NAME=FACEA'
WRITE(1,*) 'PLATEA,SPOS'
WRITE(1,*) '*SURFACE DEFINITION,NAME=FACEB'
WRITE(1,*) 'PLATEB,SNEG'
WRITE(1,*) '*SURFACE INTERACTION,NAME=FRIC'
WRITE(1,*) '*FRICTION'
WRITE(1,*) '.4,'
WRITE(1,*) '**********************CONTACT PAIRS*********'
WRITE(1,*) '*CONTACT PAIR,INTERACTION=FRIC'
WRITE(1,*) 'FACEA,FACEB'
WRITE(1,*) '*DLOAD'
WRITE(1,500)  PRES
WRITE(1,*) '*FILE OUTPUT,NUMBER INTERVAL=1'
WRITE(1,*) '*END STEP'

WRITE(1,*) '*STEP'
WRITE(1,*) '*DYNAMIC,EXPLICIT'
WRITE(1,*) ',.01'
WRITE(1,*) '*DLOAD,OP=NEW'
WRITE(1,*) '*FILE OUTPUT,NUMBER INTERVAL=1'
WRITE(1,*) '*END STEP'

END
```

APPENDIX F

Courses completed for partial fulfilment of the requirements for the Degree of Master of Science:

CAM 500 Z	Applied Mechanics I	3 credits
CAM 501 Z	Applied Mechanics II	3 credits
CAM 502 Z	An Introduction To Finite Elements	3 credits
CAM 503 Z	Finite Element Analysis	4 credits
CAM 504 Z	Engineering Software Design & Development	3 credits
MEC 524 S	Structural Impact	3 credits
MEC 435 C	Engineering Applications of Fracture Mechanics	2 credits
	Total:	21 credits

Published Papers:

G.H.FARROW, G.N.NURICK, G.P.MITCHELL, Modelling of impulsively loaded circular plates using the ABAQUS finite element code, *Proceedings of the 13th Symposium on Finite Element Methods in South Africa,* (1995).